LATE QUATERNARY GLACIER FLUCTUATIONS AT LILLOOET, DIADEM, AND BERENDON GLACIERS, COAST MOUNTAINS, BRITISH COLUMBIA

By

Lauren Annie Walker

B.Sc. University of Victoria, 2001

THESIS SUBMITTED IN PARTIAL FULFILLMENT

OF THE REQUIREMENTS FOR THE DEGREE OF

MASTER OF SCIENCE

In the Department

Of

Earth Sciences

SIMON FRASER UNIVERSITY

November 2003

APPROVAL

Name: **Lauren Walker**

Degree: Master of Science

Title of Thesis: Late Quaternary glacier fluctuations at Lillooet, Diadem, and Berendon glaciers, Coast Mountains, British Columbia

Examining Committee:

Chair: **Dr. Peter Mustard**
Associate Professor

Dr. John Clague
Senior Supervisor
Professor

Dr. Ian Hutchinson
Supervisory Committee Member
Professor, SFU Geography

Dr. Rolf Mathews
Supervisory Committee Member
Professor, SFU Biology

Dr. Brian Menounos
External Examiner
Assistant Professor
Geography Program, University of Northern BC

Date Approved: November 28, 2003

PARTIAL COPYRIGHT LICENCE

I hereby grant to Simon Fraser University the right to lend my thesis, project or extended essay (the title of which is shown below) to users of the Simon Fraser University Library, and to make partial or single copies only for such users or in response to a request from the library of any other university, or other educational institution, on its own behalf or for one of its users. I further agree that permission for multiple copying of this work for scholarly purposes may be granted by me or the Dean of Graduate Studies. It is understood that copying or publication of this work for financial gain shall not be allowed without my written permission.

Title of Thesis/Project/Extended Essay:

Late Quaternary glacier fluctuations at Lillooet, Diadem, and Berendon glaciers, Coast Mountains, British Columbia

Author: _____

(Signature)

Lauren Annie Walker

(Name)

Dec 3/2003

(Date)

Abstract

Stratigraphic and paleobiological records indicate pre-Little Ice Age advances of Lillooet, Diadem, and Berendon glaciers in the Coast Mountains of British Columbia. Subdued lateral moraines ("outer moraines") lie outside the Little Ice Age limit of each of the three glaciers. At Lillooet Glacier, sediments in dug pits, cores collected from ponds dammed by the outer moraine, and sediments exposed in a composite lateral moraine indicate four periods of advance: prior to 6200 ^{14}C yr BP and probably during late-glacial time; during the Tiedemann Advance with a maximum about 2800 ^{14}C yr BP; during the late Holocene between 1500 and 1000 ^{14}C yr BP; and during the Little Ice Age. At Diadem Glacier, sediments overlying the outer moraine similarly indicate an advance prior to 6200 ^{14}C yr BP, likely during late-glacial time. The sediments further suggest warmer conditions during the early Holocene and landscape instability during the Little Ice Age. At Berendon Glacier, stratigraphic evidence suggests that the outer moraine is older than 3500 ^{14}C yr BP. Sedimentological and paleobiological evidence provided by a core collected from a pond outside the Little Ice Age terminal moraine of Berendon Glacier further indicates a Tiedemann-age advance about 2700 ^{14}C yr BP and minor glacier fluctuations between 1800 and 1200 ^{14}C yr BP. Vegetation change at Berendon Glacier during advances prior to the Little Ice Age was relatively insignificant. Cosmogenic ^{36}Cl exposure ages on boulders on the outer moraines at all three study sites are much younger than the moraines themselves and are not easily explained.

Equilibrium-line altitude reconstructions of the modern and Little Ice Age glaciers provide estimates of climate change associated with the climactic Little Ice Age advance and the advance(s) responsible for the subdued outer moraines. Little Ice Age equilibrium-line altitude depressions calculated using the accumulation area ratio method are about 140 m, at least 30 m, and approximately 60 m for the Lillooet, Diadem, and Berendon glaciers, respectively. A comparison of calculated ELAs to modern upper air data suggests a temperature lowering of up to 0.7 °C from present values during both advances, likely accompanied by a coeval increase in precipitation.

Acknowledgements

I would like to thank the following people for their support and guidance through the course of my work.

I would first like to acknowledge my supervisor, John Clague, for his encouragement and assistance that saw me through to the end of my thesis, and for providing me with the incredible experience of working and learning in the mountains that I love. I would also like to thank Ian Hutchinson and Rolf Mathewes for their input into this project and for assistance with field logistics. I would also like to thank Mark Stasiuk, Kirsty Simpson, and Kelly Russell for their help with tephra identification, Doug Clark for facilitating magnetic susceptibility analysis of cores, Mitch Plummer and Fred Phillips for their assistance in obtaining cosmogenic ages, and Jon Riedel for his help with equilibrium-line altitude reconstructions. Multiple thank yous also go to Britta Jenson, Tracy Arsenault, Lisa Wilson, Ian Walker, Jenn Sabean, Matthew Skinner, and Jamie Dunlop for their assistance in the field, and especially to Alberto Reyes for both his assistance and constructive discussions in the field. Funding for this project was provided by John Clague from his NSERC Operating Grant and by the Northern Scientific Training Program.

In particular, I want to extend a warm thank you to my family for their continual encouragement and support over the years, to all my friends for keeping me smiling, and finally to Ella-dog for countless inspiring walks along the sand.

Table of Contents

List of Tables

List of Figures

List of Appendixes

1 Introduction

Increasing awareness of possible future climate change is accompanied by uncertainty as to how this climate change will impact our environment. Reconstructions of past glacier activity provide opportunities to assess both environmental and climate change. To properly assess past climate change, however, it is essential to have complete records of former glacier extents. This thesis presents evidence collected at three glaciers in the Coast Mountains of British Columbia. The evidence is used to reconstruct the history of glacier fluctuations at each site during late Quaternary time.

Late Quaternary Glacial History of the Coast Mountains

The majority of glaciers in the Coast Mountains of British Columbia attained their maximum post-glacial extent during the Little Ice Age, a period of variable but generally cool climate that began in the 13th century and ended in the late 19th century (ca. AD 1200- late 1800s) (Grove, 1988; Luckman, 2000). Most evidence of older Holocene and latest Pleistocene advances was lost when Little Ice Age glaciers overran older glacial deposits. The record of these earlier glacier fluctuations is thus fragmentary. However, through the use of paleobiological proxy climate indicators and by dating remaining pre-Little Ice Age glacial deposits, a more complete picture of pre-Little Ice Age glacier fluctuations and climate change in the Coast Mountains is beginning to form.

Following the maximum of the Vashon Stade of the Fraser Glaciation approximately 14,000 ^{14}C yr BP, the Cordilleran Ice Sheet rapidly decayed by downwasting and frontal retreat (Clague and James, 2002). By 9500 ^{14}C yr BP, glaciers in the Coast Mountains were of similar extent to today (Ryder and Thomson, 1986). There is, however, evidence for latest Pleistocene glacier readvance in the southern Coast Mountains about 10,700-10,500 ^{14}C yr BP (Friele and Clague, 2002a, b), and in the Fraser Lowland between 11,600 and 10,000 ^{14}C yr BP (Kovanen and Easterbrook, 2002). Advances are also postulated prior to 11,300 ^{14}C yr BP at Mt. Rainier (Heine, 1998) and prior to ca. 11,300 ^{14}C yr BP at Glacier Peak (Beget, 1981).

Arguments have been made for glacier advances on Mt. Baker between 8400 and 7700 ^{14}C yr BP (Thomas et al., 2000), on Mt. Rainier between 9800 and 9850 ^{14}C yr BP (Heine, 1998), and near Glacier Peak ca. 9300 ^{14}Cyr BP (Beget, 1981). Paleobiological evidence from Castle Peak in the southern Coast Mountains, however, indicates a warmer-than-present climate and elevated tree line between 9100 and 8100 ^{14}C yr BP (Clague and Mathewes, 1989).

Middle Holocene glacier advances recognized in the Coast Mountains cluster into two periods. The first advances are associated with the Garibaldi Phase of glaciation between ca. 6000 and 5000 ^{14}C yr BP (Ryder and Thomson, 1986; Clague, 1989). Advances are also recognized between ca. 6100 and 4600 ^{14}C yr BP at Glacier Peak, in the Washington Cascades, and between ca. 6000 and 5800 ^{14}C yr BP at South Cascade Glacier (Beget, 1984). The second group of advances is the Tiedemann Phase between ca. 3300 and 1900 ^{14}C yr BP (Ryder and Thomson, 1986). The maximum advance of Tiedemann Glacier occurred ca. 2300 ^{14}C yr BP (Ryder and Thomson, 1986), and other Tiedemann advances are recognized in the southern Coast Mountains at Monarch Icefield (Desloges and Ryder, 1990) and in the Mt. Gilbert area (Ryder and Thomson, 1986), and in the northern Coast Mountains in the Stewart area (Clague and Mathewes, 1986). These advances are roughly contemporaneous with advances on Mt. Rainier (Crandell and Miller, 1974) and in coastal Alaska (Calkin et al., 2001).

Evidence from the Coast Mountains indicates that the Little Ice Age commenced ca. 900 ^{14}C yr BP and peaked in the eighteenth or nineteenth century (Ryder and Thomson, 1986; Desloges and Ryder, 1990; Clague and Mathewes, 1996; Kershaw, 2002). At present, almost all glaciers in the Coast Mountains are significantly smaller than they were at the Little Ice Age maximum, having retreated since the beginning of the 20th century.

Study Sites

Three glaciers chosen for this study lie roughly along a north-south transect in the Coast Mountains: Lillooet Glacier, approximately 180 km north-northwest of Vancouver; Diadem Glacier, about 100 km north of Lillooet Glacier; and Berendon Glacier

approximately 40 km north-northwest of Stewart. The three glaciers are within the Coast geological belt, which formed during Cretaceous and early Tertiary time and is composed of granite and metamorphosed sedimentary and volcanic rocks (Clague, 1989). The Coast Mountains are part of the western physiographic unit of the Canadian Cordillera that extends from the Cascade Mountains of on the south to the St. Elias Mountains in southwestern Yukon (Clague, 1989). The topography is rugged, with high mountains supporting valley glaciers and icefields.

At all three study sites, sharp-crested lateral moraines and distinct trimlines associated with Little Ice Age advances attest to significant glacier downwasting and retreat over the last few centuries. Of particular interest at the three sites are more subdued lateral moraines that lie outside the Little Ice Age moraines. These outer moraines provide a rare opportunity to assess glacier fluctuations prior to the Little Ice Age.

Objectives of Study

The objectives of this study are threefold:

1. Reconstruct the late Quaternary glacial history of the three study sites, with emphasis on advances that pre-date the Little Ice Age maximum.

2. Evaluate climate changes associated with these glacier fluctuations.

3. Correlate reconstructed glacier advances with other advances identified in the Coast Mountains.

The findings of this research contribute to existing knowledge of late Quaternary climate and glacier fluctuations in the Coast Mountains. A more thorough understanding of how glaciers in the Coast Mountains oscillated in response to past climate change is an essential step in properly evaluating how future climate change will impact glaciers and the alpine environment.

Thesis Structure

Chapter 2 presents sedimentological and paleobiological data pertinent to moraines deposited during late Quaternary advances of the three glaciers investigated in this study. Chapter 3 describes the cosmogenic ^{36}Cl dating of moraine boulders used to constrain the ages of the glacier advances. Chapter 4 presents a reconstruction of modern and past glacier equilibrium-line altitudes and the climate conditions they imply. The closing chapter summarises the major findings of this study.

2 Late Quaternary Glacier Fluctuations at the Three Study Sites

This chapter describes research on the history of sediments deposited at Lillooet, Diadem, and Berendon glaciers since the last glacial maximum. The stratigraphic records come from pits dug in the vicinity of lateral moraines and from sediment cores collected in moraine-dammed ponds. The morphology and extent of pre-Little Ice Age moraines were also determined through aerial photographic interpretation and field investigations.

Lillooet Glacier

Lillooet Glacier is located approximately 70 km northwest of Pemberton, in the Pacific Ranges of the southern Coast Mountains (Fig. 1). The glacier flows northward approximately 5.25 km from its accumulation area in the Lillooet Icefield, then flows west-southwest for approximately 8.75 km. It terminates at approximately 900 m asl at Silt Lake, which marks the head of the Lillooet River. The glacier shares an accumulation area with Bishop Glacier, which flows to the northwest. The surrounding area is characterized by steep slopes with peaks over 3000 m in elevation. The local vegetation is transitional between that of the coastal Mountain Hemlock and the Englemann Spruce-Subalpine Fir biogeoclimatic zones, with alpine meadows at high elevations.

Distinct glacial trimlines and prominent lateral moraines border the lower part of Lillooet Glacier (Fig. 1). Up to five till units separated by soil horizons and woody debris constitute the prominent lateral moraine, marking Little Ice Age limit along the northeast side of the glacier. The crest of this composite moraine can be traced downvalley approximately 1.5 km beyond Silt Lake.

Just outside the Little Ice Age limit are segments of a more subdued moraine that records an earlier advance of similar magnitude (Fig. 1). This 'outer' moraine is parallel to the main lateral moraine crest and occurs in segments up to 500 m in length. The outer moraine crest is notably rounded in comparison to the main crest. A third, 'middle' moraine occurs as two small segments between the Little Ice Age moraine and

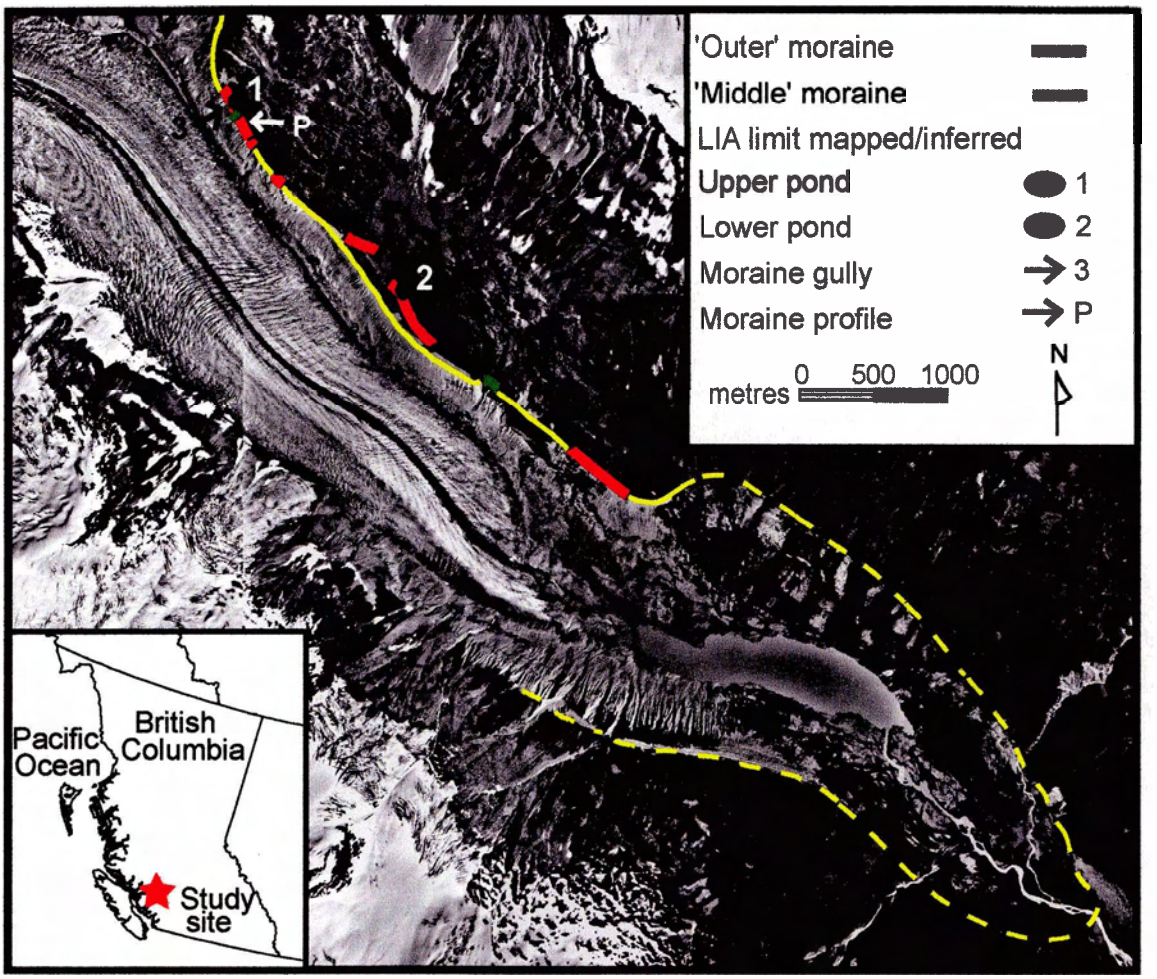

Figure 1. Composite aerial photograph of Lillooet Glacier, showing the locations of moraines, ponds, a gully, and the moraine profile discussed in the text. "LIA limit" refers to the maximum Little Ice Age extent of the glacier. Portions of British Columbia Government air photographs BC81085:144-146, 086-087 (1981); reproduced courtesy of the Ministry of Sustainable Resource Management, Base Mapping and Geomatic Services Branch.

the outer moraine (Fig. 1). It is a smaller feature than the outer moraine.

The Outer Moraine and Moraine-dammed Ponds

Methods

Two different approaches were used to constrain the age of the outer moraine. Moraine boulders were sampled for cosmogenic ^{36}Cl dating (see Chapter 3, *Cosmogenic ^{36}Cl Dating*). At two locations, the moraine dams two small ponds (Figs. 1 and 2). As the ponds are impounded by the moraine and lie outside of it, pond sediments must postdate the moraine. The sediments thus provide age constraints on the glacier advance that built the outer moraine and on subsequent advances.

Pits were dug along the edges of the two ponds to establish the relationship between the pond sediments and past advances of Lillooet Glacier (Fig. 2). Three cores were also collected from the upper pond using a simple percussion device with 7.5 cm-diameter PVC tubes. Cores LP1 and LP2 were taken from water depths of 49 and 48 cm, respectively. Core LP3 was collected from the dried surface of the pond at its edge.

Upper Pond

The upper pond (ca. 1490 m asl) extends approximately 42 m along the edge of the outer moraine and has a maximum depth of about 55 cm. The pond is fed seasonally by snowmelt and by a small stream that enters it at its north end (Fig. 2). It drains by a small stream cut into the moraine. The moraine crest rises approximately 50 cm above the level of the pond, sloping about 25°. The pond is fringed by sedges; rhododendron, huckleberry, willow, subalpine fir and sparse mountain hemlock grow on the moraine.

The pond lies on a small, possibly rock-controlled, bench; bedrock crops out approximately 20 m south of the pond. The outer moraine can be traced northwest from this bedrock knob to about 50 m beyond the pond. The outer moraine crest is only slightly lower than the crest of the Little Ice Age moraine directly to the west.

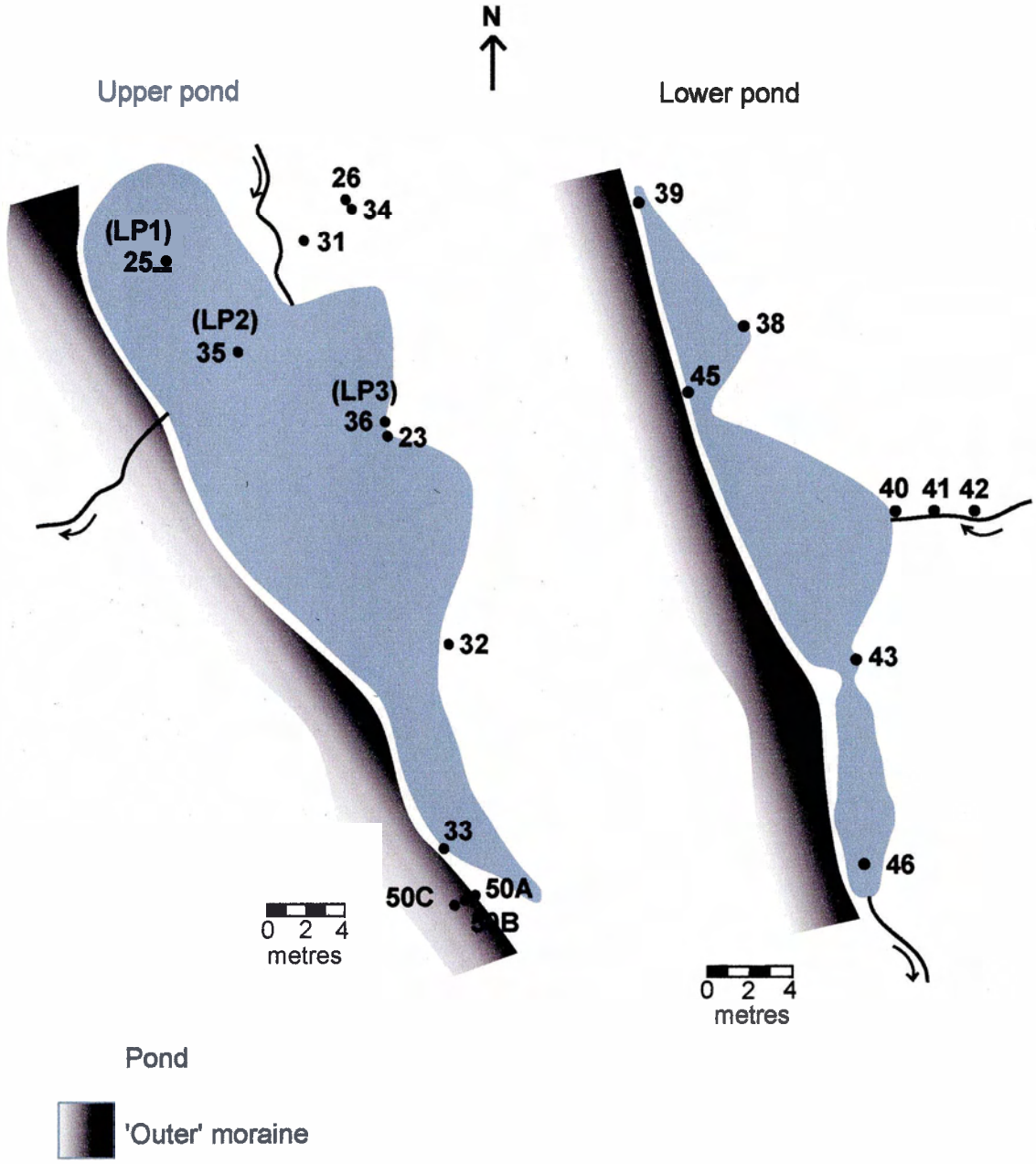

Figure 2. The lower and upper ponds, and locations of pits described in the text. The moraine and creeks are not drawn to scale. See Figure 1 for locations of ponds, and Figures 4 and 6 for pit stratigraphy.

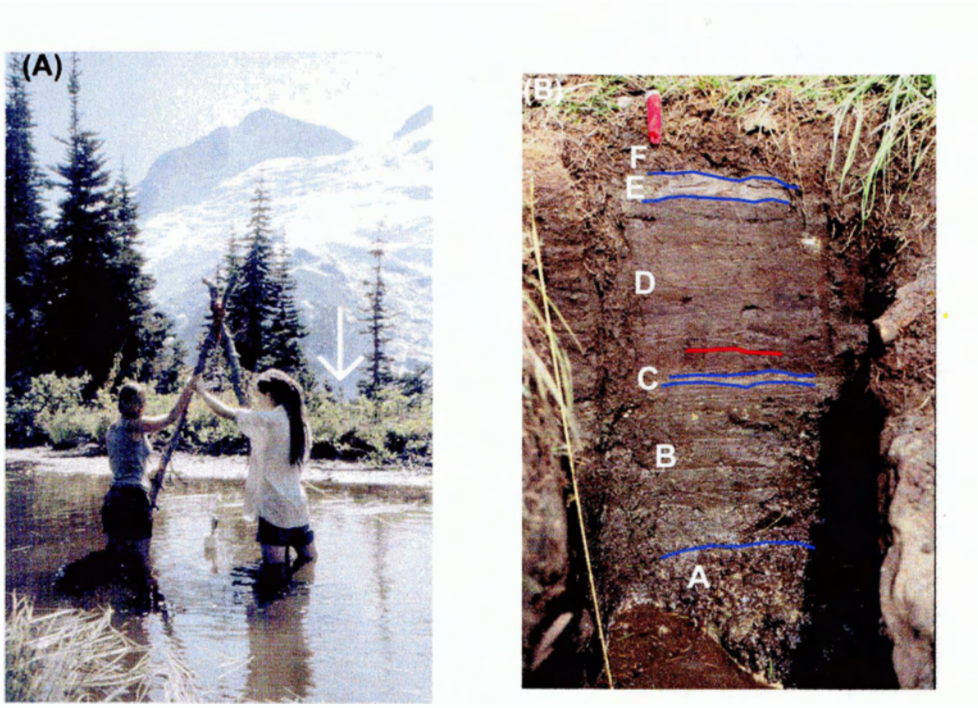

Figure 3. A. Removing core LP2 at the upper pond. Arrow indicates the position of the outer moraine. (B) Photograph showing the stratigraphy of the upper pond sediments. Photograph taken adjacent to pit 26 described in the text. The red line indicates the position of the Bridge River tephra horizon. Knife handle is approximately 9 cm in length.

Sediments

The stratigraphy of the upper pond sediments was logged in five pits, a trench dug perpendicular to the moraine (sections 50A-C, Fig. 2), and three cores (Fig. 4). A representative photograph of the sediments is shown in Figure 3. The lowest unit (A) comprises cobble-rich diamicton with a matrix of silt and sand. The base of the diamicton was not seen. The top of the unit is oxidized. Unit A grades into overlying muddy peat (unit B) over a distance of 2 to 5 cm. In pit 33 and trench 50A-C at the southern end of the pond, the lowermost few centimetres of unit B contain abundant charcoal. Small isolated pebbles occur through the lower half of unit B. The upper half of the unit is more organic-rich than the lower half. Unit B is thickest (62 cm) in pit 26. Unit B is sharply overlain by 1 to 2 cm of light grey silt and sand (unit C). Two beds of sand and silt are separated by a few centimetres of muddy peat in pits 31 and 34. Unit C is sharply overlain by humified, muddy, brown peat (unit D). In most pits, up to 2 mm of white, silty tephra is discontinuously present in the lower half of unit D. The tephra was

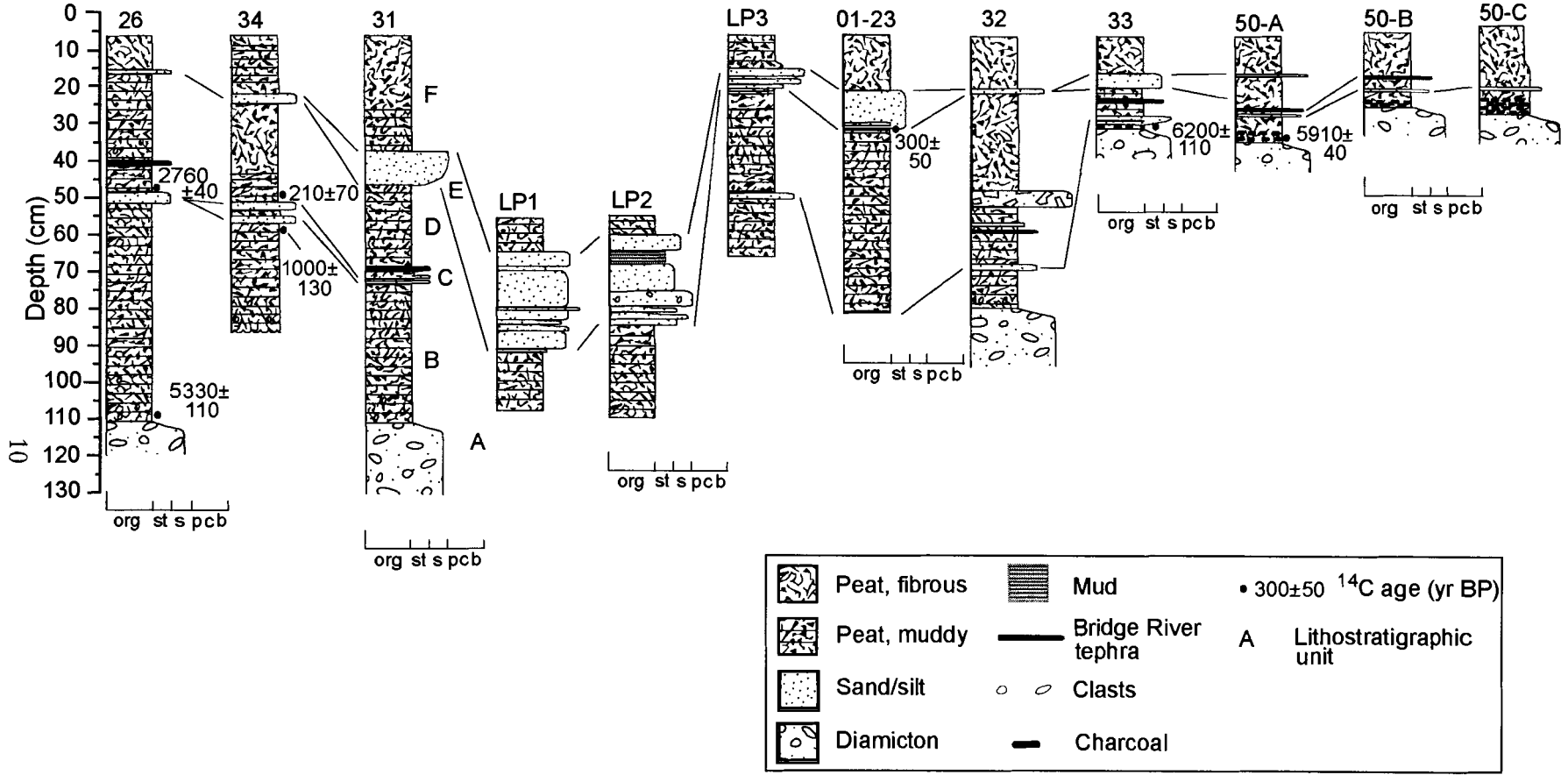

Figure 4. Stratigraphy of upper pond pits, trench, and cores (see Fig. 2 for locations). org = organic; st = silt; s = sand; p,c, and b = pebble, cobble, and boulder, respectively. See text for stratigraphic description and interpretation.

identified by Drs. M. Stasiuk, K. Russell, and K. Simpson as Bridge River tephra on the basis of mineralogy. Bridge River tephra was deposited during an eruption of Mt. Meager approximately 2360 cal yr BP (ca. 2400 ^{14}C yr BP) (Clague et al., 1995). Unit D is sharply overlain by a second silt and sand unit (E), which coarsens and thickens to a maximum of 27 cm towards the centre of the pond. Unit E is generally massive withsparse pebbles, but fining-upwards beds of sandy silt are present in cores LP1 and LP2. In LP2, unit E includes a 5 cm-thick sandy mud bed. Unit E is sharply overlain by up to 20 cm of muddy peat and fibrous peat (unit F).

Lower Pond

The lower pond (ca. 1310 m asl) is smaller and shallower than the upper pond (Figs. 2 and 5a). It is fed by ground water, snowmelt, and overland flow during rainstorms. A small ephemeral stream enters the pond at its east side and another drains the pond to the south.

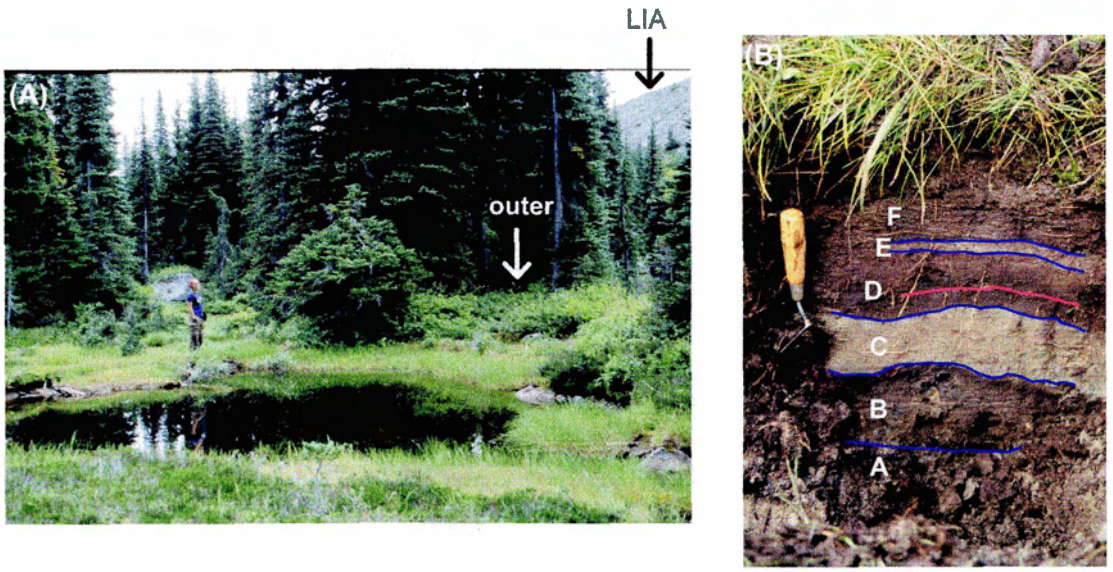

Figure 5. A. Lower pond, view to the southwest. 'LIA' and 'outer' signify the Little Ice Age and outer moraines, respectively. B. Stratigraphy of pit 38. See text and Figure 6 for details of pit stratigraphy. Red line indicates the position of the Bridge River tephra layer. Trowel handle is approximately 15 cm in length. Photograph by A. Reyes.

The Little Ice Age moraine is considerably higher at the lower pond than at the upper pond and rises steeply above the valley floor (Fig. 5a). The outer moraine is more distant from the Little Ice Age moraine at the lower pond than at the upper pond. A small stream flows between the two moraines, capturing runoff and sediment sourced on the Little Ice Age moraine.

Sediments

The stratigraphy of the lower pond sediments is similar to that of the upper pond sediments (Figs. 5b and 6). The upper part of unit A diamicton is oxidized and grades upward into unit B over a few centimetres. Unit B peat is up to 7 cm thick. It is less minerogenic than unit B peat at the upper pond, but it contains charcoal fragments in the same stratigraphic position as at the upper pond (pits 38 and 39, Fig. 6). Unit C is a bed of silty fine sand up to 14 cm thick with sharp upper and lower contacts. The unit becomes granule-rich and thicker towards the moraine. The overlying unit D peat is up to 28 cm thick and contains a discontinuous thin layer of Bridge River tephra in three of the pits (Fig. 5b). The upper part of unit D in pits at the west side of the pond has a distinct orange colour and is more fibrous than the lower part of the unit. The upper sand and silt unit (E) is up to 3 cm thick and sharply overlies unit D. It is clay-rich and massive and was only found at two pits (nos. 38 and 39). Unit E is sharply overlain by unit F peat.

Chronology

Six accelerator mass spectrometry (AMS) ^{14}C ages were obtained from sediments at the upper pond, and two from sediments at the lower pond (Figs. 4 and 6; Table 1). Charcoal and conifer needles from the base of unit B yielded ages of 5330 ± 110, 5910 ± 40, and 6200 ± 110 ^{14}C yr BP at the upper pond, and 5870 ± 80 ^{14}C yr BP at the lower pond. An age of 870 ± 100 ^{14}C yr BP was obtained on seeds and a conifer needle just below the lower silt horizon (unit C) at the lower pond. At the upper pond, ages of 1000 ± 30 and 210 ± 70 ^{14}C yr BP were obtained on rootlets 1 cm below and 1 cm above the lower silt horizon, respectively. An age of 2760 ± 40 ^{14}C yr BP was obtained on wood on top of the lower silt at the upper pond.

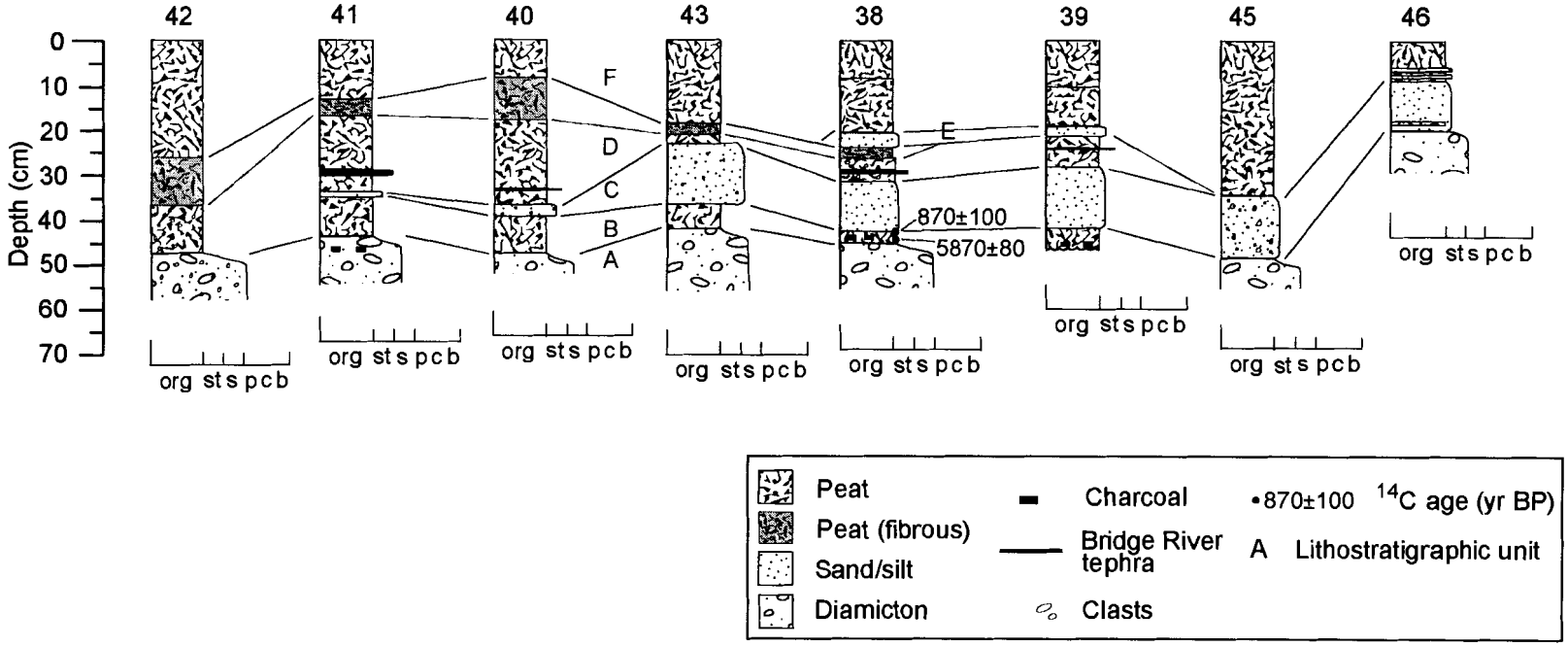

Figure 6. Stratigraphy of lower pond pits (see Fig. 2 for locations). org = organic; st = silt; s = sand; p,c, and b = pebble, cobble, and boulder, respectively. See text for stratigraphic description and interpretation.

Table 1. Radiocarbon ages from Lillooet Glacier ponds and moraine.

Radiocarbon age[1] (^{14}C yr BP)	Calibrated age[2] (cal yr BP)	Sample number	Laboratory[3] number	Depth[4] (cm)	Dated material
Upper pond					
109.9 (pMC)[5]	-	LG-48-3	B-180887	42	Wood
210±70	476-5	LG-34-1	TO-10743	44-45	Rootlets
300±50	521-5	CIA-01-23-4	TO-9756	26	Wood
1000±130	1349-536	LG-34-2	TO-10744	50-51	Rootlets
2760±40	3075-2749	LG-48-2	B-180886	42	Wood
5330±110	6534-5613	LG-26-2	TO-10741	102-105	Charcoal, conifer needle
5910±40	6907-6501	LG-50-1	B-180888	27-29	Charcoal
6200±110	7555-6570	LG-33-1	TO-10742	22	Charcoal
Lower pond					
5870±80	7156-6312	LG-38-1	TO-10745	43	Charcoal
870±100	1173-527	LG-38-5	TO-10746	42-43	Seeds, conifer needle
Moraine gully					
890±40	932-673	LG-24-2	B-180885	-	Wood
1093±45	1257-792	AVR-02-41-3	WK-12308	-	Wood
2086±49	2328-1835	LG-24-1	Wk-12313	-	Charcoal

[1] Age error terms are 1-sigma.

[2] Reference datum is AD 1950. Calibrated from data of Stuiver and Reimer (1993) and Stuiver et al. (1998). The values are the 2-sigma age ranges determined using an error multiplier of 2.0.

[3] Laboratores: Wk, University of Waikato; TO, IsoTrace (University of Toronto); B, Beta Analytical Inc.

[4] Depth below floor of pond.

[5] pMC = percent modern carbon (sample is modern).

Interpretation

The oldest glacier advance recorded at the two ponds deposited the cobble-rich diamicton of unit A. This till unit is similar at both ponds and has an oxidized upper surface. Unit A was found at all but two pits, where the lowermost sediments were below the water table, but it was not found in the cores taken from the upper pond. The PVC coring tube repeatedly broke during attempts to penetrate beyond unit B peat. It likely broke on unit A till. Alternatively, the pond may be underlain by colluvium eroded from the flank of the outer moraine.

The presence of unit B muddy peat at both ponds implies that the outer moraine predates the peat. Unit A is correlated with the till that forms the outer moraine at both ponds. This correlation was confirmed in the trench at the upper pond (sections 50A-C), where the till can be traced without break from the pond to the core of the moraine. The outer moraine was probably constructed during a single advance and, consequently is unlikely to be a composite feature. Any subsequent advance to the distal margin or crest of the outer moraine probably would have left diamicton or gravel in the adjacent ponds, and such sediments are not present above unit A.

Radiocarbon ages on charcoal at the base of unit B provide a minimum age for unit A till and the outer moraine. They indicate that the outer moraine was built before 6200 ^{14}C yr BP or before approximately 7000 cal yr BP (Table 1). As all the radiocarbon ages are from charcoal overlying the till, the moraine may be significantly older than 6500 cal yr BP. The upper 10 cm of the till in most pits is oxidized. This may reflect either exposure and soil development prior to the deposition of unit B peat and its charcoal horizon, or leaching of the overlying peat. In pit 41 at the lower pond, the dated charcoal came from the uppermost few centimetres of unit A. It may, however, have been incorporated into diamicton that was transported off the moraine after the moraine was formed. In view of this possibility, no relationship can be inferred between the time of deposition of this charcoal and the till.

The contact between the till and muddy peat of unit B is gradational. The high mineral content of the lower part of unit B likely records washing of sediment off the outer moraine. Unit B is not present in pits 45 and 46 at the lower pond, suggesting that water levels in the pond were likely lower than at present.

Unit C records rapid deposition of sand and silt, likely during a second advance of Lillooet Glacier. As the unit is massive, contains few clasts, and is present throughout both ponds, it is unlikely to be slopewash derived from the valley side walls. This inference is affirmed by the presence of a very different colluvial deposit with abundant angular stones in pit 32. Unit C is present locally in the upper pond as a couplet, possibly indicating two closely spaced advances. At the lower pond, unit C is much thicker than the second clastic unit (E) above it, suggesting that more sediment-laden meltwater entered the pond during the earlier advance.

Two radiocarbon ages on rootlets at the upper pond suggest that unit C was deposited between 1000 ± 30 and 210 ± 70 ^{14}C yr BP (Fig. 4; Table 1). However, an age of 2760 ± 40 ^{14}C yr BP on wood lying directly on top of unit C is a minimum for the time of deposition of the unit. As the Bridge River tephra is consistently above unit C, the dated rootlets likely penetrated from higher in the sequence. The age of 2760 ± 40 ^{14}C yr BP thus is a minimum age for the second advance. An age of 870 ± 100 ^{14}C yr BP was obtained on seeds and a conifer needle below unit C and just above charcoal in unit B dated at 5870 ± 80 ^{14}C yr BP. The younger age must also be in error, as the dated sample is clearly below the tephra horizon, and it is unlikely that 5000 years of accumulation is represented by the 1 cm of peat between the two dated levels.

Peat of unit D is more fibrous than that of unit B in many pits at the upper pond. Similarly, a distinct upper zone of orange fibrous peat is widespread in the lower pond. These more fibrous peats may indicate that cooler conditions prevailed during the time between deposition of the two clastic units, impeding peat decomposition.

At the upper pond, the upper silt-sand horizon (unit E) is considerably coarser than underlying unit C. The pond cores contain only one clastic unit, which is correlated with unit E, as that unit thickens towards the center of the pond. At the lower pond, unit E is thinner than unit C, probably because meltwater flow was focused along the stream between the Little Ice Age and outer moraines at the time unit E was deposited. Wood fragments at the base of unit E at the upper pond yielded an age of 300 ± 50 ^{14}C yr BP. This is a maximum age for the onset of a final period of advance at Lillooet Glacier, during the Little Ice Age.

Moraine Gully

Erosion of the Little Ice Age moraine has created numerous gullies that expose intercalated tills and organic horizons. The stratigraphy of several of these gullies and the ages of the till units and bounding paleosols are described in detail by Reyes (2003). One of the gullies, however, is described here (Figs. 7 and 8) as it connects the history of Lillooet Glacier inferred from the pond sediments to that shown by the stratigraphy of the composite moraine.

The 'moraine gully' is located directly west of the bedrock outcrop south of the upper pond (Fig. 1). Water flowing from the pond has eroded a horseshoe-shaped amphitheatre into the moraine, providing a near three-dimensional view of its sediments (Fig. 8c). The gully also truncates the smaller middle moraine in the center of the gully.

Sediments

Six sections were logged along the width of the gully (Fig. 7). Details of radiocarbon ages constraining times of sediment deposition are given in Table 1.

The lowest described unit (A) is of unknown thickness, and consists of matrix-supported grey diamicton with a silt to medium sand matrix and lenses of well-rounded gravel and massive sand. Unit B conformably overlies unit A and consists of a red-brown (10YR 3/2) peat horizon. Its maximum exposed thickness is 15 cm. The unit has a greasy texture and contains small rootlets, wood fragments, and small pebbles. Pebbles are sparse, except at section 4 where they constitute up to 15% of the unit. The upper contact of unit B is demarcated by a millimetre-thick orange horizon. Unit B is overlain by a second sequence of sand, gravel, and till (unit C). At section 3, unit C is up to 80 cm thick and comprises pebble-rich sand beds, cyclical beds of pebble gravel and fining-upward sand, and till. At section 4, unit C is approximately 115 cm thick and comprises diamicton forming the middle moraine (Fig. 7c). This diamicton is very compact and has a silt to medium sand matrix and subangular stones. Unit C is overlain by a second paleosol (unit D). This paleosol is much thinner and far less developed than unit B and does not contain preserved plant macrofossils. At sections 1 and 6, unit D is a 2 to 3-cm thick oxidized horizon. At section 3, it is a millimetre-thick orange-red stain at the top of

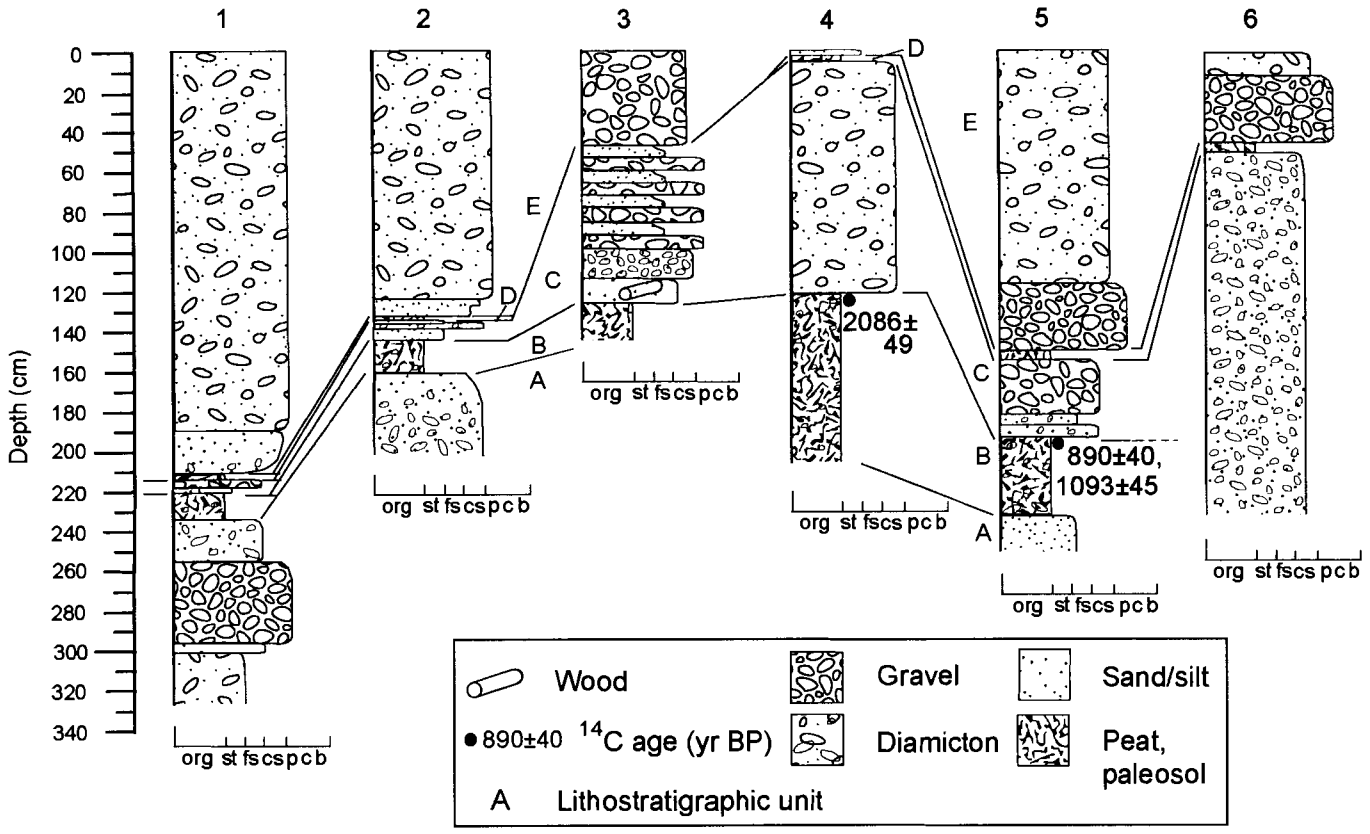

Figure 7. Stratigraphy of sections in the moraine gully. org = organic; st = silt; fs = fine sand; cs = coarse sand; p,c, and b = pebble, cobble, and boulder, respectively. See text for stratigraphic description and interpretation.

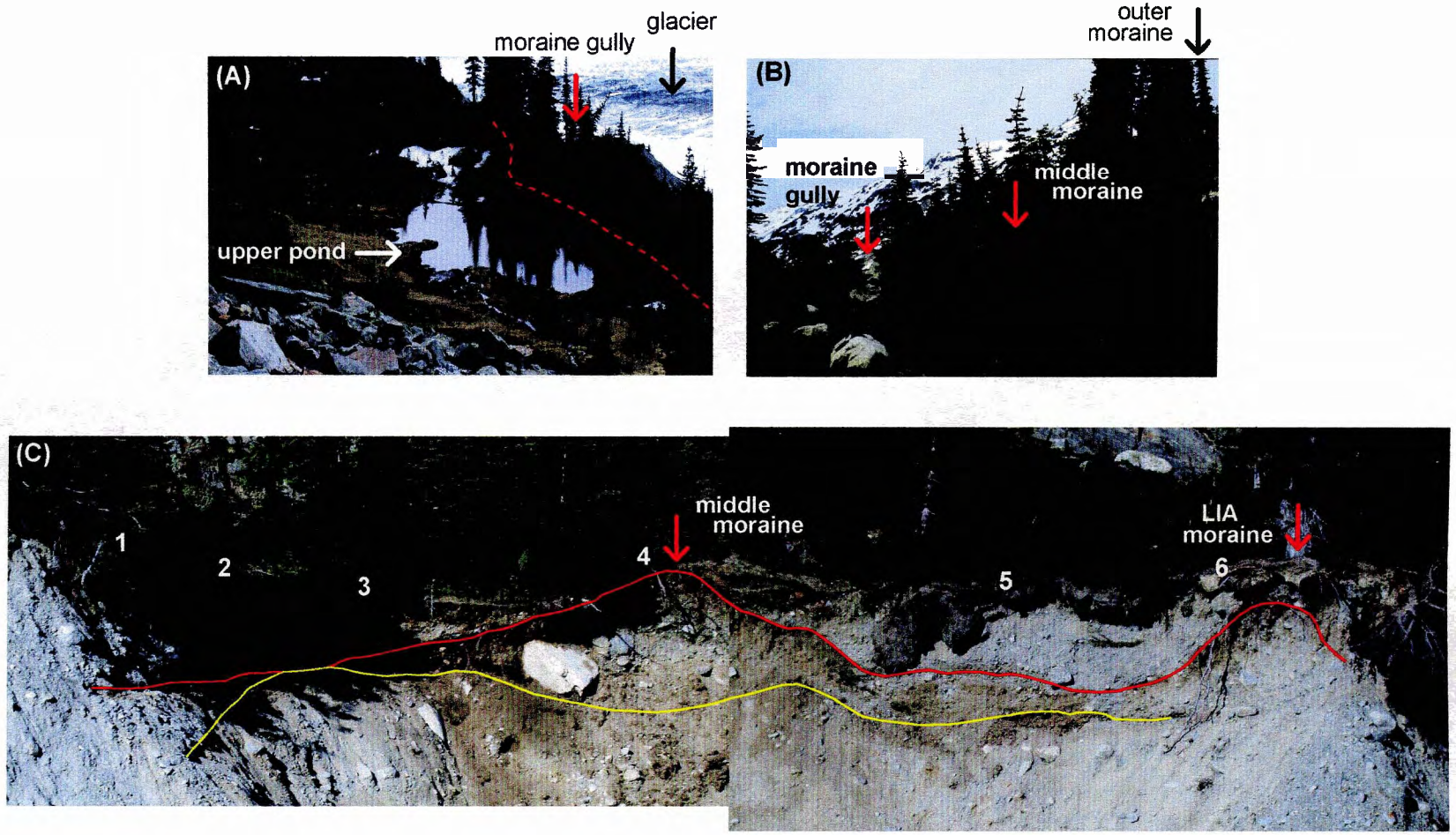

Figure 8. A. Relationship of the upper pond to the moraine gully; view to the southwest. The crest of the outer moraine is delineated by a red dashed line. B. View up-glacier of the middle moraine intersecting the moraine gully. Camera case on boulder is 10 cm high. C. Composite photograph of the moraine gully. The lower paleosol (unit B) is delineated in yellow, and the upper paleosol (unit D) in red. Numbers 1 to 6 show the locations of sections described in Fig. 7. The large white boulder is approximately 1.5 m wide. See text for details of stratigraphy. Photographs of moraine gully courtesy of J. Clague.

unit C. At section 4, unit D is a centimetre-thick paleosol developed on till of the middle moraine. The capping sediment at all sections (unit E) is clast-rich diamicton and gravel, which form the crest of the Little Ice Age moraine.

Interpretation

The lowest diamicton in the gully (unit A) is till deposited during an advance of Lillooet Glacier. This advance constructed a lateral moraine that provided a low area for sediment accumulation on its distal side. Fluvial sand and gravel overlying the diamiction were deposited during or after glacier retreat. The humified nature of unit B indicates that it likely accumulated as peat in the low area, which at that time would have been a small wetland. On each side of the gully, unit B thins into an oxidized paleosol that developed on the moraine flank concurrently with peat deposition.

A second glacier advance is recorded by unit C till, which forms the middle moraine. Radiocarbon ages obtained from the upper part of unit B provide maximum limiting ages for this advance. An age of 2086 ± 49 ^{14}C yr BP was obtained on charcoal in unit B at section 4, below the middle moraine, and ages of 1093 ± 45 and 890 ± 40 ^{14}C yr BP were obtained on wood at the contact between units B and C at section 5. Of these ages, the two younger ones likely provide better constraints on the time of the advance. The charcoal that yielded the oldest age was collected not at the top of unit B, but several centimetres below it. Furthermore, the peat below the middle moraine may have been disturbed when it was overrun during the advance that built the middle moraine, moving the charcoal out of its original stratigraphic position.

The unit B paleosol can be traced discontinuously along the length of the moraine. A peat unit morphologically similar to unit B crops out in a gully midway between the upper and lower ponds. Wood from the upper surface of this peat yielded a maximum age for renewed glacier activity of 1090 ± 50 ^{14}C yr BP (Reyes, 2003). Wood from what is thought to be a correlative paleosol near the lower pond, however, gave older ages of 1530 ± 40 and 1390 ± 50 ^{14}C yr BP (Reyes, 2003). This wood is older than the peat in the two gullies and thus predates the advance recorded by unit C. The differences among the ages may reflect fluctuations of the glacier margin between 1500 and 900 ^{14}C

yr BP. Regardless, the younger ages from the peat indicate that a glacier advance must have commenced before 900 ^{14}C yr BP.

At the moraine gully, unit D forms a paleosol on top of the middle moraine. Just down-glacier in the moraine gully, the paleosol rises to form a traceable second moraine crest below the Little Ice Age moraine crest (Fig. 8c). The second crest likely delineates a moraine deposited adjacent to the middle moraine prior to the development of the unit D paleosol, and reflects a fluctuating glacier margin between 1500 and 900 ^{14}C yr BP.

Unit D is overlain by deposits that record a readvance of Lillooet Glacier. Sand and gravel in the lower part of unit E were deposited by meltwater flowing along the linear depression between the middle moraine and glacier margin. The sand and gravel are overlain by till that forms the crest of the main valley composite moraine and records the maximum Little Ice Age advance of Lillooet Glacier. No dateable material was found in unit D at the moraine gully to constrain the age of this advance. However, radiocarbon ages from correlative sediments elsewhere along the moraine show that this advance is less than 500 years old (Reyes, 2003).

Holocene Glacier Fluctuations

The sedimentary records of the upper and lower ponds and the moraine gully provide evidence for at least four advances of Lillooet Glacier during the late Quaternary. At both ponds, basal till units correlated with the outer moraine record an advance prior to 6200 ^{14}C yr BP. Overlying silt beds bounded by peat indicate a second advance ca. 2800 ^{14}C yr BP. At the moraine gully, glacial sediments lying on a peat and paleosol record one or more later advances ca. 1500-900 ^{14}C yr BP. Silt and sand beds in both ponds and glacial sediments above a second paleosol in the moraine gully record the Little Ice Age maximum advance.

The only early or middle Holocene glacier advance currently recognized in the southern Coast Mountains is the Garibaldi Phase, dated to between 6000 and 5000 ^{14}C yr BP based on overriden trees stumps in Garibaldi Park (Ryder and Thomson, 1986). Dendroglaciological evidence exists for a Garibaldi-age advance of Tchaikazan Glacier,

30 km north of the Lillooet Glacier (Smith, 2003), and an advance of Fyles Glacier between 5980 and 4860 ^{14}C yr BP (Laxton et al., 2003).

The minimum limiting ages for the earliest recorded advance of Lillooet Glacier, from the charcoal overlying the basal till, are 5900-6200 ^{14}C yr BP. The till and moraine may reflect a late-glacial readvance after the disappearance of the Cordilleran Ice Sheet. . The oxidized nature of the till may indicate exposure of the moraine prior to peat accumulation in the ponds, with warmer and drier conditions during the early Holocene preventing peat accumulation until after 6200 ^{14}C yr BP. It is unlikely that the outer moraine dates to the Garibaldi Phase. For this to be the case, peat accumulation would have had to have commenced immediately after recession of the glacier from the outer moraine. In view of the evidence cited above, this scenario can be ruled out. The feature thus is either a late-glacial feature, or it records an early Holocene advance before the Garibaldi Phase.

The second advance of Lillooet Glacier, about 2800 ^{14}C yr BP, correlates with the Tiedemann Advance, a period of renewed glacier activity between 3300 and 1900 ^{14}C yr BP, recognized at Tiedemann and Gilbert glaciers (Ryder and Thomson, 1986), Jacobsen Glacier (Desloges and Ryder, 1990), and Berendon Glacier (see section *Berendon Glacier*). At its type locality (Tiedemann Glacier), the Tiedemann Advance was more extensive than all subsequent Neoglacial advances. The absence of Tiedemann-age moraines at Lillooet Glacier indicates that this advance was less extensive than the climactic Little Ice Age advance.

Renewed glacier activity occurred at Lillooet Glacier between 1500 and 900 ^{14}C yr BP. Berendon Glacier also advanced at this time (see section *Berendon Glacier*), and evidence exists for glacier expansion in the southern Coast Mountains prior to ca. 900 ^{14}C yr BP (Ryder and Thomson, 1986). As the segments of the middle moraine lie just outside the Little Ice Age moraine, Lillooet Glacier must have been as extensive at this time as at the Little Ice Age maximum.

Summary

The combined sedimentary records from two moraine-dammed ponds and one gully dissecting a composite lateral moraine provide evidence for at least four phases of advance of Lillooet Glacier:

1. Prior to 6200 ^{14}C yr BP, probably during late-glacial time.
2. About 2800 ^{14}C yr BP, correlative with the Tiedemann Phase.
3. Between 1500 and 900 ^{14}C yr BP.
4. During the Little Ice Age.

Diadem Glacier

Diadem Glacier lies adjacent to Mt. Queen Bess (3289 m asl), approximately 100 km north of Lillooet Glacier (Fig. 9). It flows approximately 4.5 km eastward out of a small icefield that is contiguous with the larger Homathko Icefield to the south. The glacier toe is adjacent to Queen Bess Lake (Fig. 10a), which drains into the west fork of Nostetuko River at approximately 1500 m asl. Vegetation in the area is characteristic of the Englemann Spruce-Subalpine Fir biogeoclimatic zone.

Queen Bess Lake lies within a basin created by the Neoglacial lateral and end moraines of Diadem Glacier (Fig. 9). The moraines surrounding the lake record at least two Neoglacial advances. A rounded glacially overridden moraine lies inside a prominent Little Ice Age terminal moraine. The inner moraine coalesces with the Little Ice Age terminal moraine on the north and south sides of the lake, forming a composite lateral moraine (Fig. 9). A till and an associated linear concentration of large boulders define a segment of a third highly weathered lateral moraine outboard of the Little Ice Age moraine crest on the north side of the lake (Figs. 9 and 10b)

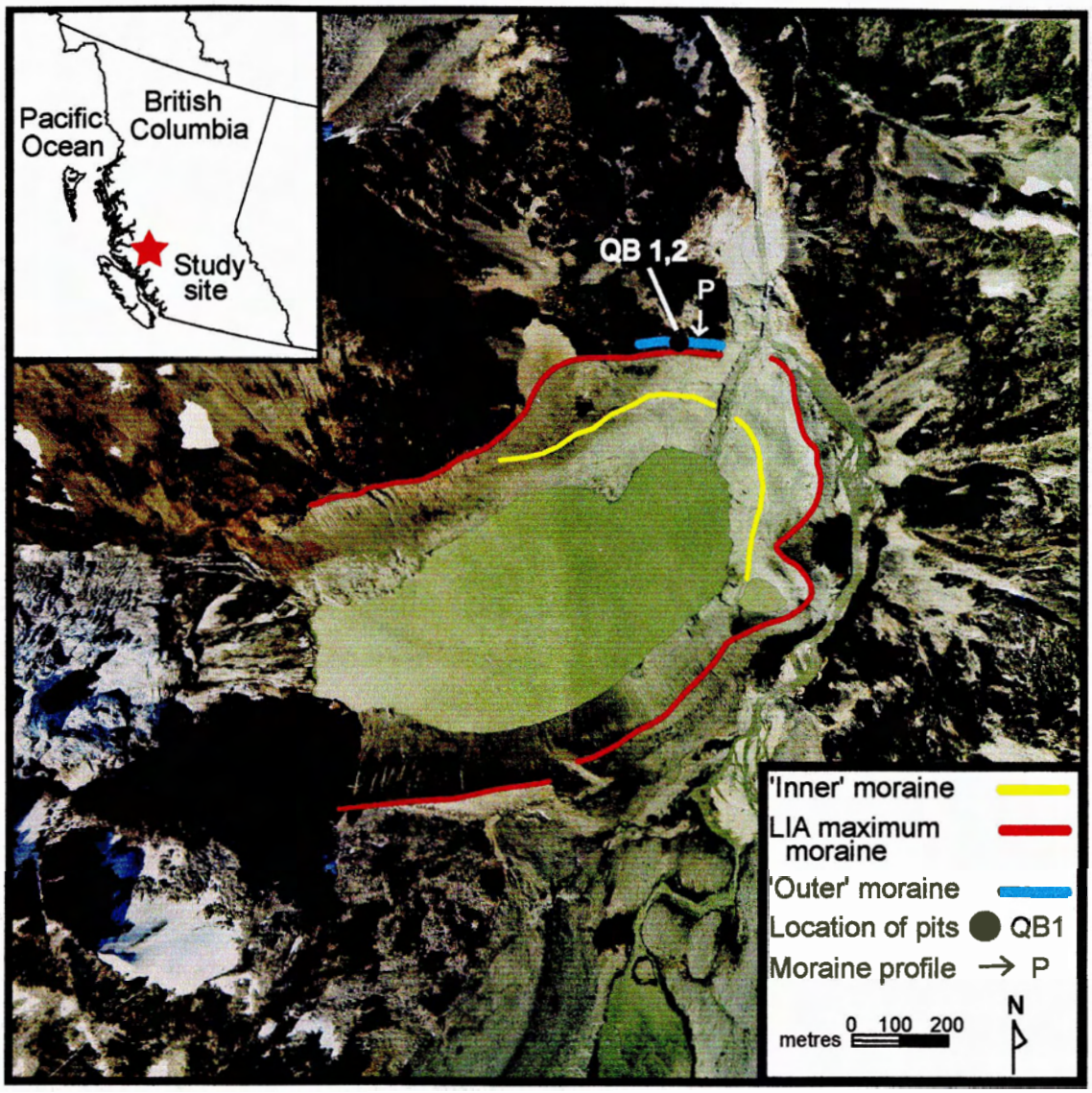

Figure 9. Aerial photograph of Queen Bess Lake and Diadem Glacier, taken in July 1998, about one year after the lake partially drained. See the text for descriptions of the outer, inner, and Little Ice Age (LIA) moraines, and the moraine profile. The stratigraphy of pits QB1 and QB2 is shown in Figure 10. Part of Selkirk Remote Sensing Ltd. photograph SRS5944-11 (July 1998); reproduced courtesy of S.G. Evans, Geological Survey of Canada.

Prior Work

On August 12, 1997, the snout of Diadem Glacier collapsed into Queen Bess Lake, generating displacement waves that overtopped and incised the end moraine, lowering the lake by 8 m (Kershaw, 2002). A gully was eroded through the moraine by the outflow. It provides excellent exposures of sediments forming the moraine (Kershaw, 2002).

Interbedded till, fluvial deposits, and paleosols exposed in the breached moraine record at least two Holocene advances of Diadem Glacier. The advance that constructed the inner moraine probably occurred before 1260 ± 50 ^{14}C yr BP (ca. 1340 cal yr BP). Kershaw (2002) argues that this advance likely is a Tiedemann-phase event. During the climactic Little Ice Age advance, Diadem Glacier overrode the inner moraine and constructed the prominent moraine that surrounds the lake. A radiocarbon age of 370 ± 50 ^{14}C yr BP from a root in growth position below outwash deposited during this advance indicates that the moraine was constructed within the last 500 years. Kershaw (2002) suggests that the outer moraine on the north side of Queen Bess Lake pre-dates the Little Ice Age and possibly records a late Pleistocene advance.

I attempted to further constrain the age of the outer moraine on the north side of the lake and determine if it correlates with the outermost moraines at Lillooet and Berendon glaciers (see sections *Lillooet Glacier* and *Berendon Glacier*). Several pits were dug on the outer moraine to document soil development and thus indirectly constrain the age of the moraine. Moraine boulders were also sampled for cosmogenic ^{36}Cl dating (see Chapter 3, *Cosmogenic ^{36}Cl Dating*).

Moraine Pits

Stratigraphy

The stratigraphy of two pits dug on the outer moraine is shown in Figures 10c and 11. The basal sediment in both pits is a compact, fissile, grey, matrix-supported diamicton with a sand-silt matrix (unit A). Clasts within unit A are predominantly pebble-sized and subangular. Unit A is sharply overlain by 20 to 30 cm of well-sorted fine to medium sand with interbeds of pebble gravel (unit B). The sand shows mottled oxidation and, in part,

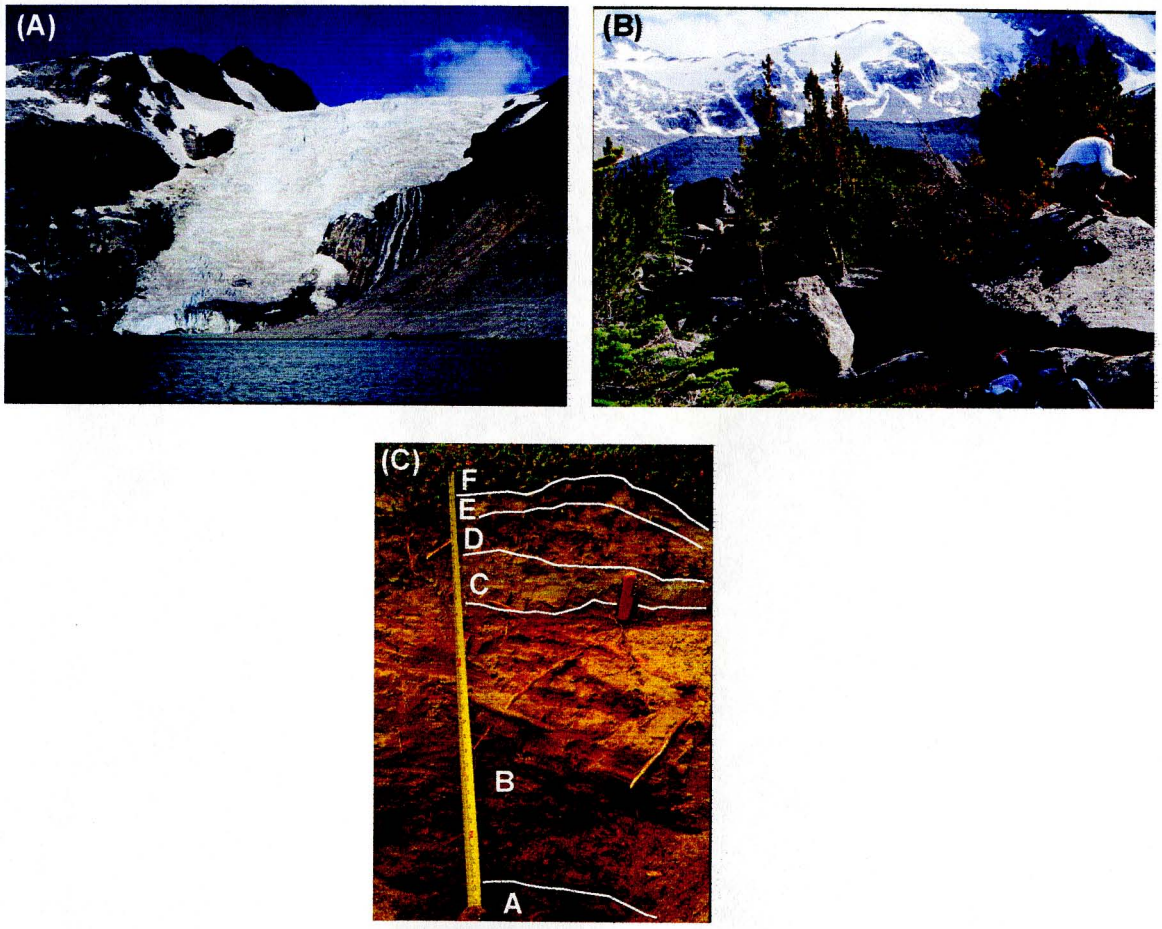

Figure 10. A. Steep terminus of Diadem Glacier, 2002. B. Sampling a boulder on the outer moraine for cosmogenic dating. The Little Ice Age moraine on the opposite side of the lake is visible in the background. View is to the southwest. C. Sediments on the outer moraine in pit QB-2. The red knife handle is approximately 8 cm in length. See Figure 9 for the location of the pit, and the text and Figure 11 for a description of units.

is cemented into small clasts. The gravel beds consist of oxidized, subangular to subrounded granitic pebbles in a medium to coarse sand matrix. Unit B sharply overlain by a light grey, well-sorted, silty fine sand (unit C), which ranges in thickness from 3 to 10 cm and has a convolute lower contact. The silty fine sand is capped by a medium brown (10YR 4/2) paleosol (unit D). The paleosol is 4 to 7 cm thick, and has a loose texture with numerous rootlets. Unit D is gradationally overlain by unweathered, well-sorted fine to medium sand (unit E).Unit E is 7 to 10 cm thick and is capped by a modern, rooty soil (unit F).

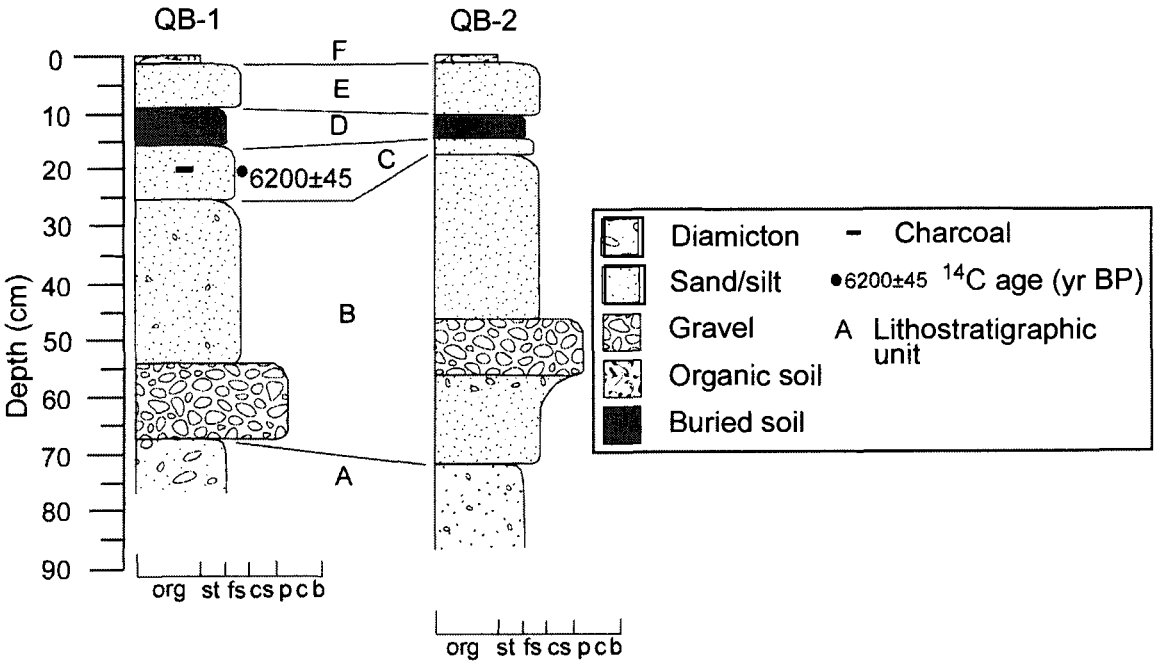

Figure 11. Stratigraphy of pits dug into the outer moraine at Diadem Glacier (see Fig. 9 for location). org = organic; st = silt; fs = fine sand; cs = coarse sand; p,c,b = pebble, cobble, and boulder, respectively. See text for stratigraphic details and interpretation.

Interpretation

Sediments in the two pits record deposition during and after construction of the outer moraine. Unit A diamicton is till deposited during the final stage of moraine construction. It lies about 65 cm below the surface of the moraine. Considering the height of boulders

on the moraine surface (Fig. 10; Appendix B), a significant amount of erosion has occurred since moraine formation.

Sand and gravel of unit B were likely deposited by meltwater as Diadem Glacier retreated from the outer moraine. The highly oxidized character of the unit likely indicates significant exposure and soil formation following glacier retreat.

Two possible origins are suggested for unit C. It may be an Ae horizon that developed on the sand of unit B through leaching of organic matter and iron. The fine texture, sorting, lack of clasts, and sharp lower contact with unit B, however, indicate that unit C is likely an aeolian deposit.

A radiocarbon age of 6200 ± 45 ^{14}C yr BP (OS-38190) was obtained on charcoal recovered from unit C in pit QB-1 (Fig. 11), indicating that the outer moraine was constructed prior to 7000 cal yr BP. The presence of charcoal within unit C may further indicate that climate during deposition of the unit was warmer than at present. This interpretation agrees with other records of early Holocene climate in the Coast Mountains of British Columbia (e.g., Clague and Mathewes, 1989).

Unit D is interpreted to be a soil that developed on the moraine some time after 7000 cal yr BP. It was subsequently buried by unit E sand. As the outer moraine is above the inner and Little Ice Age moraines, unit E could not have been deposited by meltwater during those advances. The sediment of unit E, however, may be aeolian, blown from the Diadem Glacier forefield during one of these advances. The coarseness of unit E relative to aeolian unit C suggests a proximal source. Given the distal position of the inner moraine (Fig. 9), unit E was probably deposited during construction of the nearby Little Ice Age moraine. The lack of weathering of the unit further suggests that it is young, which favours deposition during the Little Ice Age rather than during the Tiedemann Phase. The capping soil (unit F) records moraine stability since the Little Ice Age.

Summary

1. The outermost weathered moraine of Diadem Glacier was constructed prior to 7000 cal yr BP and probably during late-glacial time.

2. A charcoal-bearing aeolian sand on the outer moraine may indicate warmer conditions during the early Holocene than today.

3. Unweathered sediments directly below the surface soil on the outer moraine may record landscape instability during the Little Ice Age.

Berendon Glacier

Berendon, Frank Mackie, and Salmon glaciers flow eastward from icefields in the Boundary Ranges of the northern Coast Mountains at the British Columbia-Alaska boundary (Fig. 12). The highest mountain peaks approach 2600 m asl and local relief exceeds 1600 m. The three glaciers are linked hydrologically by two lakes. Summit Lake lies between Berendon and Salmon glaciers and, since 1961, has discharged to the south into Salmon River, on occasion by jökulhlaups (Mathews, 1973; Mathews and Clague, 1993). Prior to 1961, Summit Lake drained northward into Bowser River via a channel at 826 m asl (Fig. 13). Tide Lake, to the north, was dammed by Frank Mackie Glacier (Clague and Mathews, 1992), but it drained in the early 20th century.

The ecology of the area is governed by cold, snowy winters and a short, cool growing season. The area lies within the wet, cold subzone of the Englemann Spruce-Subalpine Fir biogeoclimatic zone (Meidinger and Pojar, 1991). The climate encourages a unique vegetation assemblage, with high-elevation parkland supporting a mix of coniferous trees, subalpine meadow, and heath. Subalpine fir (*Abies lasiocarpa*) and mountain hemlock (*Tsuga mertensiana*) are the dominant conifers (Mackinnon et al., 1992).

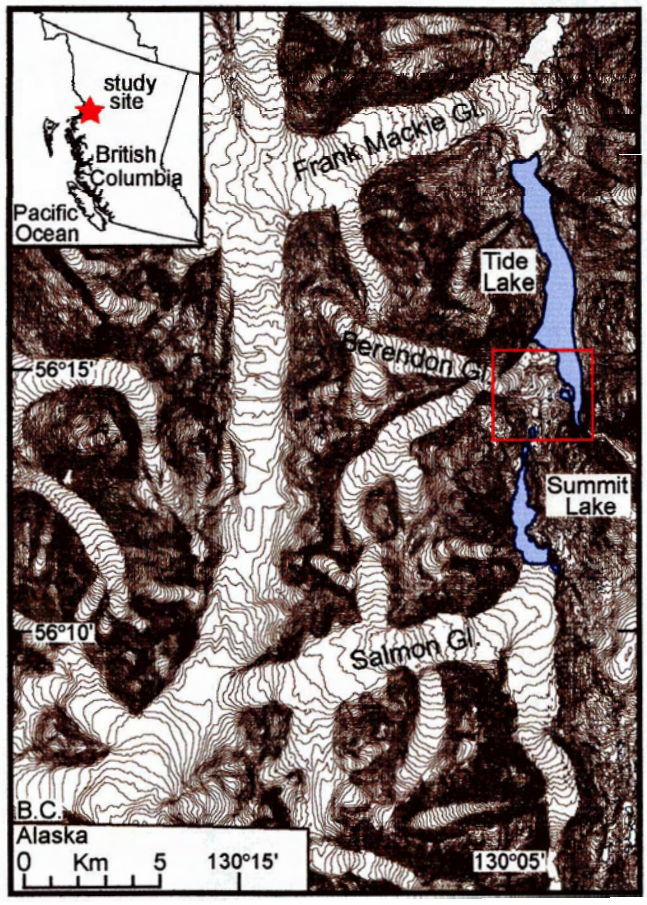

Figure 12. Map showing locations of Salmon, Berendon, and Frank Mackie glaciers, and Summit and Tide lakes. Tide Lake is shown at its maximum Little Ice Age extent. Inset red rectangle delineates the area shown in Figures 13 and 14. Reproduction of part of TRIM map 104B, courtesy of the Government of British Columbia, Base Mapping and Geomatic Services Branch

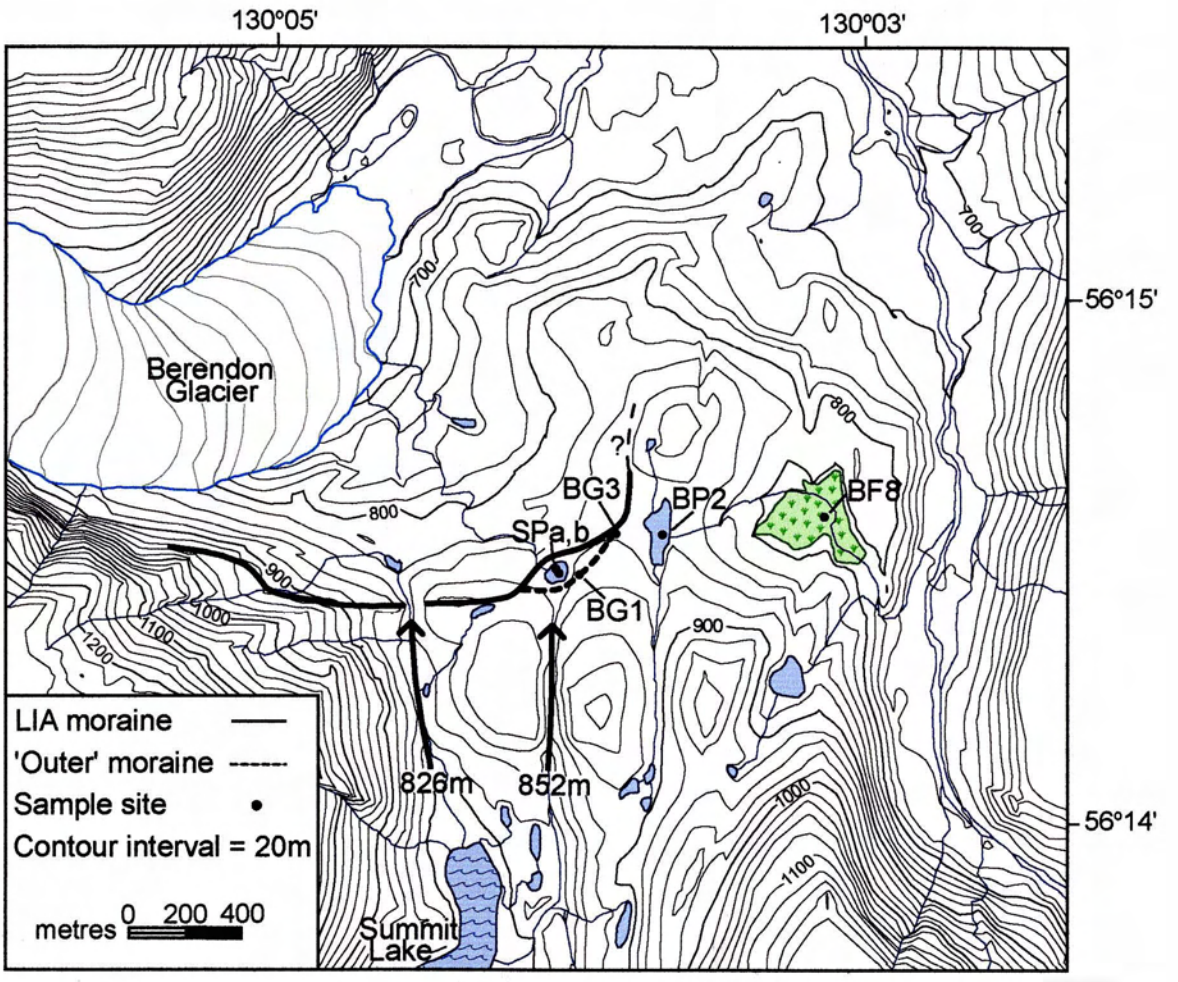

Figure 13. Map showing Summit Lake, Spillway Pond (SP), Berendon Pond (BP), Berendon Fen (BF), and the moraines discussed in the text. Arrows indicate paths taken by Summit Lake overflow. During the maximum Little Ice Age (LIA) advance of Berendon Glacier, meltwater was routed along the 852 m channel. BG1 and BG3 are cosmogenic age samples taken from the 'outer' moraine. Reproduction of part of TRIM map 104B030, courtesy of the Government of British Columbia, Base Mapping and Geomatic Services Branch.

Berendon Pond

Berendon Pond (ca. 835 m asl) is situated northeast of Spillway Pond and southwest of Berendon Fen (Figs. 13 and 14). It is approximately 6 ha in area and has a maximum depth of 4.3 m. The pond is fed mainly by catchment overland flow produced by snowmelt and rain.

A prominent moraine borders the pond on its west and north sides. The moraine delineates the maximum Little Ice Age advance of Berendon Glacier, approximately 1 km from the present terminus of the glacier (Figs.13 and 14) (Clague and Mathewes, 1996). When the moraine was constructed, Berendon Glacier blocked the 826-m-asl channel of Summit Lake, and the lake overflowed along a higher 852-m-asl channel to Spillway Pond (Fig. 13) (Clague and Mathewes, 1996).

A trimline along both sides of the Tide Lake basin delineates the maximum level of the lake during the Little Ice Age. It can be traced to the prominent Berendon terminal moraine to the south. Several other smaller moraines occur inside the terminal moraine and formed during advances and stillstands of Berendon Glacier after the Little Ice Age maximum.

A low, subdued morainal ridge and line of erratic boulders lie outside the Little Ice Age terminal moraine on the south side of Spillway Pond (Figs. 13 and 14). The moraine and boulders have been interpreted as possibly middle Neoglacial in age, based on their morphology and position in relation to Spillway Pond (Clague and Mathewes, 1996). As Berendon Glacier advanced over what is now Spillway Pond, water from Summit Lake would have flowed along the margin of the glacier into Berendon Pond.

Vegetation surrounding Berendon Pond is parkland dominated by mountain hemlock, subalpine fir, Sitka alder (*Alnus viridis*), willow (*Salix spp.*), mountain ash (*Sorbus*), and huckleberry (*Vaccinium*) (Clague and Mathewes, 1996). Herbaceous species include arctic lupine (*Lupinus arcticus*), Sitka valerian (*Valeriana sitchensis*), Indian hellebore (*Veratrum viride*), and arrow-leaved groundsel (*Senecio triangularis*). On well-drained and rockier substrates, common pioneering species include alder, willow, grasses (Poaceae), sedges (Cyperaceae), and willow-herb (*Epilobium latifolium*).

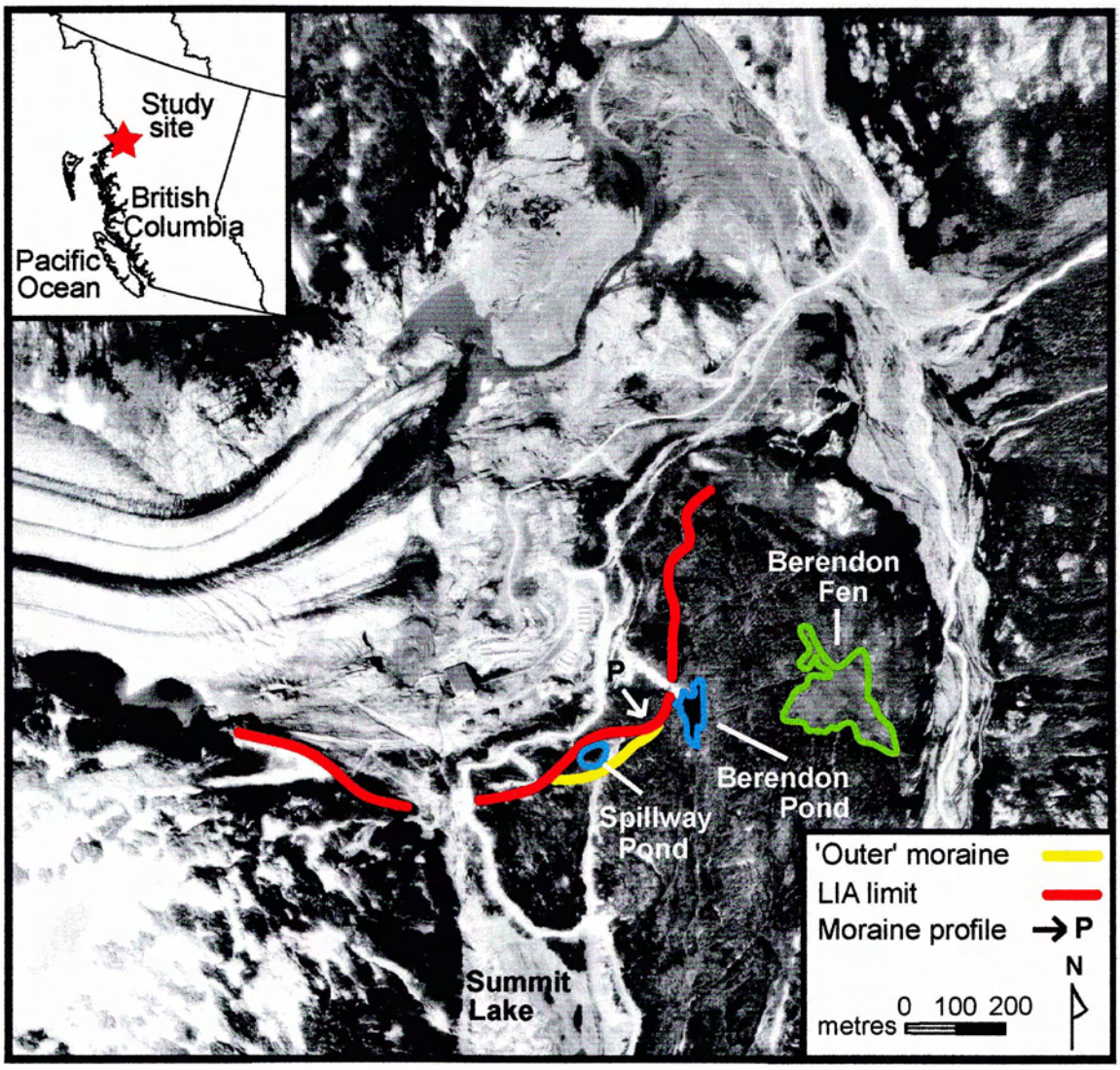

Figure 14. Aerial photograph of Berendon Glacier study area, showing locations of moraines discussed in the text and their positions relative to Spillway and Berendon ponds, Berendon Fen, and Summit Lake. 'LIA limit' refers to the limit of the maximum Little Ice Age advance of the glacier. Part of British Columbia Government air photograph BC5505.170 (August 1972); reproduced courtesy of the Ministry of Sustainable Resource Management, Base Mapping and Geomatic Services Branch.

Stratigraphy of Core BP2

Six Russian cores and three percussion cores were taken from Berendon Pond in September 2000. Of these, percussion core BP2 provided the longest record of sedimentation and hence was selected for analysis. The core was collected near the centre of the lake (Fig. 13), in water approximately 4.25 m deep.

The lowermost sediments of core BP2, from 200 to 180 cm depth (unit A, Fig. 15), are peaty mud with some plant macrofossils. Overlying this is a unit of grey-brown organic-rich mud (unit B, 180-147 cm), which includes thin beds of silt at 172-171 cm, clayey gyttja at 171-169 cm, laminated clayey silt at 158-157 cm, and two 1 cm-thick mud layers between 152 and 147 cm. An abrupt erosional contact separates unit B from overlying stratified olive-grey clayey silt of unit C (147-33 cm). Some of the strata in unit C are contorted. Clasts of organic-rich mud occur within the lower part of the unit. The uppermost sediments of the core (unit E, 33-0 cm) consist of fine to medium sand with laminated mud lenses. A clay gyttja unit up to 25 cm thick overlies unit E in other cores from Berendon Pond (Clague et al., submitted).

Chronology

Chronological control for core BP2 is provided by six accelerator mass spectrometry (AMS) ^{14}C ages (Figs. 15, 16, and 17; Table 2). Five samples of wood recovered from units A and B yielded radiocarbon ages of 3510 ± 60, 2710 ± 60, 2700 ± 60, 1780 ± 50, and 1910 ± 50 ^{14}C yr BP. An AMS age of 615 ± 85 ^{14}C yr BP on needle and leaf fragments was obtained from unit C.

Palynology

Methods

The lower, organic-rich part of core BP2 (units A and B) was analyzed for pollen and spores. The core was subsampled at intervals of 1 to 3 cm, with 1 mL volumes extracted for processing. Each sample was spiked with a known quantity of marker grains (*Lycopodium clavatum*, batch no. 201890, 11,300 ± 400 grains per tablet) to calculate

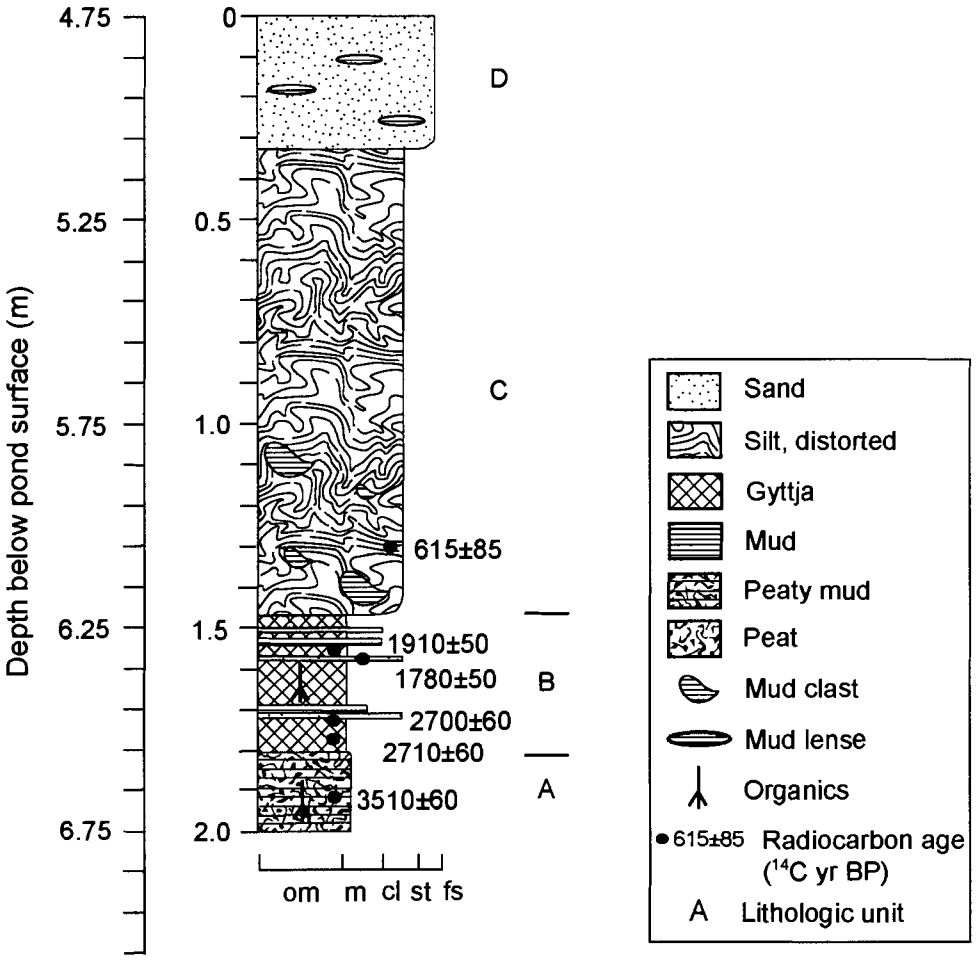

Figure 15. Stratigraphy of core BP2 taken from Berendon Pond (see Fig. 13 for location). See text for description and interpretation of stratigraphy. om = organic mud (gyttja); m = mud; cl = clay; st = silt; fs = fine sand.

Table 2. Radiocarbon ages from Berendon Pond.

Radiocarbon age[1] (^{14}C yr BP)	Calibrated age[2] (cal yr BP)	Sample number	Laboratory[3] number	Location Lat. (N) , Long. (W)	Depth[4] (m)	Dated material
615±85	915-306	BP121-140	LuA-5113	56°14.5' , 130°03.7'	1.21-1.40	Needle, leaf fragments
1780±50	1925-1423	BP20	TO-8978	56°14.5' , 130°03.7'	1.57-1.58	Wood
1910±50	2113-1574	BP22	TO-9662	56°14.5' , 130°03.0'	1.54-1.55	Wood fragment
2700±60	3156-2473	BP12	TO-8877	56°14.5' , 130°03.7'	1.72-1.74	Wood
2710±60	3158-2491	BP9	TO-8976	56°14.5' , 130°03.7'	1.76-1.79	Wood (twig)
3510±60	4143-3472	BP1	TO-8975	56°14.5' , 130°03.7'	1.92-1.94	Wood (twig)

[1] Age error terms are 1-sigma.

[2] Reference datum is AD 1950. Calibrated from data of Stuiver and Reimer (1993) and Stuiver et al. (1998). The values are the 2-sigma age ranges determined using an error multiplier of 2.0.

[3] Laboratories: LuA: University of Lund; TO, IsoTrace (University of Toronto).

[4] Depth below lake floor.

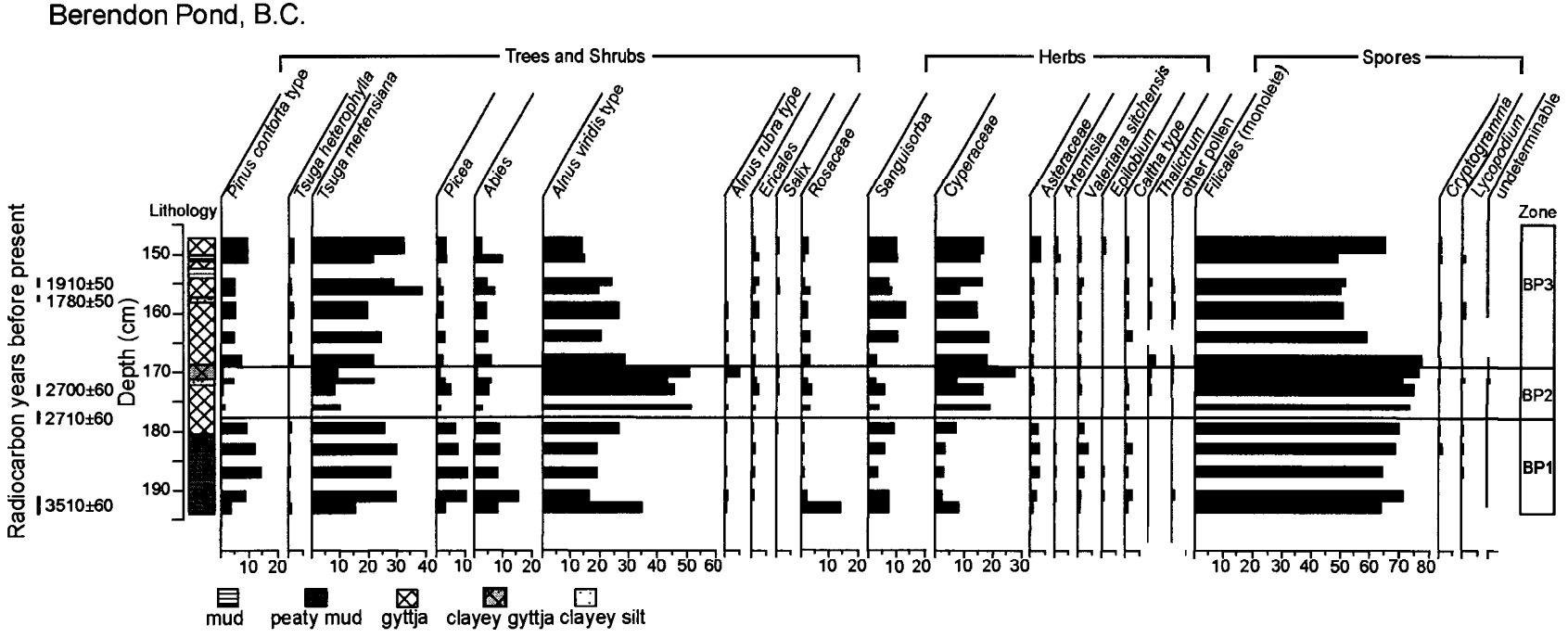

Figure 16. Pollen and spore percentage diagram for core BP2. Pollen and spore percentages are calculated excluding *Filicales* for clarity; *Filicales* is shown as a percentage of the total pollen and spores. See Table 2 for details of radiocarbon ages, Figure 15 for lithologies, and Figure 17 for pollen concentrations.

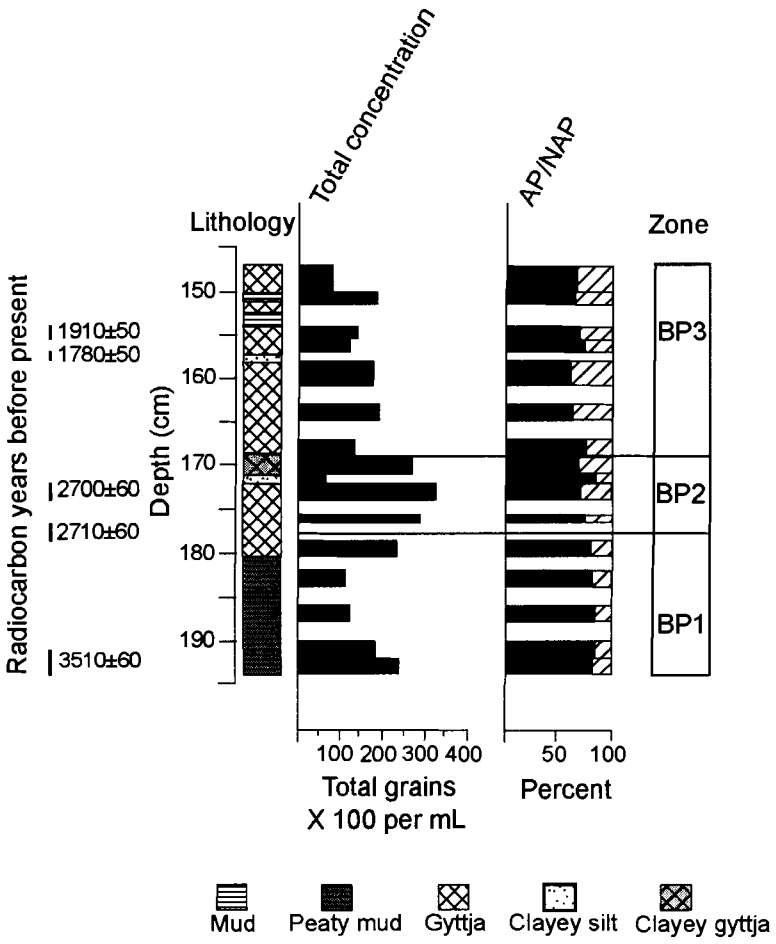

Figure 17. Plot of total concentration and relative abundance of arboreal (AP) and non-arboreal (NAP) pollen in core BP2. See Table 2 for radiocarbon ages and Figure 15 for lithologies.

fossil pollen concentrations. Samples were prepared using standard techniques (Faegri and Iversen, 1975), including 10% HCl, 10% KOH, HF, and acetolysis. All samples were sieved to remove coarser debris. The more peat-rich sediments from the base of the core were also treated with 10% bleach.

Pollen residues were mounted in silicone oil and counted under a light microscope at 400X magnification. A minimum of 250 arboreal pollen grains were identified in each sample, with the exception of two samples at 170 and 168 cm, which had low pollen concentrations. Pollen and spores were identified using keys (e.g., Moore and Webb, 1978) and the Simon Fraser University reference collection. Pollen and spore abundance and concentrations were determined in Microsoft Excel and plotted using Adobe Illustrator. Relative abundances of species are shown in Figure 16. Figure 17 shows changes in the total concentration of fossil pollen over the length of the analyzed portion of the core, as well as total arboreal and non-arboreal pollen abundance. Figure 18 shows photographs of representative pollen grains.

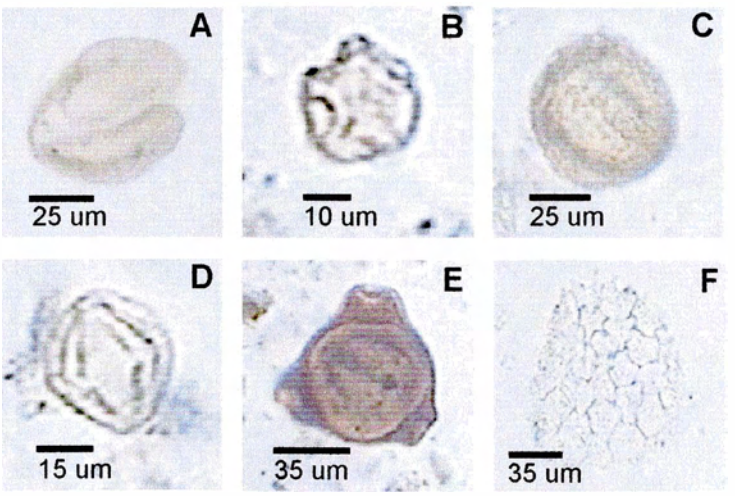

Figure 18. Representative pollen grains from Berendon Pond samples. A. Mountain hemlock (*Tsuga mertensiana*). B. Sitka alder (*Alnus viridis*). C. Sitka valerian (*Valeriana sitchensis*). D. Sitka burnet (*Sanguisorba canadensis*). E. Willow-herb (*Epilobium*). F. Colony of planktonic alga *Pediastrum*.

Pollen Zones

Three pollen zones were identified by visual assessment of the relative abundance data (Fig. 16) and trends in the absolute concentration of pollen grains (Fig. 17): zone BP1 (194-178 cm; lithologic unit A and lowermost unit B); zone BP2 (178-169 cm; lower part of lithologic unit B); and zone BP3 (169-147 cm; upper part of lithologic unit B).

The basal pollen zone (BP1) is characterized by a high relative abundance of arboreal pollen, dominated by *Tsuga mertensiana*. *Abies*, *Picea*, and *Pinus* pollen are present as secondary components, in comparable amounts. Alder is present predominantly as *A. viridis*. Herbaceous species include *Sanguisorba* (Sitka burnet), Asteraceae (sunflower family), *Valeriana sitchensis*, and *Caltha* type (marsh-marigold). Total pollen concentration is relatively constant through the zone.

Zone BP2 is dominated by *Alnus viridis*. *Alnus rubra* (red alder) reaches its peak in this zone. The relative abundance of arboreal pollen decreases slightly from BP1. Most herbaceous species show a slight decrease from BP1 values, with the exception of Cyperaceae, which increases steadily to the top of the zone. *Thalictrum* (meadowrue) and Caryophyllaceae (pink family) first occur in zone BP2. Silt- and clay-rich layers near the top of BP2 have elevated values of non-arboreal pollen. Total pollen concentration increases markedly from zone BP1 (Fig. 17).

Arboreal pollen is present in slightly lower abundances in zone BP3 than in BP1, but *T. mertensiana* persists as the dominant conifer. Herbaceous pollen abundance is generally elevated, as in BP2. *Sanguisorba* attains its highest abundance in zone BP3. Total pollen concentration is lower than in BP2, and there is an abrupt decrease in concentration at the BP2-BP3 boundary. Sparse colonies of the planktonic alga *Pediastrum* were observed in the uppermost sediments of BP3.

Carbon Content and Magnetic Susceptibility

The lower part of core BP2 was analyzed for magnetic susceptibility and carbon content at the University of Lund, Sweden. Magnetic susceptibility provides a measure of the relative abundance of ferromagnetic minerals in a sample and, therefore, serves as a proxy for allochthonous mineral sedimentation in a lake (Thompson and Oldfield, 1986).

The organic carbon values are a proxy for autochthonous, organic-rich sediment. Magnetic susceptibility measurements were made according to the method of Walden et al. (1999). Organic carbon was determined by stepwise heating in a LECO RC-412 multiphase analyzer.

Magnetic susceptibility values are lowest in unit A, rapidly increase to a maximum at 172-171 cm in the lower part of unit B, and then decline (Fig.19). The decline is interrupted by two subtle increases at 159-158 cm and 152-151 cm.

The analyzed sediments are relatively organic-poor (Fig. 19). The highest values are in unit A, with a maximum of 15% total carbon. Samples from 172-171 cm and 158-157 cm have very low (ca. 1%) total carbon values.

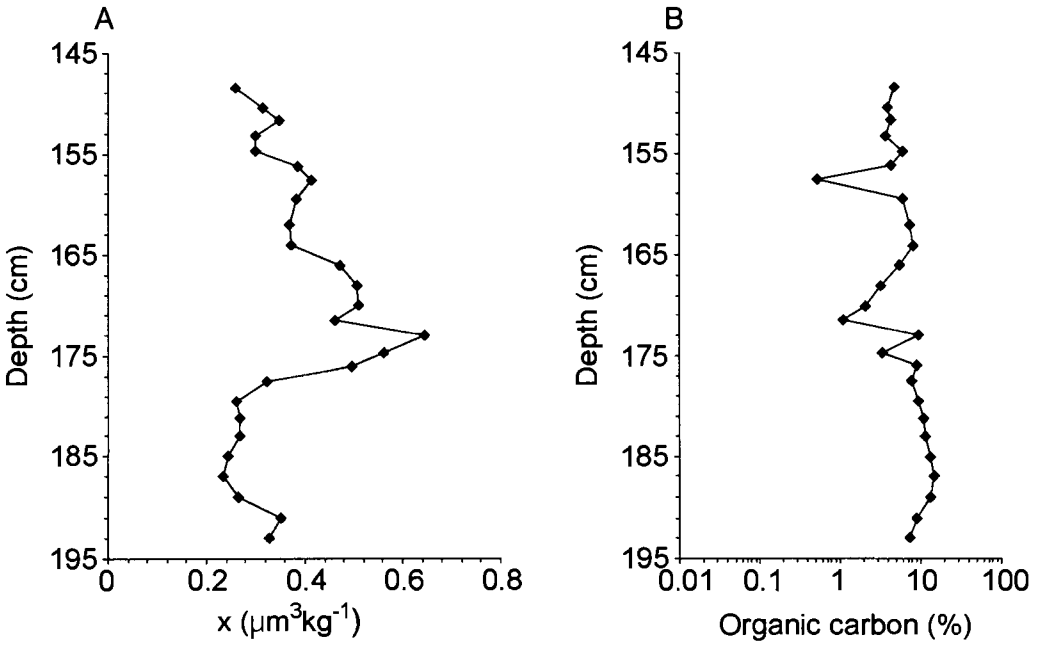

Figure 19. A. Plot of magnetic susceptibility of the lower part of core BP2. The curve shows changes in the concentration of ferromagnetic minerals. B. Organic carbon profile for core BP2. See text for description of stratigraphy and Figure 13 for location of core.

Interpretation

The pollen assemblage of the basal sediments of core BP2 (unit A, zone BP1) records a high elevation, subalpine parkland at Berendon Pond. Herbaceous elements and a variety of conifer species indicate conditions comparable to the modern environment. The presence of *Epilobium*, an entomophilous species, shows that sand or gravel substrates were near the pond. *Sanguisorba* and Caltha-type pollen and *Cryptogramma* (parsley fern) spores suggest the presence of open, wet areas at the site. The more peaty nature of unit A may indicate low water levels during this interval. Carbon values associated with these sediments, while relatively low, are elevated in comparison to carbon values in overlying sediments, supporting low water levels and more bog-like conditions. Influx of mineral sediment at this time was likely decreased, as magnetic susceptibility is consistently low over this interval. Based on the pollen assemblage and the character of the associated sediments, Berendon Glacier was likely less extensive during this interval than during the Little Ice Age, with water input to the pond occurring via overland flow. Deposition of unit A commenced prior to 3510±60 ^{14}C yr BP.

The environment surrounding Berendon Pond was disturbed during zone BP2. Disturbance is inferred from the striking dominance of *Alnus viridis*, a shade-intolerant, pioneering species that thrives on moist or gravelly substrates. The associated peak in total pollen concentration likely reflects the proliferation of this species in the area at this time (Fig. 17). A disturbed environment is supported by increased abundance of Cyperaceae, also an open-canopy pioneering species, and by a significant decrease in arboreal pollen. The apparent relative increase in arboreal pollen at 172-171 cm (Fig. 16) is misleading, as it coincides with a low pollen count. The shift to less peat-rich sediments during this period may indicate deepening of the lake.

The silt- and clay-rich horizons at the top of zone BP2 and their associated peaks in magnetic susceptibility indicate increased sedimentation ca. 2700 ^{14}C yr BP. These data, along with decreased organic carbon values during this interval, suggest an input of sediment-laden meltwater from either Berendon Glacier or Summit Lake. The sustained increase in magnetic susceptibility, coupled with the environmental disturbance recorded by the pollen further suggest that these changes were sustained over some time and may have been associated with a prolonged advance of Berendon

Glacier. The radiocarbon ages associated with zone BP2 indicate that the advance correlates with the Tiedemann Phase of Neoglaciation (Fig. 20).

Following this period of disturbance, the environment surrounding Berendon Pond returned to a state similar to that of zone BP1. Slightly lower abundance of *Pinus*, *Picea*, and *Abies*, and sustained higher levels of *Cyperaceae*, however, may indicate less favourable growing conditions than during BP1, and perhaps more open parkland. The elevated abundance of *Sanguisorba* may indicate that moisture levels in the area were higher than before the disturbance event. Pond water depth and pond productivity may also have increased, as *Pediastrum* and other algae are present in the more mud-rich upper sediments.

The laminated, inorganic mud of unit C, which yielded a radiocarbon age of 615±85 ^{14}C yr BP, was deposited during the Little Ice Age. It indicates that sometime after about 600 yr BP, Berendon Glacier was sufficiently advanced to block the lower Summit Lake overflow channel and re-route meltwater into Berendon Pond via Spillway Pond. The coarse sediments of unit D likely reflect sedimentation from meltwater flowing into the pond directly from Berendon Glacier when it reached its maximum extent.

A decrease in magnetic susceptibility and low organic carbon values in the upper part of unit B indicate a return to more quiescent pond sedimentation. The conspicuous silt layer and two laminated mud horizons near the top of the unit may indicate increased sedimentation about 1800 ^{14}C yr BP. The silt layer is associated with a sharp decrease in carbon content and a slight increase in magnetic susceptibility. These clastic layers are not associated with any changes in vegetation. They may, however, record brief meltwater pulses related to minor glacier advances.

A ^{210}Pb profile through the capping clay gyttja unit in another Berendon Pond core indicates that this unit began to accumulate about 300 years ago (Clague et al., submitted). As the clay gyttja represents very low energy, slow sedimentation, the upper overflow channel must have been abandoned, and Berendon Glacier had retreated from its Little Ice Age end moraine, by that time.

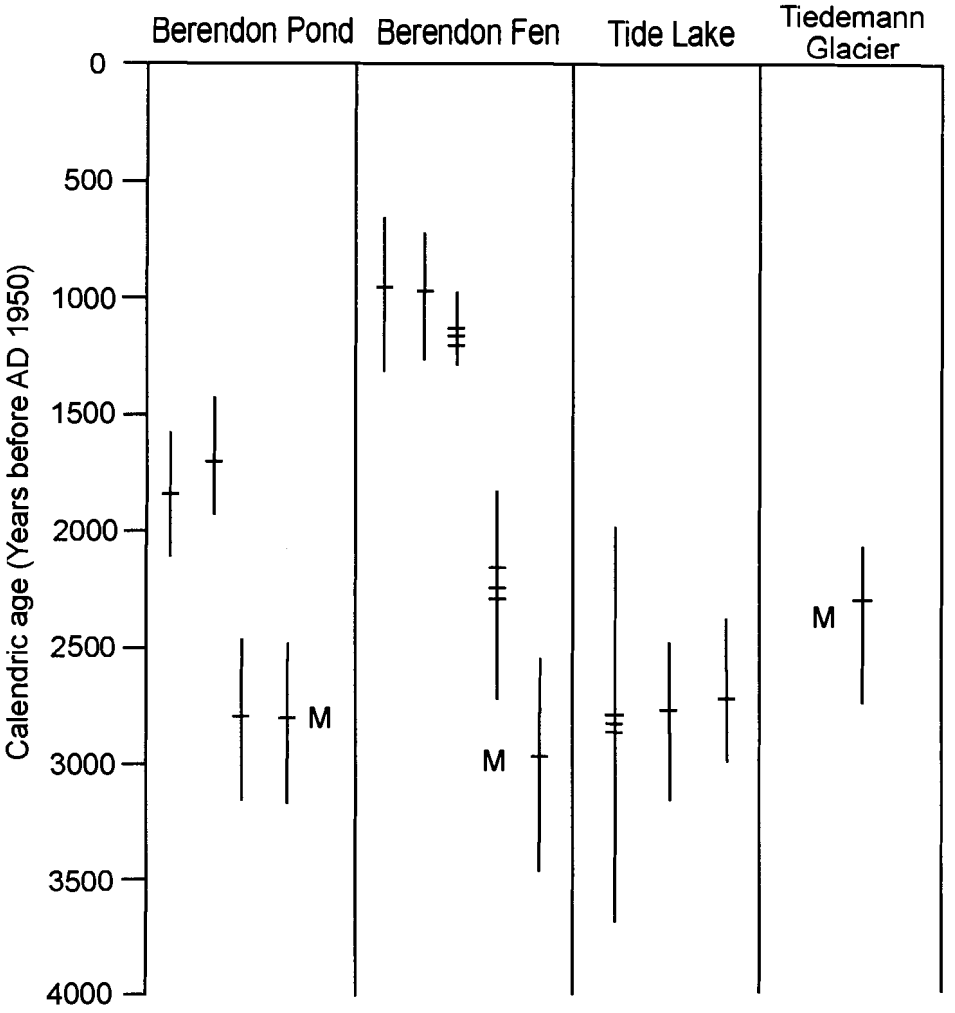

Figure 20. Plot of calibrated radiocarbon ages associated with Neoglacial advances of Berendon and Tiedemann glaciers. Berendon Fen ages are from Clague and Mathewes (1996); Tide Lake ages from Clague and Mathews (1992); and Tiedemann Glacier ages are from Ryder and Thomson (1986). 'M' denotes inferred maximum age for the Tiedemann Advance. Radiocarbon ages were calibrated using CALIB 4.3 (Stuiver and Reimer, 1993). The vertical lines denote the 2-sigma age range calculated with an error multiplier of 2.0. Horizontal ticks are intercept ages. (Based on Clague and Mathewes, 1996).

Spillway Pond

Spillway Pond (842 m asl) lies southwest of Berendon Pond and Berendon Fen (Figs. 13, 14, and 21). It is approximately 0.5 ha in area and has with a maximum depth of 3 m. The lake is recharged by overland flow during snowmelt and rain events.

Spillway Pond is located between the Little Ice Age terminal moraine and a subdued older moraine (Figs. 13, 14, and 21). A short segment of a second, even more subdued moraine lies just outside the outer moraine west of the pond. This outermost moraine is parallel to the outer moraine and merges with it and the Little Ice Age moraine west of Berendon Pond.

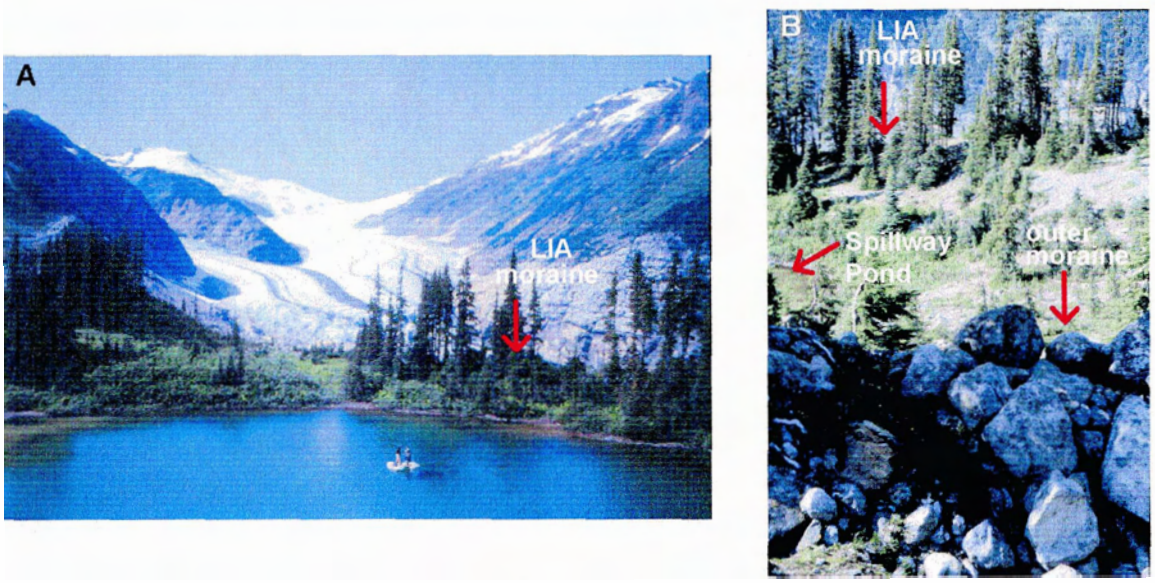

Figure 21. A. Spillway Pond, Berendon Glacier, and the Little Ice Age (LIA) moraine. B. Outer and Little Ice Age moraines at the northeastern edge of Spillway Pond.

A delta is inset into the outer moraine just south of Spillway Pond. The delta formed when Summit Lake discharged into Spillway Pond via the upper overflow channel (Fig. 13). The channel became active in the 17th century when Berendon Glacier advanced to its maximum Little Ice Age position (Clague and Mathewes, 1996) and re-routed Summit Lake drainage from the lower channel to the upper channel. The delta top is

approximately 7 m above the surface of Spillway Pond, indicating that the pond was deeper during the Little Ice Age than today.

Spillway Pond was cored by Clague and Mathewes (1996), but they were able to penetrate only 65 cm of sediment (core SP1, Fig. 22). Spillway Pond was cored again as part of this study in an attempt to extend the record of sedimentation and to constrain the age of the outer moraine south of the pond.

Stratigraphy of Cores SPa and SPb

Two cores (SPa and SPb) were collected from Spillway Pond using a percussion coring system modified from Reasoner (1993). The cores were collected near the center of the pond in water 2.55 m deep. The stratigraphy of the two cores and core SP1 of Clague and Mathewes (1996) is shown in Figure 22, with units corresponding units to those in Berendon Pond core BP2.

The lowest cored sediments (unit C) consist mainly of rhythmically laminated clayey silt. In core SPb, unit C extends from 44 cm to at least 272 cm. Strata range from 1 mm to 4 cm thick and consist of clay to fine sand. Zones of contorted laminated sediments, similar to those in unit C at Berendon Pond, occur within the sequence (Figs. 22 and 23). One coarse sand bed occurs at 230 cm depth in SPb. Unit C is abruptly overlain in all three cores by unit D, which consists of up to 15 cm of massive, granule-rich coarse sand (Fig. 23). Unit D has an oxidized reddish colour (5YR 3/4). Rhythmically laminated clayey silt (unit F), similar to unit C, overlies the granule-rich sand. The rhythmites are interrupted by thin, oxidized, medium sand stringers near the base of unit F. The uppermost rhythmites are more clay-rich than rhythmites lower in the unit. A thin layer of clay gyttja (unit G) caps the sequence.

Magnetic Susceptibility

The magnetic susceptibility of cores SPa and SPb was measured at 2 cm intervals at Western Washington University using a Bartington Instruments MS2 magnetic susceptibility system with a MS2C whole core scanning sensor (Bartington Instruments

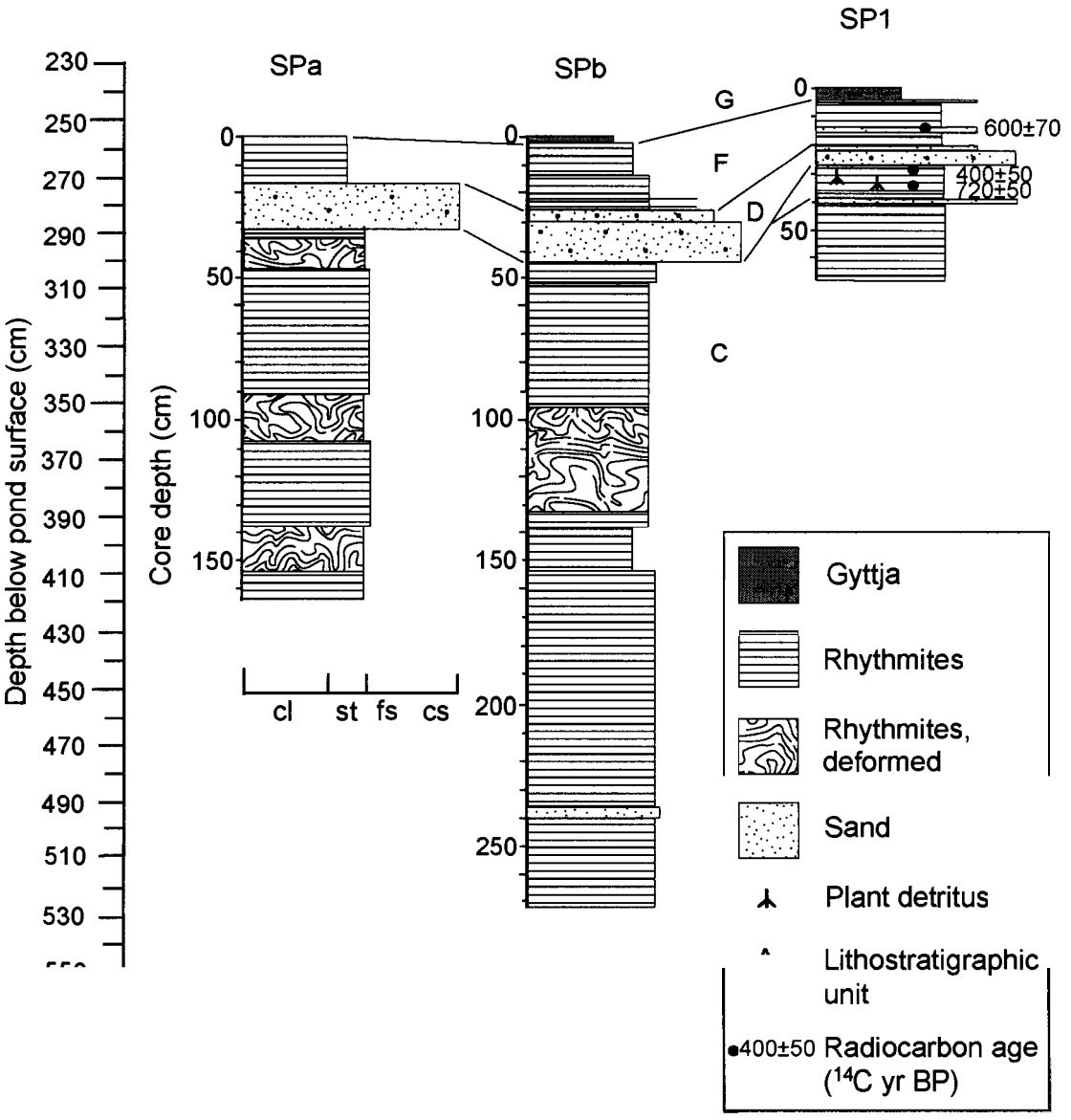

Figure 22. Stratigraphy of Spillway Pond cores (SPa and SPb) and their relationship to core SP1 of Clague and Mathewes (1996). See text for description of stratigraphy and Figure 13 for core locations. cl = clay; st = silt; fs = fine sand; cs = coarse sand.

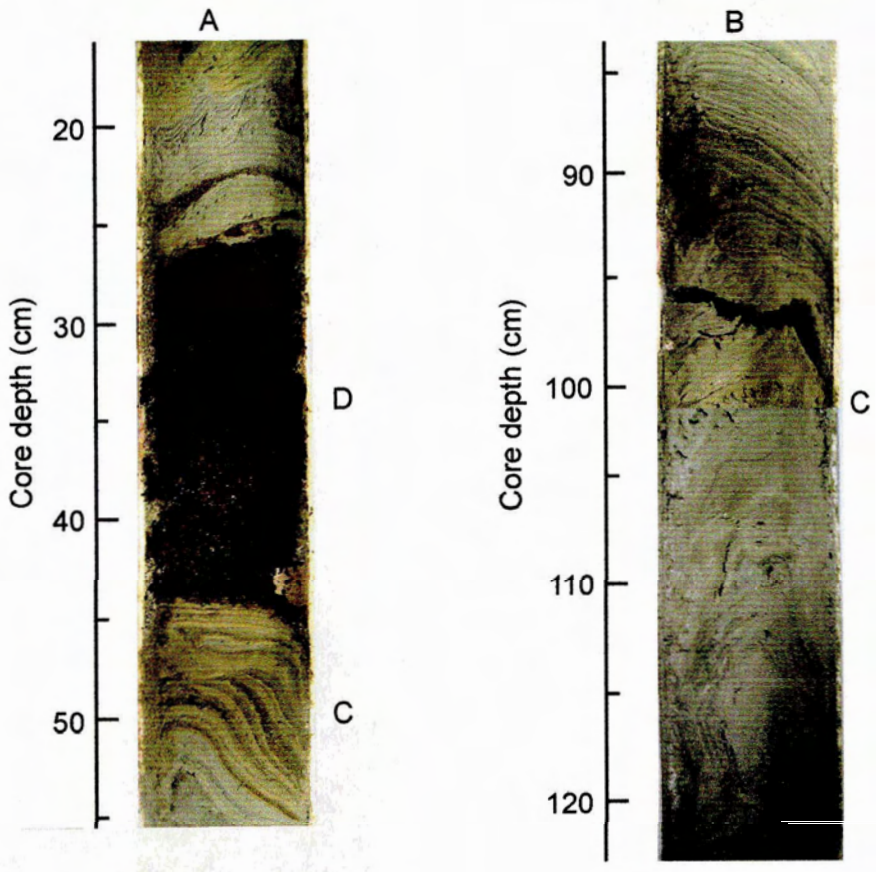

Figure 23. Photographs of parts of core SPb. A. Coarse sand of unit D sharply overlies laminated sediments of unit C. B. Clay-rich laminated sediments above deformed rhythmites of unit C.

Inc., 1993) (Fig. 24). Trends in susceptibility can be correlated with changes in stratigraphy. Both cores show a rapid linear increase in susceptibility to 23 cm depth,reflecting sediment compaction and increasing bulk density below the sediment-water interface. The decrease in values at 23 cm corresponds stratigraphically with unit D sand, which has low susceptibility. The spike at 40 cm in core SPb is due to a clast. The relatively uniform susceptibility values below 40 cm are from laminated clayey silt of unit C. Two derivations at 96-74 cm in SPa and at 120-92 cm in SPb correspond to contorted zones in the middle of unit C.

Interpretation

The stratigraphy of cores SPa and SPb correlates well with that of core SP1 (Fig. 22). The rhythmites of unit C comprise couplets of clay, silt, and sand (Fig. 23). As this unit is not dated, it is not known whether or not the couplets are varves. The unit extends to an unknown depth, as neither core extends to the base of the sediment fill in the pond. The zones of deformed rhythmites may be coring-induced. Alternatively, they could represent syndepositionary deformation resulting from sudden dewatering or slumping. Disturbances may have been initiated by meltwater discharge from advancing Berendon Glacier or overflow from Summit Lake.

Unit C contains abundant silt and fine sand, and contemporaneous deformation structures. These characteristics suggest that the unit was deposited relatively rapidly, probably by Berendon Glacier meltwater during the Little Ice Age. Overlying coarse sand of unit D was deposited when Berendon Glacier attained its maximum Little Ice Age extent, at which time sediment would have been carried into the pond both from Summit Lake via the upper channel and directly from the glacier front. The rhythmites of unit F may reflect continued Little Ice Age sedimentation as the glacier began to retreat from the moraine.

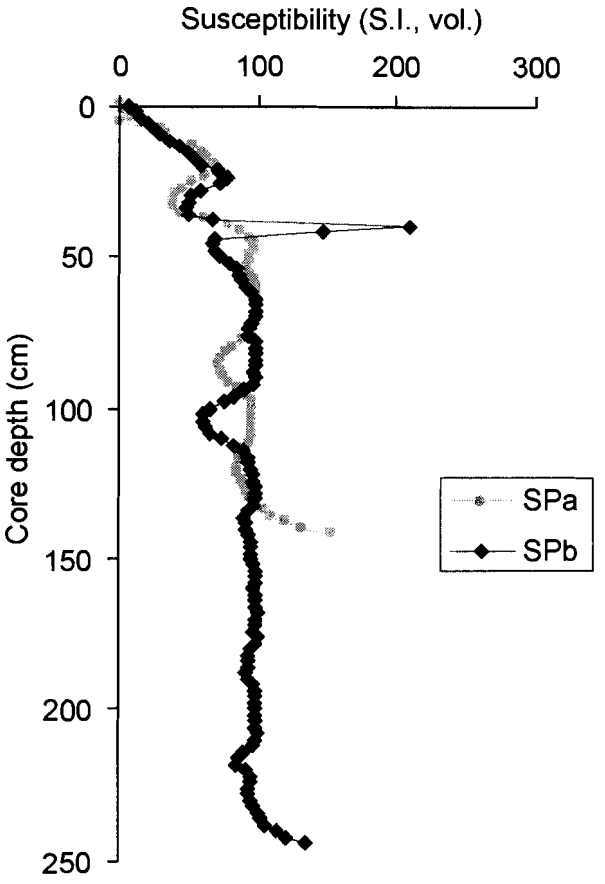

Figure 24. Magnetic susceptibility profiles of cores SPa and SPb. The increase in values at the base of each core likely reflects the presence of core catchers. See text for description of stratigraphy and Figure 13 for locations of cores.

In core SP1 of Clague and Mathewes (1996), a mud bed containing abundant pollen and macrofossils overlies unit C (Fig. 22). As the mud bed must have been deposited without input of meltwater from Summit Lake or Berendon Glacier, Clague and Mathewes interpret it as possibly indicting a period of glacier retreat between 260 and 660 cal yr BP, during the Little Ice Age. A second core was also taken by Clague and Mathews (their SP2), but it did not contain this organic unit. Given the absence of this unit in core SP2 and also in the cores SPa and SPb, described here, the possibility of a period of retreat seems unlikely. It is possible that the organic unit was eroded from cores SP2, SPa, and SPb when the sand of unit D was deposited. However, plant matter in core SP1 may be locally derived and not present throughout the pond. The interpretation of only one Little Ice Age advance is further in accord with the stratigraphy of core BP2 from Berendon Pond.

The capping clay gyttja layer (unit G) records very low-energy deposition in the pond without meltwater input. This layer implies that the upper overflow channel was inactive. The ages of living trees adjacent to Summit Lake below the elevation of the upper channel indicate abandonment since at least the early 1700s (Clague and Mathewes, 1996).

Berendon Fen

The Neoglacial history of Berendon Fen and Tide Lake is described in detail by Clague and Mathewes (1996) and Clague and Mathews (1992), respectively. A brief review is given here in order to relate events at these sites to the records from Berendon Lake and Spillway Pond.

Frank Mackie Glacier repeatedly advanced during the Neoglacial period, blocking Bowser River and creating Tide Lake. Frank Mackie Glacier attained its maximum Little Ice Age extent in the early to middle 17th century. At that time, Berendon Fen was inundated by Tide Lake. This event is recorded in the fen by silt and sand layers within the upper part of the peat sequence (Fig. 25). Prior to the Little Ice Age, Tide Lake was not extensive enough to flood the fen. Mud layers, however, indicate that Berendon Glacier at times was sufficiently advanced to route Summit Lake overflow into the fen. The mud layers date to ca. 2800 and 2200 ^{14}C yr BP and 1200-1000 ^{14}C yr BP. Clague and Mathewes (1996) correlate the two earlier events with the Tiedemann Phase (Fig. 20). The third mud layer may record a limited post-Tiedemann, pre-Little Ice Age glacier advance.

Glacier Fluctuations and Drainage Changes

Advances of Berendon Glacier caused meltwater to be routed into Spillway Pond. Local topography (Fig. 13) similarly directed meltwater into Berendon Pond. Meltwater entering Berendon Pond, in turn, flowed into Berendon Fen. Thus, the sedimentary record from Berendon Pond provides a link between the previously established records of Neoglacial activity from Spillway Pond and Berendon Fen.

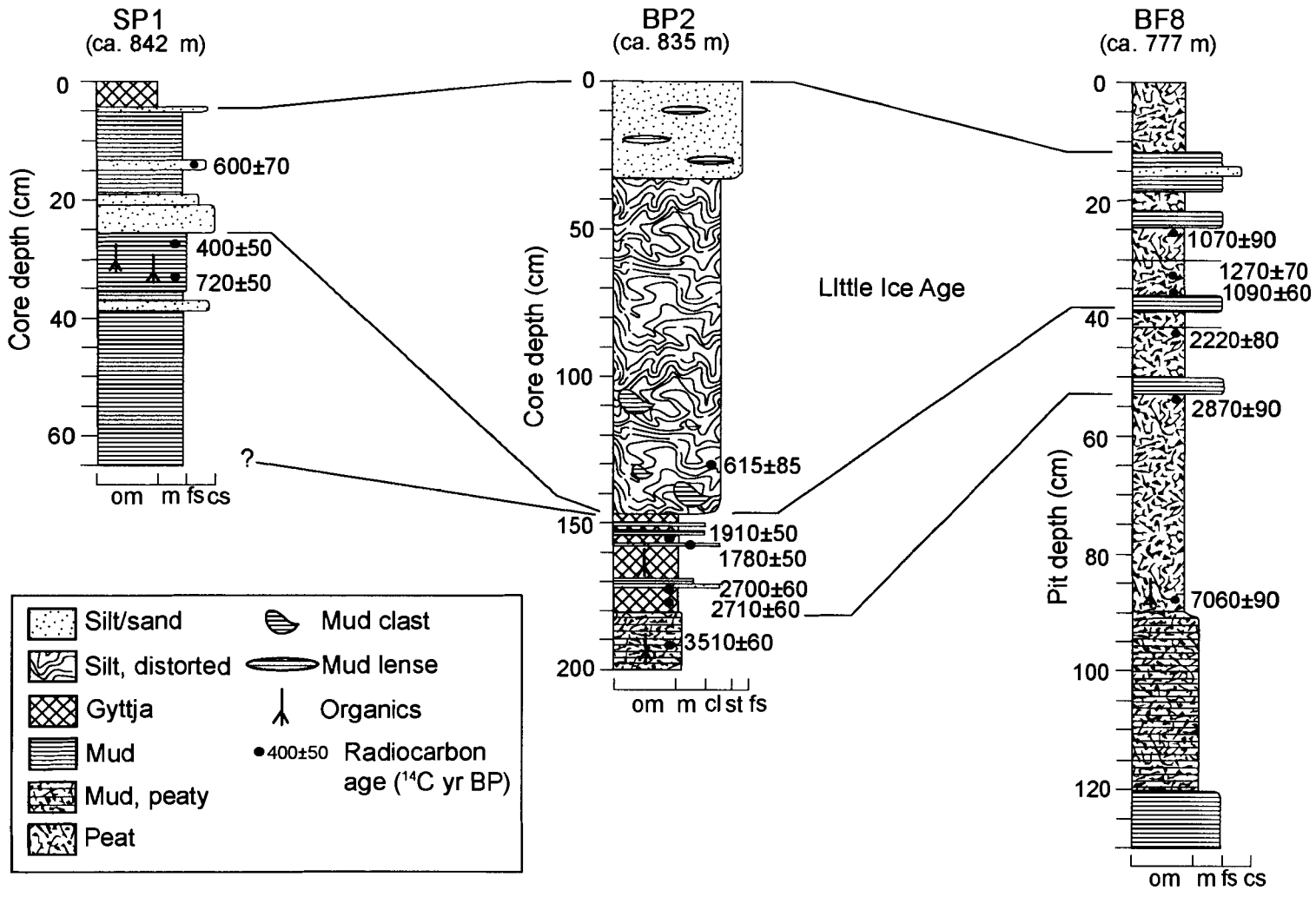

Figure 25. Stratigraphy of Berendon Pond core BP2, core SP1 from Spillway Pond, and pit BF8 at Berendon Fen. Details of relationships between cores are given in the text. om = organic mud (gyttja); m = mud; cl = clay; st = silt; fs = fine sand; cs = coarse sand.

At all three sites, Little Ice Age sedimentation is represented by sand and silt beds. Little Ice Age sediments at Spillway and Berendon ponds were deposited by diverted Summit Lake overflow and by meltwater issuing directly from Berendon Glacier. Little Ice Age sediments at Berendon Fen are the result of inflow of meltwater from Berendon Pond and flooding of the fen by Tide Lake. Radiocarbon ages indicate that this Little Ice Age sedimentation commenced ca. 600 cal yr BP.

The thick package of Little Ice Age sediments (units C and D in core BP2) contrasts with the thin silt- and clay-rich layers ascribed to the Tiedemann Phase (within unit B in core BP2), indicating that Berendon Glacier had a far greater influence on sedimentation in Berendon Pond during the Little Ice Age (Fig. 15). Berendon Fen shows a similar pattern: Tiedemann Phase silt layers are thinner than silt and sand layers deposited during the Little Ice Age. These observations indicate that Berendon Glacier was less extensive during the Tiedemann Phase than at the Little Ice Age maximum.

The age of the outermost Berendon Glacier moraine is problematic. The ice-front position inferred from the moraine implies a clastic signal in the sediments of Berendon Pond at least as great as that of the Little Ice Age. No such signal is evident in core BP2, which spans the last 3500 years. The moraine thus likely predates the Tiedemann Phase and is the product of a late-glacial or early Holocene advance. Alternatively, the moraine may record an early Little Ice Age advance prior to the formation of Spillway Pond. While there is no record of an early Little Ice Age advance at Berendon Pond, its evidence may have been eroded from the record at the hiatus between units B and C in core BP2. However, no silt or sand layers of sufficient thickness or extent were deposited early during the Little Ice Age in Berendon Fen to support the idea of construction of the outer moraine at that time. Boulders on the outer moraine boulders were sampled for cosmogenic ^{36}Cl dating but they, unfortunately, do not help to constrain the age of the moraine (see Chapter 3, *Cosmogenic ^{36}Cl Dating*).

The pre-Little Ice Age silt and laminated mud beds in the upper part of unit B in core BP2 also raise some interesting questions. As Berendon Pond is connected to Berendon Fen by a channel, these layers should correlate with the pre-Little Ice Age mud layers in the fen. Although event beds associated with the Tiedemann glacial maximum at the two sites correlate well (Fig. 25), those postdating it do not. Mud beds at the fen suggest a

glacier advance at 1200-1000 ^{14}C yr BP, whereas silt and laminated mud layers at Berendon Pond were deposited ca. 1800-1700 ^{14}C yr BP. Ryder and Thomson (1986) describe recession of Tiedemann Glacier from its maximum position ca. 2300 ^{14}C yr BP as slow and pulsatory, ending about 1900 ^{14}C yr BP. The 1800-1700 ^{14}C yr BP clastic layers at Berendon Pond may reflect late-stage glacier fluctuations near the end of the Tiedemann Advance that were too small to convey a signal to the fen. The pollen and magnetic records of core BP2 support only minor fluctuations of the glacier at this time.

Clague and Mathewes (1996) recognized that the 1200-1000 ^{14}C yr BP mud beds at Berendon Fen do not temporally fit with the Tiedemann Advance. They interpreted the beds to possibly record a separate period of limited glacier advance. While the Berendon Pond record does not show evidence for an advance at this time, the record of any such event may have been eroded during the following Little Ice Age glacier advance.

Neoglacial Climate Change at Berendon Glacier

Climate during the Neoglacial period in British Columbia fluctuated, ranging from warmer to cooler than today at decadal to millennial timescales (Hebda, 1983; Hebda and Whitlock, 1997; Brown, 2000; Walker, 2001). The pollen, sediment, and geochemical proxy data obtained from Berendon Pond, in conjunction with sedimentary records from Spillway Pond and Berendon Fen, demonstrate the response of a near-coastal, high elevation environment to Neoglacial climate change.

A high elevation parkland with alpine meadows and coniferous groves persisted at the site from at least 4100 years ago to approximately 3000 years ago. Berendon Glacier was less extensive than today and sediment-laden water was delivered to Berendon Pond and Berendon Fen primarily by overland flow. Berendon Glacier advanced between 2800 and 2700 ^{14}C yr BP, disturbing its immediate environment and increasing sediment input to both Berendon Pond and Berendon Fen. This time has been identified in other records as an interval of cool and wet climate in coastal British Columbia (e.g., Pellatt and Mathewes, 1994), and renewed glacial advance in the Coast Mountains (Ryder and Thomson, 1986). Climate deteriorated further with the onset of the Little Ice

Age, as Berendon and Spillway ponds, and Berendon Fen all indicate that Berendon and Frank Mackie glaciers advanced at that time.

The Berendon Pond record indicates that climate changes between 2800 and 1700 ^{14}C yr BP were insufficient to cause a significant vegetation response. Climate change during the Tiedemann Phase, however, was sufficient to cause Berendon Glacier to advance. Furthermore, the similarity between the sedimentary records from both ponds and the fen indicate that the three hydrologically linked glaciers were responding to Holocene climate changes in relative synchrony.

Summary

1. Stratigraphic and paleoenvironmental data from Berendon Pond indicate a Tiedemann-aged advance of Berendon Glacier about 2800 ^{14}C yr BP that was less extensive than the mid-17th century Little Ice Age advance. Minor fluctuations of the glacier also occurred between 1800 and 1000 ^{14}C yr BP.

2. The pollen record from Berendon Pond indicates a vegetation disturbance during the 2800 ^{14}C yr BP advance, due to either general climate deterioration or to the proximity of Berendon Glacier to the pond.

3. The age of the outer moraine at Spillway Pond remains unknown, however, it is older than 3500 ^{14}C yr BP.

Summary of Reconstructed Glacier Advances

The combined stratigraphic and paleobiological records of Lillooet, Diadem, and Berendon glaciers provide evidence for at least four periods of glacier advance in the Coast Mountains of British Columbia following the Vashon Stade of the Fraser Glaciation:

1. Prior to 6200 ^{14}C yr BP, probably during late-glacial time.

2. During the Tiedemann Phase, with a maximum advance about 2800-2700 ^{14}C yr BP.

3. During the late Holocene, between 1500 and 900 ^{14}C yr BP.

4. During the Little Ice Age, with a maximum advance after 400 years ago.

3 Cosmogenic ^{36}Cl Dating of Outer Moraines

Introduction

The use of terrestrial cosmogenic nuclides in dating Quaternary landforms has grown significantly over the last decade, due largely to the development of accelerator mass spectrometry (AMS) techniques and, recently, refinement of in-situ cosmogenic nuclide production rates (see Gosse and Phillips, 2001, and references therein). A variety of nuclides are now used in dating Quaternary surfaces, including ^{3}He, ^{21}Ne, ^{10}Be, ^{26}Al, and ^{36}Cl. Of these nuclides, ^{36}Cl is often chosen to date Quaternary surfaces due to its half-life of 301 ka and its ubiquitousness (Zreda and Phillips, 1994).

The cosmogenic ^{36}Cl method has been used to date glacier advances in the mountains of the western United States (Phillips et al., 1990; Zreda et al., 1994; Zreda and Phillips, 1995; Phillips et al., 1996a; Swanson and Porter, 1997; Briner et al., 2001; Swanson and Caffee, 2001). In Canada, ^{36}Cl dating studies currently are limited to the Mackenzie Mountains (Duk-Rodkin et al., 1995), southwestern Alberta (Jackson et al., 1999), and southern British Columbia (McCrumb and Swanson, 1998).

The goal of this study was to assess the utility of the cosmogenic ^{36}Cl method for dating Holocene glacier advances in the mountains of western Canada. The method was applied to pre-Little Ice Age moraines at Lillooet, Diadem, and Berendon glaciers (see Chapter 2). The moraines could not be dated directly by any other method.

Background

Cosmic ray energy derives mainly from galactic cosmic radiation, which consists largely of high-energy protons and heavier atomic nuclei (Gaisser, 1990). As the cosmic ray flux penetrates Earth's upper atmosphere, collisions with gas nuclei create a secondary fast neutron flux capable of reaching Earth's surface (Lal and Peters, 1967). This secondary radiation is composed of high- and low-energy components that produce cosmogenic nuclides.

High-energy neutrons undergo spallation reactions, involving direct collisions of neutrons with other target nuclei, regardless of composition. The neutrons attenuate exponentially along their path, proportional to the amount of mass through which they travel (Lal, 1991).

The behaviour of low-energy neutrons depends on the medium through which the neutrons travel (Bethe et al., 1940). These thermal neutrons diffuse as a function of the absorption cross-section of particles, preferentially reacting with particles with larger reaction cross-sections, such as atomic gases (Kurz and Brook, 1994). The atmosphere has a bulk absorption capacity approximately one order of magnitude larger than most rock types (Phillips et al., 2001), creating what is known as the 'air-ground boundary effect', with relative depletion in the near-surface part of rocks (Kurz and Brook, 1994). This phenomenon creates a path flux of increasing production to a certain depth, followed by exponential decay.

Cosmogenic nuclides are also produced by low-energy muon capture, whereby muons fall into the electron shells of atoms and then are captured by the nucleus (Gosse and Phillips, 2001). The probability that a muon will be captured by a nucleus to form a cosmogenic nuclide is a function of the nucleus cross-section (Gosse and Phillips, 2001).

Production of Cosmogenic ^{36}Cl

The three types of reactions producing cosmogenic ^{36}Cl follow four main pathways:

1) and 2) High-energy spallation:

$$^{39}K \xrightarrow{(n,2n,2p)} {}^{36}Cl$$

$$^{40}Ca \xrightarrow{(n,2n,3p)} {}^{36}Cl$$

3) Low-energy thermal neutron activation:

$$^{35}Cl \xrightarrow{(n,\gamma)} {}^{36}Cl$$

4) Negative muon capture:

$$^{40}Ca \xrightarrow{(\mu^-,\alpha)} {}^{36}Cl$$

High-energy spallation reactions and low-energy thermal neutron activation of ^{35}Cl dominate the production of ^{36}Cl at Earth's surface. The importance of muon capture is still not well understood. In total, ^{36}Cl can be produced by slow muon absorption by Ca, low-energy neutron absorption, and photodisintegration reactions (Phillips et al., 2001). Although muon capture becomes more important with depth (Rama and Honda, 1961), absorption by ^{39}K, and thermal neutron capture of ^{39}K are considered only minor surface reactions and are generally not considered in age calculations (Swanson and Caffee, 2001). Production of ^{36}Cl by muon capture, however, is increasingly being incorporated into production rate calibrations.

The production rate (P) of cosmogenic ^{36}Cl in rock can be described by the following formula (Zreda and Phillips, 1994):

$$P = \psi_{Ca}(C_{Ca}) + \psi_K (C_K) + \phi_n(\sigma_{35}N_{35}/\Sigma\sigma_i N_i),$$

where ψ_{Ca} and ψ_K are production rates due to spallation of Ca and K, respectively, C_{Ca} and C_K are concentrations of Ca and K, ϕ_n is the rate of thermal neutron absorption per unit mass of rock, σ_{35} and σ_i are the reaction cross-sections of ^{35}Cl and all other elements in the rock matrix, and N_{35} and N_i are their relative abundance.

Sources of Error

Geomagnetic field effects on ^{36}Cl production rates are perhaps the most significant, yet least understood, source of error in determining exposure ages. The effects are of two types, spatial and temporal field effects. The spatial effect refers to the difference in the amount of particles penetrating Earth's geomagnetic field due to location. Because primary particles from galactic cosmic radiation are charged, they are subject to deflection by Earth's magnetic field. They preferentially penetrate the field at high latitudes (Kurtz and Brook, 1994). A correction for the spatial effect is made with a set of scaling coefficients, based on a polynomial correction equation developed by Lal (1991). Temporal field effects involve variations in the orientation and intensity of the geomagnetic field, which affect the ability of the field to shield incoming ray flux (Gosse et al., 1996). Secular variation of the dipole axis of Earth, which changes the geomagnetic latitude of sampling sites (Gosse and Stone, 2001), and fluctuations in field

intensity and orientation induced by variations in solar wind (Kurtz and Brook, 1994) influence terrestrial cosmogenic nucliide production rates.

The atmosphere itself affects production rates, because lower atmospheric pressure at high altitudes provides less shielding, and hence allows a greater neutron flux, than higher pressure at low altitudes. This altitude affect is taken into account in Lal's (1991) correction equation. Changes in climate affect the strength of dominant high and low atmospheric pressure systems and can also affect production rates at ground level (Stone, 2000).

Shielding of moraine boulders either by adjacent topography or snow alters production rates. A correction can be made for topographic shielding if the angle of incidence between sampled boulders and the surrounding topography is known (Zreda and Phillips, 1994). Snow cover is more difficult to assess. Hydrogen atoms have light nuclei and effectively moderate neutron energy by transferring energy to target nuclei (Phillips et al., 2001). Both snow and rock interstitial water will, therefore, influence thermal neutron distribution. Snow cover can increase the thermal neutron production rate and hence increase the apparent ^{36}Cl age of the boulders.

Assumptions

Several assumptions must be satisfied to successfully use cosmogenic nuclides to date moraines. The assumptions are described in greater detail elsewhere (e.g., Kurtz and Brook, 1994; Zreda and Phillips, 1994) and will only be given cursory treatment here. The primary assumption underlying ^{36}Cl dating of moraine boulders is that the boulders were eroded from fresh rock and shielded from cosmogenic radiation until they were deposited at the land surface. Boulders deposited during the construction of a moraine can then be used to date a glacier advance. Other assumptions are: (1) that ^{36}Cl production rates are known; (2) the relation between cosmic ray flux and time is linear, thus there is a direct relationship between nucliide concentration and exposure time; (3) the boulder surface was immediately exposed to cosmic rays at the time of deposition; (4) all samples are 'zeroed' prior to deposition, i.e. the boulders were sufficiently eroded that they have no inherited exposure; (5) the isotopic system is closed and there is,

therefore, no ^{36}Cl contamination; and (6) boulders have remained at the surface of a moraine and have not moved since deposition.

Calibration Production Rates

Two recently published ^{36}Cl production rates are those of Phillips et al. (2001) and Swanson and Caffee (2001) (Table 3). Both Phillips et al. and Swanson and Caffee use the scaling equations of Lal (1991), which normalize samples with respect to latitude and sea level. The two production rates differ, however, as Phillips et al. (2001) account for the effects of hydrogen by reassessing the low-energy flux and also include muon production effects based on the calculations of Stone et al. (1998). ^{36}Cl production from calcium, due to slow muon absorption, is excluded, resulting in a ca. 9% lower $P_{s,Ca}$ (production rate by spallation of Ca). Swanson and Caffee (2001) do not separately account for production from calcium resulting from slow muon absorption. In order to compare apparent moraine ages obtained in this study using both datasets, the rate of muon capture of 5±2 (atoms $^{36}Cl(gCa)^{-1}yr^{-1}$) (determined by Stone et al., 1998, and used by Phillips et al. 2001) was subtracted from Swanson and Caffee's (2001) published value of $P_{S,Ca}$= 91±5 (atoms $^{36}Cl(gCa)^{-1}yr^{-1}$).

Phillips et al. (2001) use a different dataset from that used in their 1996 calibration (Phillips et al., 1996b). The 2001 dataset comprises 33 samples ranging in age from 2 to 55 ka, collected over a wide range of elevations and latitudes. The calibration dataset compiled by Swanson and Caffee (2001) consists of 50 samples validated with radiocarbon ages. Their samples are from a limited geographic area and are near to sea level (Table 3), consequently they required little scaling to get calibrated production rates.

Table 3. Production rate calibration datasets discussed in the text.

Study	Latitude	Altitude (m)	Exposure age (ka)	Calibration production rates[1] $P_{S,Ca}(O)$	$P_{S,K}(O)$	$P_f(O)$
Swanson and Caffee (2001)	47.5 - 48.4°N	10 - 140	15.5	86 ± 5	228 ± 18	762 ± 28
Phillips et al. (2001)	20 - 80°N	20 - 2578	2 - 55	66.8 ± 6.8	137 ± 60	626 ± 105
Phillips et al. (1996b)	20 - 80°N	20 - 2578	2 - 55	72.5 ± 5	154 ± 10	586 ± 40

[1] Production normalized to sea level and high geographic latitude (>60°). $P_{S,Ca}$ (O) = total production due to spallation of Ca [atoms $^{36}Cl(gCa)^{-1}yr^{-1}$]; $P_{S,K}$ (O) = total production due to spallation of K [atoms $^{36}Cl(gK)^{-1}yr^{-1}$]; $P_f(O)$ = ground-level secondary neutron production rate in air [neutrons $(g\ air)^{-1}yr^{-1}$].

Methods

Sampling

Boulders were selected for dating based on several criteria. Where possible, the largest boulder on a given moraine crest was chosen to minimize the possibility of post-depositional movement and exhumation. Samples were taken from the uppermost few centimetres of boulders to minimize depth-dependent nuclide production differences, and as far from boulder edges as possible to avoid the loss of nuclides produced by thermal neutron activation. Three one-kilogram samples were taken from each moraine using a hammer and chisel.

Shielding due to surrounding topography was measured in four quadrants with a clinometer. The surface slope angle, slope direction, and dimensions of each boulder were measured, and observations were made of weathering such as surface pitting and weathering rinds.

Laboratory Analysis

Two samples from each moraine were submitted for analysis. Sample preparation and major element analyses were done at the New Mexico Institute of Mining and Technology. The bottoms of samples were trimmed if necessary, and lichens and other plant material were removed from the upper surfaces with a wire brush. Samples were crushed, ground, and screened, and the > 150 μm fraction was retained. The residues were leached in 3% HNO_3 to remove possible meteoric chloride and secondary carbonate. Major element compositions, including U and Th, were determined by X-ray fluorescence. Initial chloride concentration was determined with an ion selective electrode in a Teflon diffusion cell (Aruscavage and Campbell, 1983), with a spike of ^{35}Cl of known concentration added. Portions of samples were sent to SGS Geochemical Laboratories, Don Mills, Ontario, for Gd and B analyses by prompt gamma emission spectrometry. Accelerator mass spectrometry determination of ^{36}Cl was done at CAMS, Lawrence Livermore National Laboratories, California.

Age Calculation

CHLOE (Chlorine-36 Exposure Age Calculation Workbook, v. 98-2.1) was used to calculate boulder ages. CHLOE is a Microsoft Excel-based workbook developed by Mitch Plummer and Fred Phillips (Phillips and Plummer, 1996) at the New Mexico Institute of Mining and Technology. The program calculates neutron fluxes as a function of both depth and composition, using sample elemental data. The program also allows corrections to be made for cosmic-ray flux variations due to latitude and altitude, erosion, snow cover, and topographic shielding. The program was modified to incorporate the most recent production rate data of Swanson and Caffee (2001) in order to compare the effects of the two datasets (Table 3) on calculated boulder ages. CHLOE will calculate a range of ages using different boulder erosion rates. A maximum erosion rate of 1.1 mm/ka was chosen based on calculations by Bierman et al. (1999). This rate was calculated for a nonglacial environment in Arctic Canada, but it has been used in a coastal, mountainous environment (Briner et al., 2001). Erosion rates can be determined quantitatively by measuring two nuclides with different half-lives, such as ^{10}Be and ^{26}Al, and using production rates to solve for an erosion rate (Zreda and Phillips, 1994), but this method was not used here.

Researchers have modeled snowpack conditions to account for the effects of snow cover where extended records are not available (Jackson et al., 1999; Briner et al., 2001). For this study, an average snow density of 0.4 g/cm^3 was used, less than the 0.6 g/cm^3 determined for North Cascade glaciers (Pelto and Reidel, 2001), but greater than the 0.2 g/cm^3 assumed for both southwestern Alaska (Briner et al., 2001) and southeastern Alberta (Jackson et al., 1999). Average monthly snowpack depths were calculated for each glacier using records from the nearest climate station (Bridge Glacier, Nostetuko River, and Granduc Mine, for Lillooet, Diadem, and Berendon glaciers, respectively). The average snowpack depths were then converted to water equivalent, which CHLOE uses in conjunction with boulder height to calculate a shielding correction.

Results

Calculated apparent ^{36}Cl ages for each sample are given in Table 4. This table includes both corrected and uncorrected values obtained using both sets of production rate data. Additional sample details are given in Appendixes B, C, and D.

Figure 26 compares the calculated ages, with an uncertainty of 7% (Appendix E). The uncertainty incorporates only the maximum random error, that is the precision component, which includes errors associated with the characteristics of the sample itself (geometry and shielding corrections), sample preparation, elemental analyses, and the AMS error (Gosse and Phillips, 2001). The uncertainty term does not include systematic errors, such as those associated with production rates and geomagnetic field effects. The systematic error component can be large, but it is difficult to isolate. Uncertainties due to errors in production rates and geomagnetic field effects are often ignored in ^{36}Cl dating studies (e.g., Jackson et al., 1999). Commonly, the only uncertainty stated is that due to AMS error (e.g., Briner et al., 2001). Although this approach ignores what could be significant sources of error, it is perhaps acceptable if ^{36}Cl ages are not compared to other independently determined chronologies.

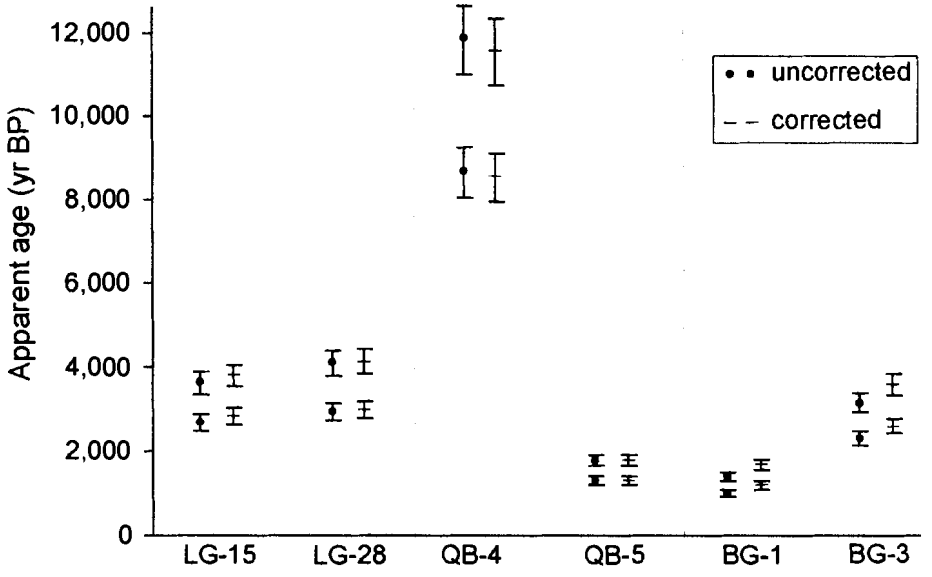

Figure 26. Plot of cosmogenic ^{36}Cl ages of sampled boulders. Blue symbols are ages calculated using production data of Phillips et al. (2001); pink symbols are ages calculated using data of Swanson and Caffee (2001). Corrected values have been adjusted for snow cover and erosion, assuming an erosion rate of (1.1 mm/ka). Error bars indicate uncertainty related only to analytical imprecision. See Appendix E for details of error magnitude calculations.

Table 4. Apparent ^{36}Cl ages of moraine boulders using two sets of production rate data.

Sample number	Thickness-averaged production rates [atoms $^{36}Cl(g^*yr)^{-1}$]			^{36}Cl Age (yr)			
	Ψ Ca	ΨK	ΨN	Zero erosion	1.1 mm[ka]$^{-1}$ erosion	Snow cover	Snow cover and erosion
Phillips et al. (2001)							
SF-LG-15	5.226	2.081	1.772	3629	3615	3821	3806
SF-LG-28	5.854	5.585	3.882	4093	4064	4177	4147
SF-QB-4	8.683	6.635	7.092	11,843	11,547	11,843	11,547
SF-QB-5	8.802	7.055	6.980	1790	1783	1790	1783
SF-BG-1	4.634	6.393	6.732	1414	1408	1684	1676
SF-BG-3	4.407	6.393	10.163	3163	3124	3638	3586
Swanson and Caffee (2001)							
SF-LG-15	6.706	3.461	2.159	2689	2695	2839	2832
SF-LG-28	7.511	9.288	4.003	2938	2926	3013	3000
SF-QB-4	11.143	11.029	8.623	8664	8528	8664	8528
SF-QB-5	11.297	11.731	8.492	1306	1303	1306	1303
SF-BG-1	5.947	10.631	8.180	1023	1010	1201	1197
SF-BG-3	5.656	10.632	12.350	2331	2312	2655	2632

Notes: Thickness-averaged production rates assume no snow cover. ΨCa = from spallation of Ca; ΨK = from spallation of K; ΨN = from thermal neutron activation.

The ages calculated using the data of Phillips et al. (2001) are older than those determined using the data of Swanson and Caffee (2001). Assuming no snow cover or erosion, boulder ages determined using the Phillips et al. (2001) data are approximately: 4100 and 3800 ^{36}Cl yr BP for Lillooet Glacier; 11,500 and 1800 ^{36}Cl yr BP for Diadem Glacier; and 3600 and 1700 ^{36}Cl yr BP for Berendon Glacier. Using the data of Swanson and Caffee (2001), they are approximately: 3000 and 2800 ^{36}Cl yr BP for Lillooet Glacier; 8500 and 1300 ^{36}Cl yr BP for Diadem Glacier; and 2600 and 1200 ^{36}Cl yr BP for Berendon Glacier.

Regardless of which production rate data are used, the calculated ages, with the exception of the 11,500 ^{36}Cl yr BP age at Diadem Glacier, suggest that moraine construction at each site later than predicted by other indirect evidence (Chapter 2). Potential causes of the discrepancy between the ages of glacier advances inferred by the cosmogenic dating and by the data presented in Chapter 2 are discussed in the next section.

Factors Producing Error in Age Interpretation

Erosion and Shielding

The dated boulders showed little evidence of erosion. Weathering rinds are less than 3 mm thick and grain relief is 1-2 mm (see Appendix B). Similar observations on late-glacial boulders led Jackson et al. (1999) to apply no correction for erosion to their ^{36}Cl ages. In view of the lack of obvious erosion, a zero erosion rate was also applied in this study.

The accuracy of the snow cover correction used in this study is questionable, because of the lack of snowpack data. Available modern snow course data are limited in duration and quality, and likely are not representative of past conditions. CHLOE assumes a planar snow surface, in which boulders are only covered if their height is less than the assigned monthly snow depth. This assumption is oversimplistic. According to CHLOE, the Diadem Glacier samples require no snow cover correction because the sampled boulders are higher than the predicted snowpack.

Exhumation

Hallet and Putkonen (1994) and Putkonen and Swanson (2003) examined the uncertainty in moraine ages caused by erosion of the moraine itself. In both studies, numerical simulations of moraine surface evolution are used to quantify the observation that moraines become wider and flatter with time. They modeled erosion as a diffusive sediment-transport process using moraine slopes between the angle of repose (34°), representative of initial conditions, and 31° taken as a lower end estimate.

To examine the possibility of boulder ages being too young due to exhumation, hypothetical profiles of the outer moraines at the three study sites (Figure 27) were constructed with moraine slopes of both 34° and 31°. The initial moraine crests were inferred by projecting these slopes (Figure 28). The profiles of the Lillooet and Berendon glacier moraines using angles of 34° and 31° are similar to the present outer moraine profiles. At an angle of 31°, sample SF-BG-1 could have been exhumed, as the boulder height is less than the projected moraine height. At an angle of 34°, both of the Berendon boulders could have been exhumed, but the Lillooet boulders remain above the projected initial moraine height and therefore were likely not exhumed.

The Diadem Glacier moraine profile is problematic. It is possible that sample SF-QB-5, which yielded an erroneous young age, is exhumed. The reconstructed moraine profiles and projected initial moraine heights, however, require almost 6 m of exhumation, which seems unrealistic. The moraine slope angle for Diadem Glacier's Little Ice Age moraine averages 15-16°, which is notably less than the slope angles of the Little Ice Age moraines at Berendon and Lillooet glaciers. It is, therefore, unlikely that the low angle slope of both the outer and Little Ice Age Diadem moraines is purely the result of erosion since construction. A more probable explanation is that the moraine profiles are partly controlled by underlying bedrock. A bedrock ridge forms the distal side of the outer moraine, dropping off steeply to the valley below. This drop off gives the moraine an asymmetrical appearance (Fig. 27). The moraine probably never had a typical moraine-type profile, and it is unlikely that the young boulder age is due to exhumation.

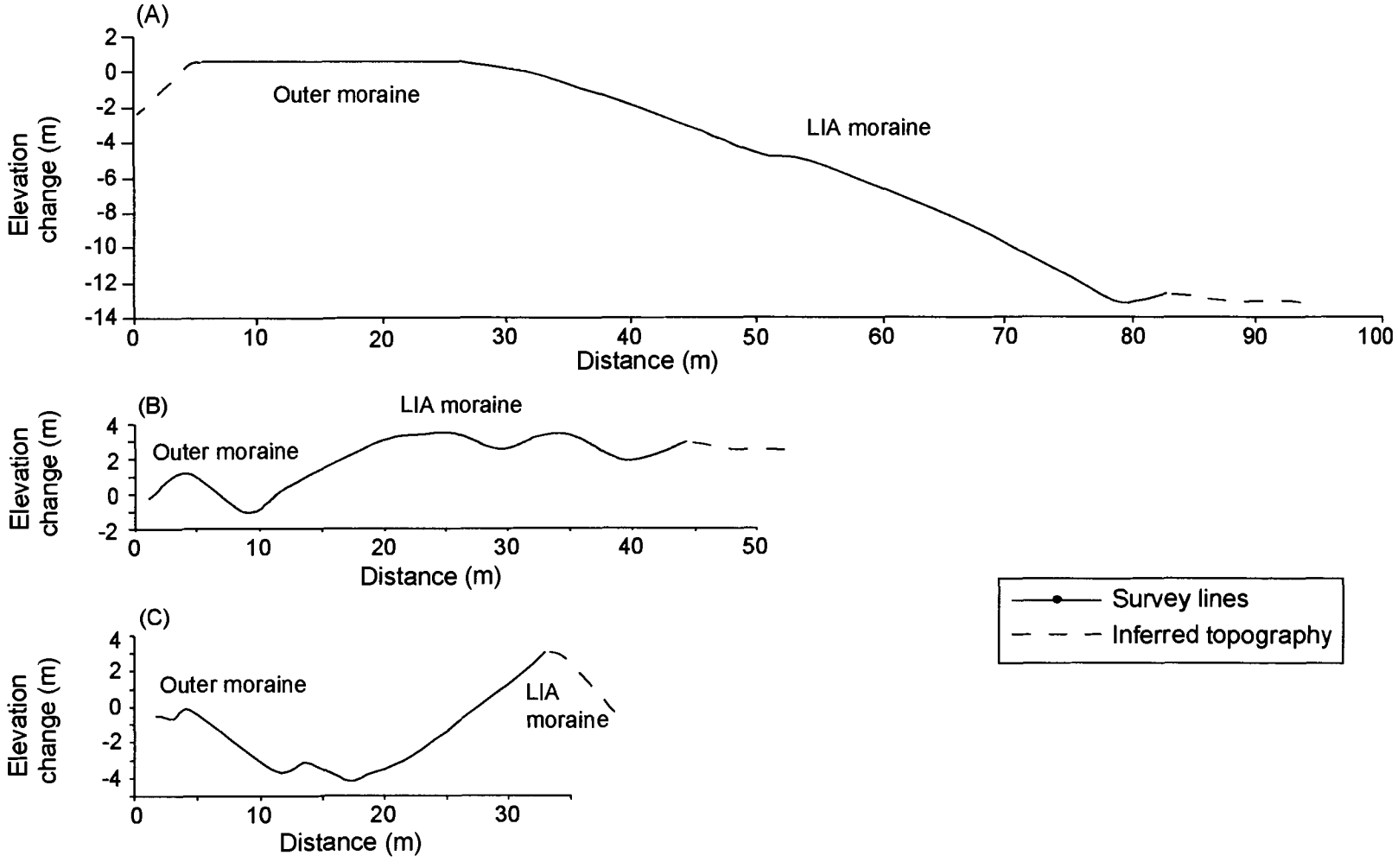

Figure 27. Profiles of moraines at (A) Diadem Glacier, (B) Berendon Glacier, and (C) Lillooet Glacier. Transects are approximately perpendicular to the crests of the moraines. LIA refers to Little Ice Age. See Figures 1, 8, and 13 for profile locations.

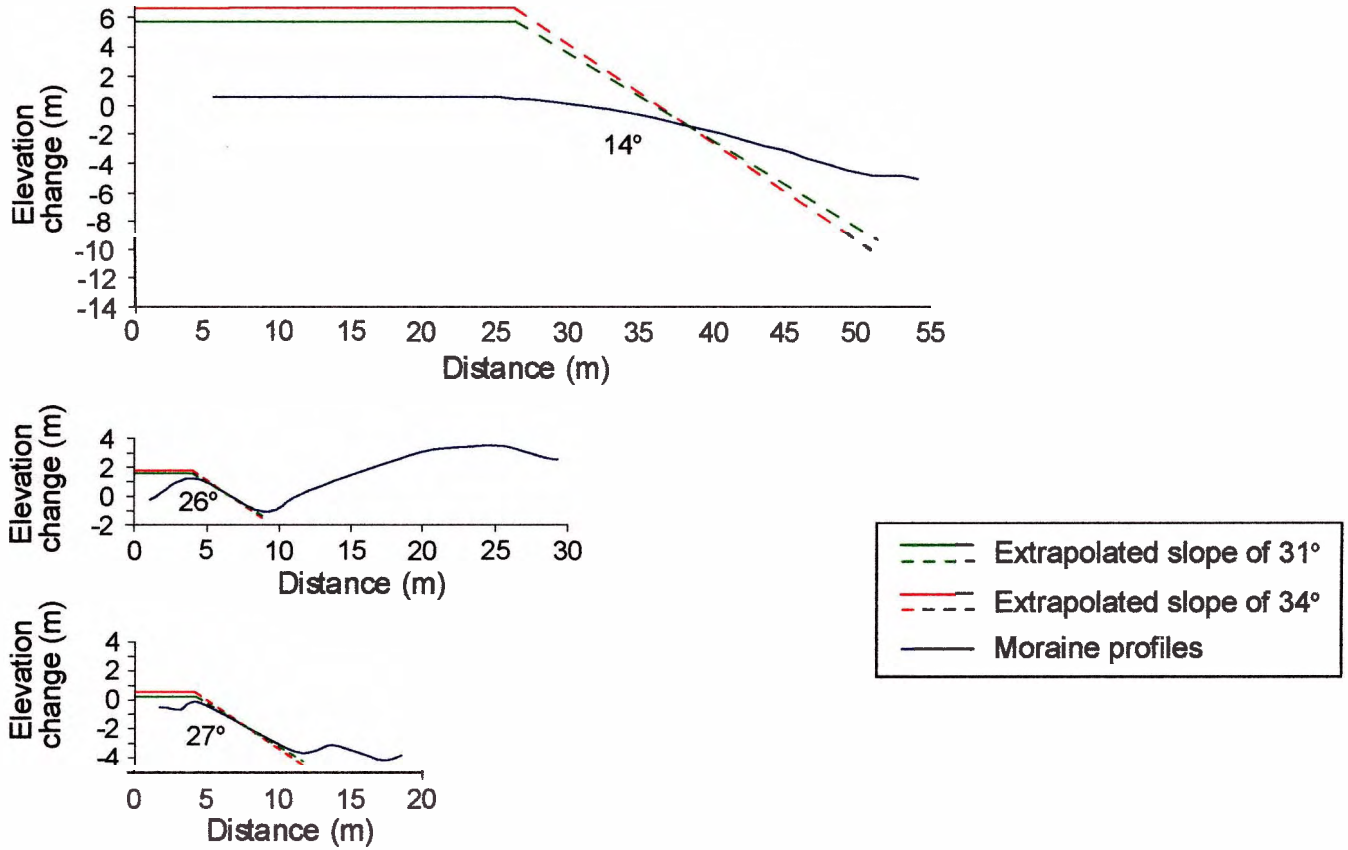

Figure 28. Moraine profiles with extrapolated pre-exhumation slopes of 31° and 34°. Angles shown are the measured slope angles of the ice-proximal side of the outer moraines at the time of boulder sampling.

Production Rates

The significant difference in ages obtained using the two sets of production rate data mentioned earlier renders the corrections made for snowpack and erosion comparatively minor. This study uses the rates of Swanson and Caffee (2001) for two reasons. First, their calibration dataset is better constrained geographically. It is also based on samples collected in the Puget Lowland, close to the southern Coast Mountains of British Columbia. This proximity minimizes the amount of scaling required for the samples in my study, with the exception of the Berendon samples. Second, the production rate data of Swanson and Caffee (2001) are based on samples of similar age to those in this study.

Discussion

Anomalous Boulder Ages

Lillooet Glacier

The Lillooet samples suggest an age for the outer moraine of ca. 2800 yr BP, assuming no snow cover or erosion. The two ages accord with each other, and the sampled boulders do not appear to have been eroded or exhumed. However, stratigraphic data and radiocarbon ages from the moraine-dammed ponds indicate that the moraine is older than 6200 ^{14}C yr BP, and there is no evidence that the boulders were deposited on the outer moraine during a second, Tiedemann-age advance (see Chapter 2, *Lillooet Glacier*).

This evidence calls into question the credibility of all the boulder ages. McCrumb (2001) was able to constrain a late-glacial advance in Howe Sound to between 12,400 ± 500 and 10,600 ± 600 ^{36}Cl yr BP, a result that is consistent with radiocarbon-dated records. The calibration data of Swanson and Caffee (2001) are based partly on the Ring Creek lava flow, independently dated at 12,800-10,600 cal yr BP. Given the proximity of both the lava flow and Howe Sound to Lillooet Glacier, it might seem reasonable that valid ^{36}Cl ages could be obtained on the Lillooet boulders if they both were late-glacial as suggested by other evidence.

Diadem Glacier

The age obtained for sample SF-QB-5 (ca.1300 ^{36}Cl yr BP) is anomalously young. A radiocarbon age on charcoal within aeolian sediments on top of the moraine (see Chapter 2, *Diadem Glacier*) indicates that the moraine is older than 6200 ^{14}C yr BP. As previously mentioned, the young age is likely not due to exhumation. Post-depositional movement of the boulder is further unlikely given its position and large size. One possible explanation is that the boulder was subject to fire spalling (Bierman and Gillespie, 1991), which resulted in a significant loss of surface material. Regardless of the explanation for the young age, the second boulder (SF-QB-4) is much older, ca. 8500 ^{36}Cl yr BP. While this age is consistent with the radiocarbon age, it cannot be assumed to date the moraine.

Berendon Glacier

The two ^{36}Cl ages of the Berendon Glacier boulders (ca. 2331 and 1023 ^{36}Cl yr BP) differ by 1300 years. It is possible that one or perhaps both of the boulders are younger than the moraine due to exhumation. Core BP2 from Berendon Pond, however, indicates that the moraine is likely older than 3500 ^{14}C yr BP (see Chapter 2, *Berendon Glacier*). Berendon Fen also shows no evidence for moraine construction in the middle or early Holocene. Regardless of the production rate data used, the ^{36}Cl ages predicted for the boulders are too young.

Summary

All six boulder ages are in error to some extent, suggesting that some unknown factor is responsible for the much younger-than-expected cosmogenic ages. It is possible that geomagnetic field effects are responsible for the problem. Geomagnetic field intensity has varied over 10 ka timescales for the past 5 Ma (Gosse and Stone, 2001). This effect is negligible over long time scales, but variations in intensities over the past 10 ka have been accompanied by changes in production rates of up to 20% (Gosse and Stone, 2001). Similarly, effects of magnetic secular variation on production rates are negligible for integrated production rates at timescales greater than 8 ka, but rates for the past 4 ka

have varied up to 20% (Gosse and Stone, 2001). These effects may perhaps explain errors in the Berendon boulder ages. They cannot, however, account for the Diadem and Lillooet ages as those moraines are likely late-glacial. To obtain the minimum age of 6000 ^{14}C yr BP for the outer moraine at Lillooet Glacier, the cosmogenic ages must be at least 50% too young. One final possibility is laboratory error. It seems unlikely that all the samples were analyzed incorrectly, but this possibility cannot be precluded.

Conclusion

The ^{36}Cl ages determined in this study contribute only limited insight into the times of glacier advances at the three study sites, but the conflicting evidence demands a critical reassessment of the cosmogenic ^{36}Cl dating method. Given the possible errors in cosmogenic age dating, it is essential to have a large sample population that allows spurious ages to be detected and eliminated. Putkonen and Swanson (2003) compiled a dataset of all published cosmogenic ages and found that the difference between the oldest and youngest boulder on a single moraine commonly exceeds the uncertainty terms of individual ages by an average of 38%. This result demonstrates the susceptibility of boulders to age-altering geologic factors and reinforces the need for a large sample size. Dating of moraines using multiple nucliides, such as ^{10}Be in conjunction with ^{26}Al, would be beneficial in similar studies in the future to determine possible weathering effects on boulder age and, further, to provide a check on the accuracy of individual boulder ages.

This study also brings into question the validity of attempting to constrain the age of young moraines. While it is hypothesized that some of the boulders in this study are late-glacial in age, the boulders may be too young to conform to the theoretical relationship between apparent age and actual age. Given the variations in the Earth's geomagnetic field (Gosse and Stone, 2001), it is further likely that apparent ages of less than 4 ka will be in error.

A final issue is the difference in apparent ages resulting from the use of different calibration data. While there has been a significant increase in the use of ^{36}Cl in Quaternary studies during the last decade, the increase has not been matched by proper

calibration studies. The result is likely to be a proliferation of errant cosmogenic ages in the literature. This problem must be dealt with before the ^{36}Cl dating method can be reliably used in Quaternary studies. Finally, comparison of ^{36}Cl ages from different studies requires standardization of cosmogenic sampling and age calculation methods.

4 Equilibrium-line Altitude Reconstructions

Introduction

The impact of climate variations on glaciers is commonly assessed by determining changes in glacier mass balance. Comparison of a glacier's present and past equilibrium-line altitudes (ELA) provides a robust means of documenting long-term mass balance changes. The ELA of a glacier is the elevation on the glacier surface where annual ablation equals annual accumulation. Changes in ELA position reflect either gains or losses in net mass balance.

Several methods can be used to determine the position of modern and paleo ELA. Determination of modern ELA from direct mass balance measurements is preferred, but this method is costly and, therefore, rarely done. The transient snowline, visible on air photographs as the upper limit of perennial snow cover at the end of an ablation season, commonly coincides with the ELA on temperate glaciers (Ostrem, 1966). Air photo coverage of modern glaciers, however, is rarely sufficient to use snowlines as an approximation of ELA.

In view of these limitations, mathematical relationships between glacier mass balance and altitude have been established to estimate modern ELA when mass balance data are not available. These relationships are also used to estimate the ELAs of former glaciers. Of these relationships, the accumulation area ratio (AAR) is the most widely used. AAR relates a glacier's accumulation area to its total area and assumes that a specific proportion of glacier mass is above the equilibrium line (Benn and Evans, 1998; Brugger and Goldstein, 1999, and references therein). Another area-altitude relationship is the toe-to-headwall ratio (THAR), which fixes ELA at a determined position between the glacier toe and the cirque headwall (Porter, 1964; Meierding, 1982). ELAs of glaciers have also been approximated by their median elevation and by the elevation of a glacier's highest lateral moraine, which, it is assumed, is the place where glacier erosion changes to deposition (Meierding, 1982).

Few reconstructions of glacier ELA have been done in the Coast Mountains of British Columbia. Ostrem (1966) indirectly determined the ELA of glaciers in the Coast Mountains by mapping the glaciation limit, a surface that is parallel to the ELA. Ohmura

et al. (1992) provide a summary of modern ELA for 70 mid- and high-latitude glaciers, of which eleven are in the Coast Mountains. Mayo (1984) includes Berendon Glacier in a compilation of mass balance gradients for several U.S. glaciers, calculated using modern mass balance data. Modern ELA values have also been calculated for Sentinel and Place glaciers using mass balance records (Ostrem, 1973; Letreguilly, 1988; Ohmura et al., 1992; Moore, 1993). Hurley (1996) estimated modern and Neoglacial ELAs for several glaciers in the North Cascades, Washington.

This chapter estimates modern ELA for the three glaciers in this study and compares the values to ELA calculated for former glaciers defined by Little Ice Age moraines at each site. The older outer moraines are much more fragmentary than the Little Ice Age moraines, but lie just outside of them. ELAs of the glaciers that built these outer moraines are nearly the same as the ELAs of the Little Ice Age glaciers and, therefore, the Little Ice Age moraines serve as proxies for the older advances.

Methods

The Little Ice Age limits of the three glaciers were mapped on air photos using locations of glacial trimlines and moraines. Ice extents were then transferred to 1:50 000-scale maps.

Areas between index contours on ice surfaces were measured with a planimeter to calculate modern and Little Ice Age ELAs. The mean of at least three area measurements was used for each increment. All measurements for the larger Berendon and Lillooet glaciers were repeated to verify results. Area values were converted to percentages of total glacier area and then plotted as cumulative percentage graphs. Toe-to-headwall altitude ratios were calculated to assess the credibility of individual ELA values. Glacier median altitudes and elevations of highest lateral moraines were also determined.

Modern and Little Ice Age ELAs were interpolated from the area distribution curves using an AAR value of 0.65±0.05, rounded off to the nearest 5 m. Assuming steady-state conditions, mid- and high-latitude glaciers have AAR values between 0.50 and 0.80, and

most glaciers have values between 0.55 and 0.65 (Benn and Evans, 1998, and references therein). A mean value of 0.65 was chosen based on Hurley's (1996) reconstructions of ELA for valley glaciers in the North Cascades.

THAR values ranging from 0.35 to 0.50 have been used to estimate ELAs of former glaciers (Brugger and Goldstein, 1999, and references therein). Meierding (1982) found that a THAR value of 0.40 and an AAR of 0.65 best described larger glaciers (> 3 km^2) in the Colorado Front Range. For smaller cirque glaciers in the Pacific Northwest, Porter (1964) concluded that a THAR value of 0.50 or the median altitude best approximates ELA.

Results

Ice extents of modern and Little Ice Age maximum glaciers are shown in Figures 29, 31 and 33. Corresponding glacier hypsometries and ELAs are depicted in Figures 30, 32, and 34. Calculated glacier areas, THAR values, and ELAs are presented in Table 5, and interval area data are given in appendixes F, G, and H.

Lillooet Glacier

The tributary glacier north of Lillooet Glacier contributed significantly to the latter's downvalley extent during the Little Ice Age. The glacier was approximately 75% greater in size than it is today. However, the overall hypsometry of Lillooet Glacier during the Little Ice Age was similar to that of the modern glacier, because the increase in mass due to the addition of the second, northern accumulation area was counterbalanced by glacier growth in the Silt Lake area. ELAs calculated using an AAR of 0.65 are 1740 ± 80 m asl for the modern glacier and 1600 ± 60 m asl for the Little Ice Age glacier. THAR values calculated using these ELA values are 0.45 and 0.39 for the modern and Little Ice Age glaciers, respectively. ELAs predicted by the median altitude method are 1829 m asl for both glaciers, whereas the elevation of the highest lateral moraine gives an ELA of 1690 m asl for the Little Ice Age glacier. Assuming an AAR of 0.65, the Little Ice Age ELA depression is approximately 140 m.

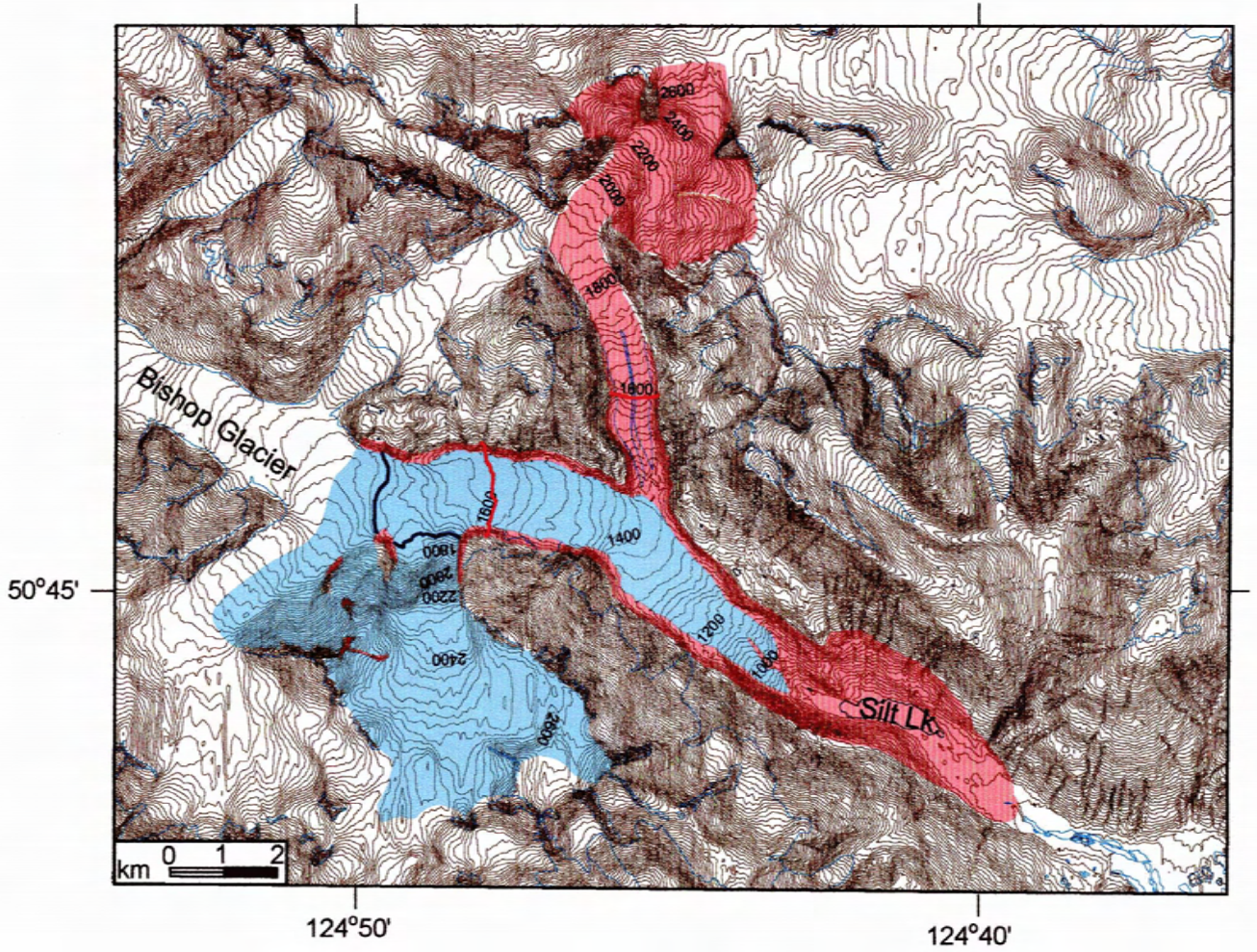

Figure 29. Map of Lillooet Glacier showing its modern (blue) and Little Ice Age (red) extent. The red lines indicate the approximate position of the equilibrium line of the glacier during the Little Ice Age. The blue line is the equilibrium line of the modern glacier. Reproduction of B.C. TRIM maps 92J.071, 92J.072, 92J.081, and 92J.082, courtesy of the Government of British Columbia, Base Mapping and Geomatic Services Branch.

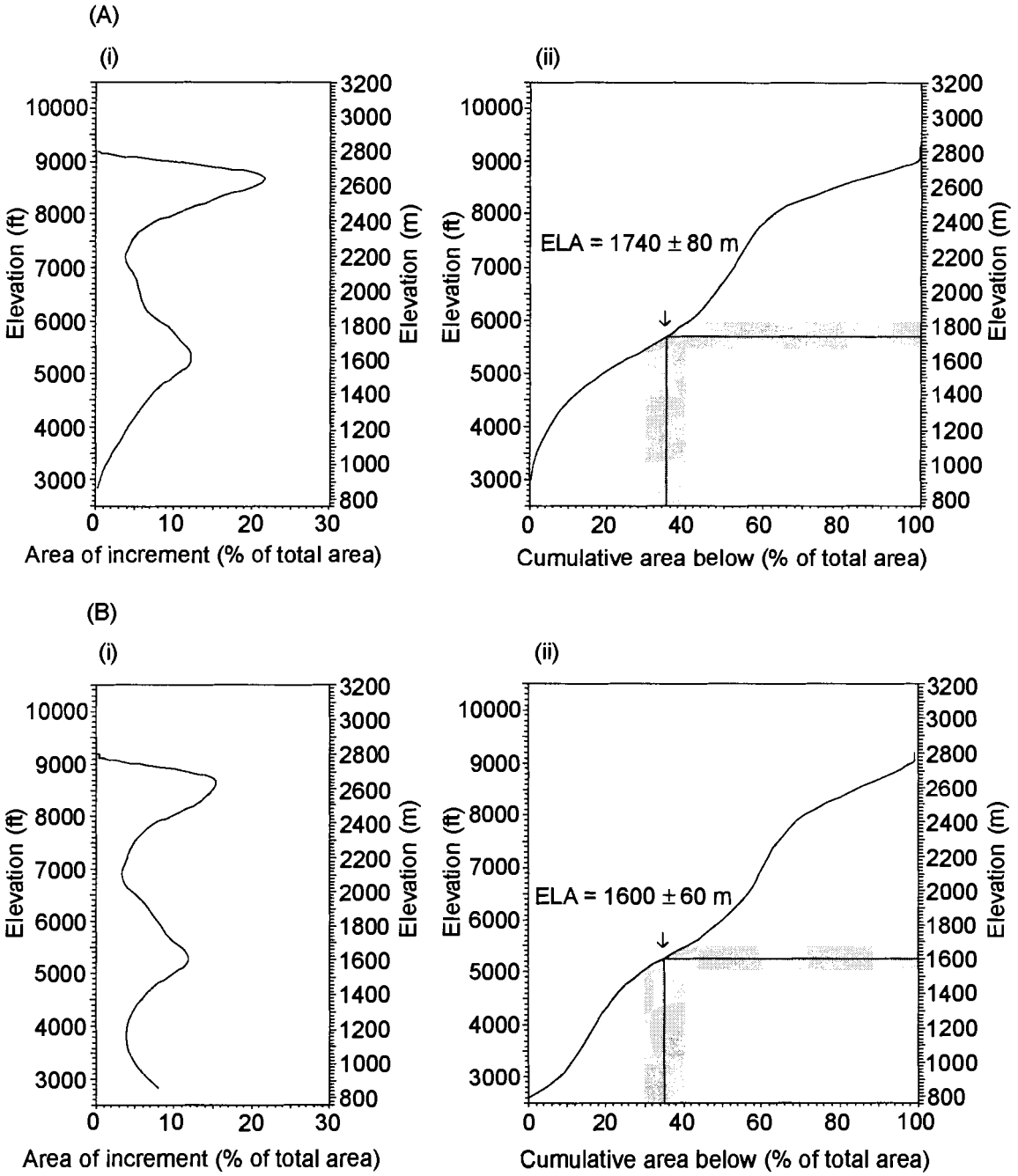

Figure 30. Distribution of surface area of Lillooet Glacier (A) today and (B) at the Little Ice Age maximum. (i) Hypsometry. (ii) Calculated equilibrium-line altitude.

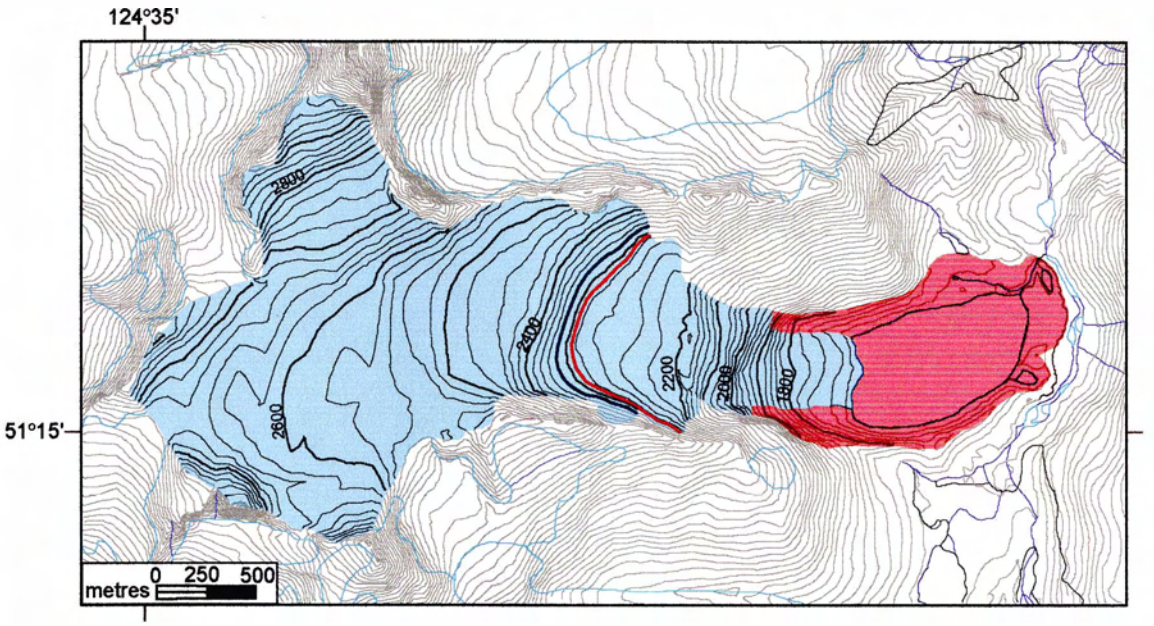

Figure 31. Map of Diadem Glacier showing its modern (blue) and Little Ice Age (red) extent. The red line indicates the approximate position of the equilibrium line of the glacier during the Little Ice Age maximum. The blue line is the equilibrium line of the modern glacier. Reproduction of B.C. TRIM map 92N.028, courtesy of the Government of British Columbia, Base Mapping and Geomatic Services Branch.

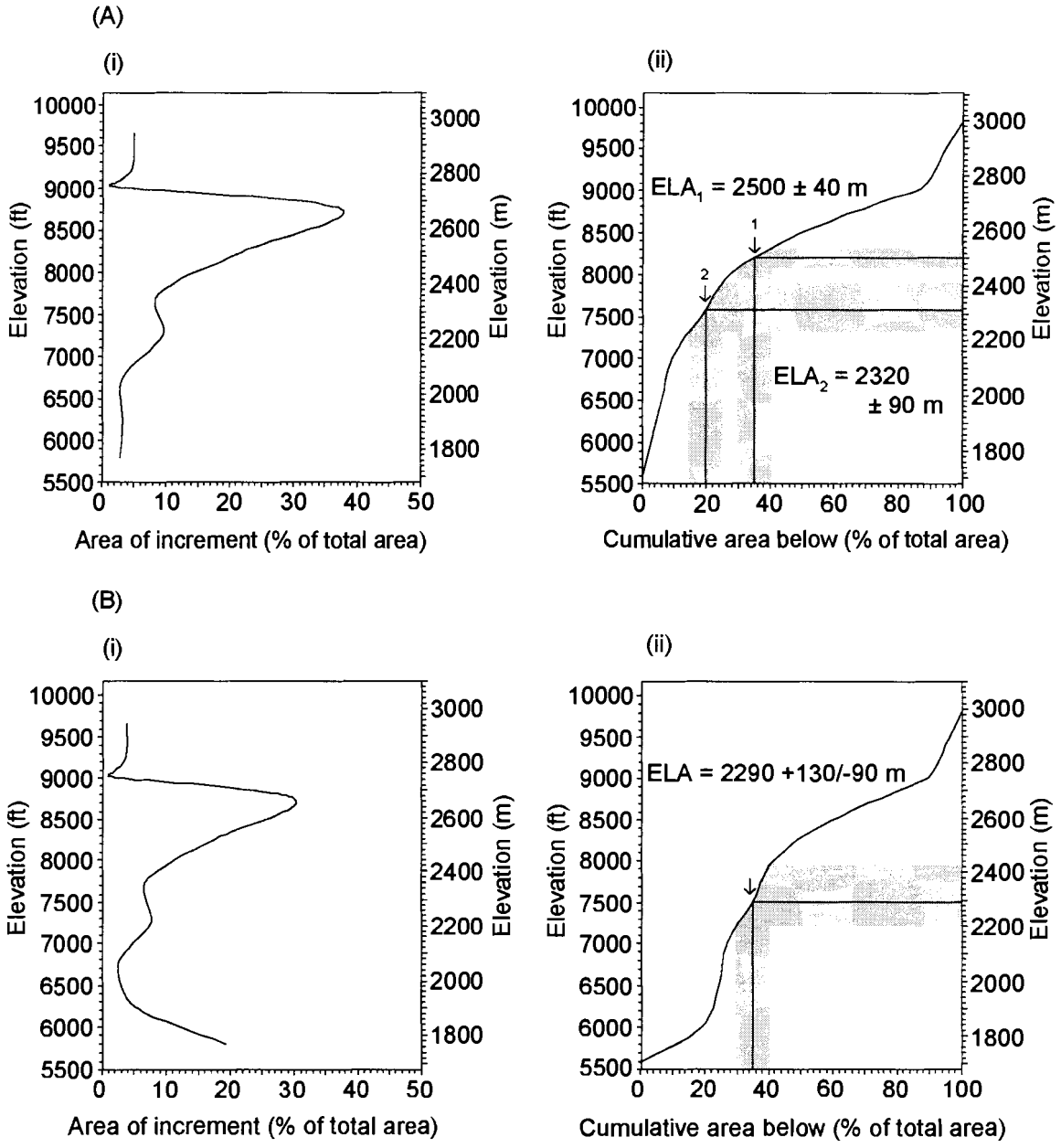

Figure 32. Distribution of surface area of Diadem Glacier (A) today and (B) at the Little Ice Age maximum. (i) Hypsometry. (ii) Calculated equilibrium-line altitude.

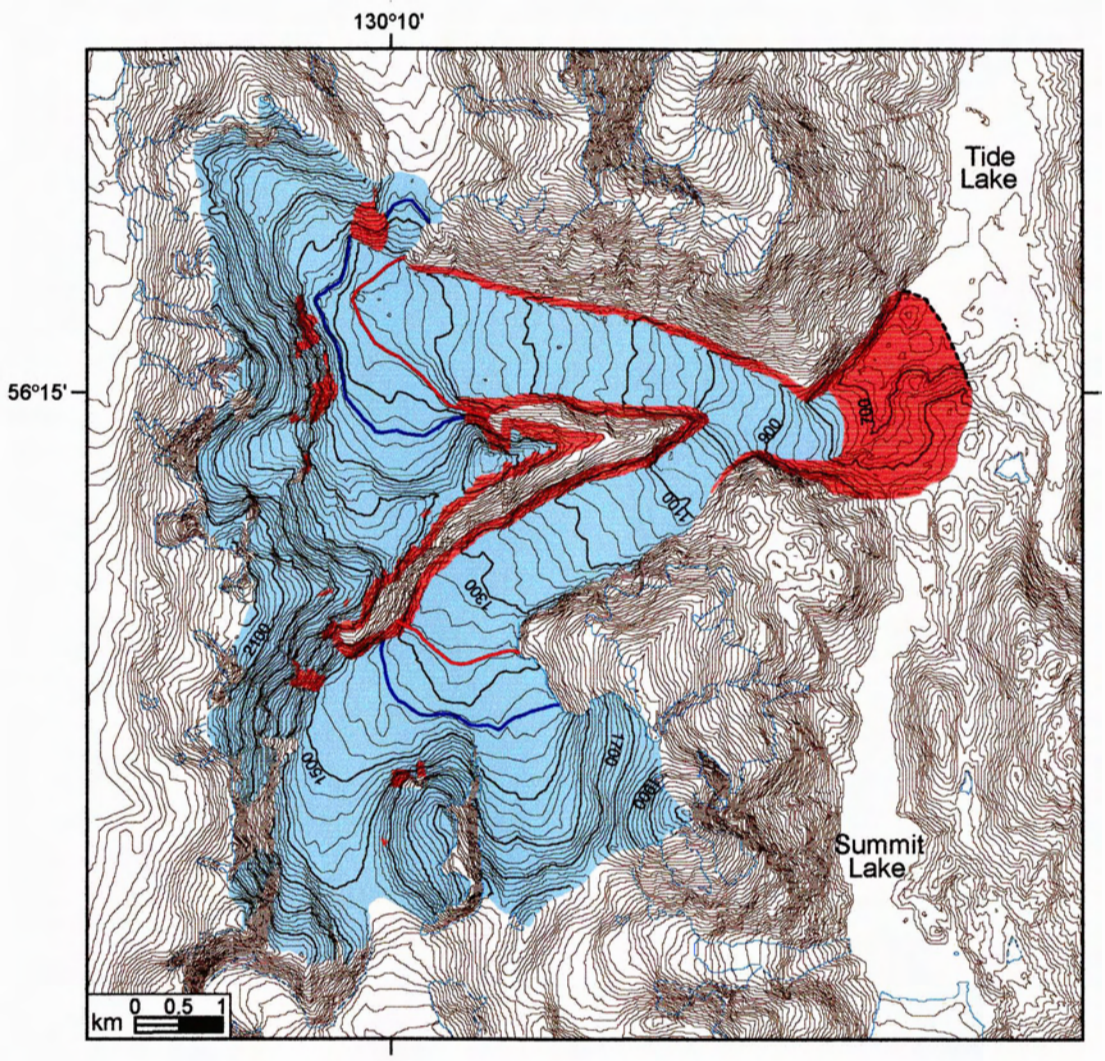

Figure 33. Map of Berendon Glacier showing its modern (blue) and Little Ice Age (red) extent. The red lines indicate the approximate position of the equilibrium line of the glacier during the Little Ice Age. Blue lines indicate the equilibrium line of the modern glacier. The dashed line is the interpolated segment of the Little Ice Age margin (see text for details). Reproduction of B.C. TRIM maps 104B019, 104B.020, 104B.029, and 104B.030, courtesy of the Government of British Columbia, Base Mapping and Geomatic Services Branch.

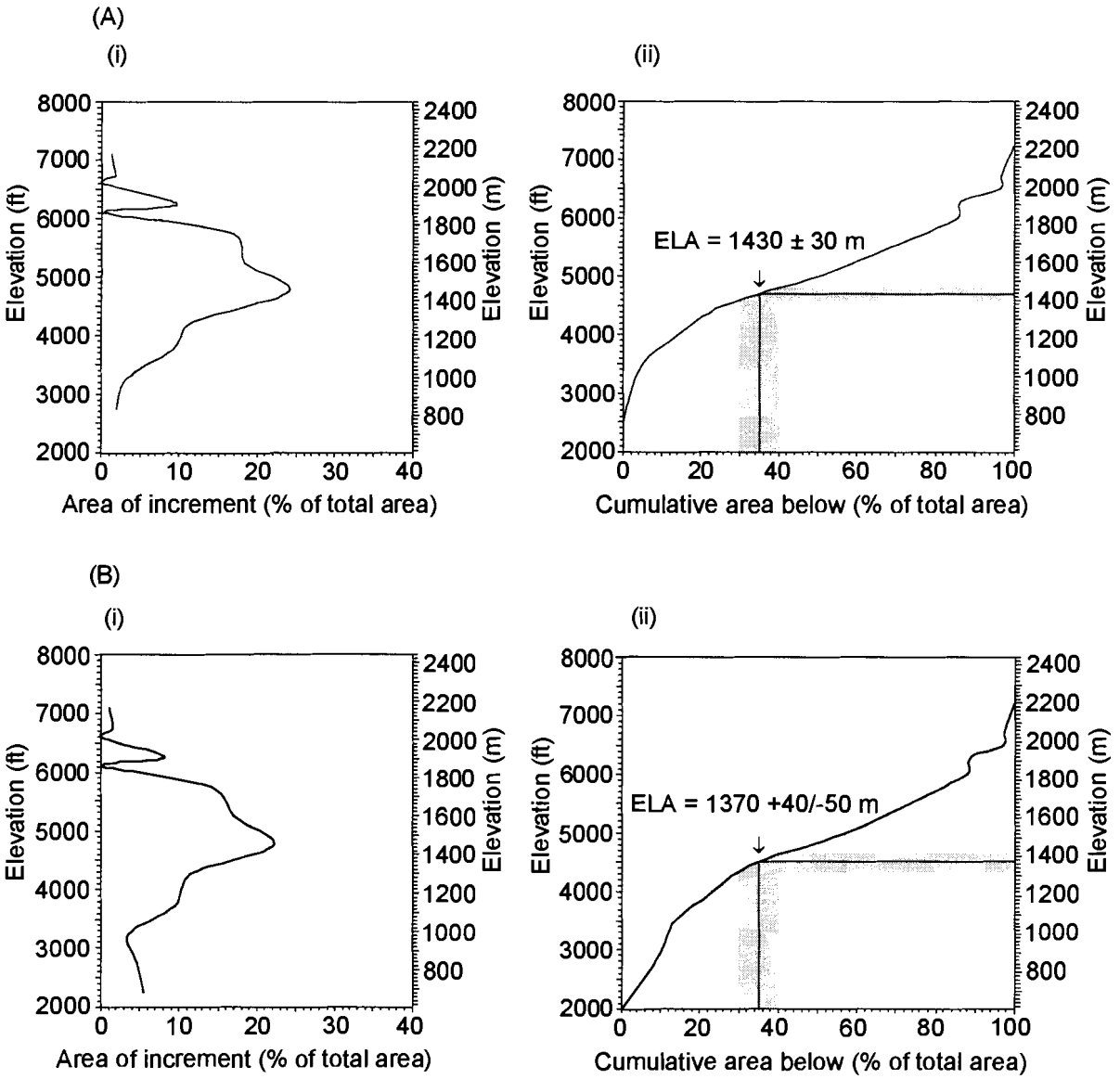

Figure 34. Distribution of surface area of Berendon Glacier (A) today and (B) at the Little Ice Age maximum. (i) Hypsometry. (ii) Calculated equilibrium-line altitude.

Table 5. Modern and Little Ice Age (LIA) equilibrium-line altitudes (ELA) and reconstructed glacier areas.

	Lillooet Glacier		Diadem Glacier		Berendon Glacier	
	Modern ELA	LIA ELA	Modern ELA	LIA ELA	Modern ELA	LIA ELA
Accumulation area ratio (m)[1]	1740	1600	2500/2320[4]	2290	1430	1370
Median altitude (m)	1829	1829	2363	2363	1524	1448
Highest moraine elevation (m)	-	1690[3]/1600	-	1900	-	1200
Toe-to-headwall ratio	0.45	0.39	0.62/0.48	0.46	0.47	0.47
Total glacier area (km^2)	32.14	56.29	5.96	7.43	34.42	41.27
ELA depression (m)[2]	-	140	-	210/30[4]	-	60

[1] Elevations calculated using an AAR of 0.65 unless otherwise stated.

[2] ELA depressions calculated using the AAR method.

[3] 1690 m elevation is from small valley glacier; 1600 m elevation is from the main Lillooet valley.

[4] ELA elevation of 2320 m calculated using an AAR of 0.80, with a THAR of 0.48.

Diadem Glacier

The accumulation area of Diadem Glacier was not significantly different at the Little Ice Age maximum than today. The hypsometry of the Little Ice Age glacier shows a shift of glacier mass to lower elevations, with the formation of a small piedmont lobe where Queen Bess Lake sits today.

The glacier was approximately 25% larger during the Little Ice Age than today. The hypsometries of the modern and Little Ice Age glaciers, however, reveal complex area-altitude distributions that necessitate the use of different AAR values (see following discussion). An ELA of 2500 ± 40 m asl was initially calculated for the modern glacier using an AAR of 0.65. The corresponding high THAR value of 0.62, however, led to a re-assessment of the AAR value. After recalculating ELAs using a range of AAR values between 0.65 and 0.80, an AAR of 0.80 was found to give the most reasonable THAR value (0.48). The recalculated modern ELA using an AAR of 0.80 is 2320 ± 90 m asl. A Little Ice Age ELA of 2290 +130/-90 m asl was obtained using an AAR of 0.65. This AAR value gives an acceptable THAR of 0.46. ELA predicted from the median altitude for both the Little Ice Age and modern glaciers is ca. 2363 m asl. The highest moraine elevation gives a much lower ELA of 1900 m asl. Using values obtained by the AAR method, the Little Ice Age ELA depression is at least 30 m.

Berendon Glacier

The hypsometry of Berendon Glacier differed little between the Little Ice Age and the present. The only major addition in mass during the Little Ice Age was at the glacier terminus. The Little Ice Age increase in glacier size of approximately 18% is small compared to the increases in size of Lillooet and Diadem glaciers (75% and 25%, respectively). ELAs calculated using an AAR of 0.65 are 1430 ± 30 m asl for the modern glacier and 1370 +40/-50 m asl for the Little Ice Age glacier. ELAs calculated using the median altitude method are higher, 1524 m asl and 1448 m asl, for the modern and Little Ice Age glaciers respectively. The highest moraine elevation predicts a Little Ice Age ELA of 1200 m asl. Assuming an AAR of 0.65, the Little Ice Age ELA depression is approximately 60 m.

Discussion

Errors

Several errors are inherent in determining ELAs using the AAR and THAR methods, the most significant being that the methods don't directly account for glacier hypsometry. They instead assume uniform mass balance over the entire glacier, which can lead to skewed area-altitude distributions (Brugger and Goldstein, 1999). This issue becomes apparent when dealing with, for example, piedmont-type glaciers, which have surplus area at low elevations and consequently would have AAR values lower than the average of 0.65.

There are also errors associated with the measurement of area increments and definition of ice margins. The ± 0.05 uncertainty value commonly associated with AAR values is thought to be sufficient to account for these errors (Brugger and Goldstein, 1999). The steep topography bordering the valley glaciers analyzed in this study and large size of the glaciers also minimize these errors. It is important to note, however, that the ± 0.05 uncertainty reflects glacier hypsometry and not precision of the area increment measurements.

Finally, ELA analysis assumes that the glaciers were in an equilibrium state when the moraines were deposited. This assumption is valid as long as the glaciers were not rapidly gaining or loosing mass, for example by surging or calving. None of the glaciers is known to have surged, and the Little Ice Age moraines must have formed during an extended period of advance, which is not characteristic of surging. Calving may have affected the Little Ice Age ELA value calculated for Berendon Glacier, as this glacier terminated in Tide Lake.

Assumptions Made in Equilibrium-Line Altitude Reconstructions

Lillooet Glacier

Two problems were encountered in reconstructing Little Ice Age Lillooet Glacier. The main southern accumulation area was assumed to be similar to that of today, except for several small areas that are presently ice free. Ice cover in these areas was

extrapolated to elevations of adjacent valley trimlines. Any error in calculated ELA values resulting from the inclusion of these areas is insignificant, as similar ELA values were obtained by including and excluding the areas. The second assumption is that the ice divide between Bishop and Lillooet glaciers during the Little Ice Age was in the same position that it is today. Bishop Glacier currently calves into a rapidly expanding proglacial lake. The lake did not exist at the Little Ice Age maximum. A consistent mass balance relationship between the two glaciers since the Little Ice Age maximum is, therefore, unlikely, but it is impossible to infer anything other than a stable ice divide position without a better understanding of Bishop Glacier's Little Ice Age history.

Diadem Glacier

It was assumed that the Little Ice Age accumulation area of Diadem Glacier was similar to that of today. This assumption is reasonable because the accumulation area is within steep terrain that shows no evidence for overtopping of ridges by the Little Ice Age glacier.

Berendon Glacier

The reconstructed Little Ice Age accumulation area of Berendon Glacier is very similar to the present-day accumulation area. The glacier is connected to a large icefield, but steep valley walls on the north side of the glacier probably limited mass balance shifts with Frank Mackie Glacier during the Little Ice Age. Small exposed areas in the accumulation area below the elevation of mappable trimlines were included in the Little Ice Age area calculations. As in the case of the Lillooet Glacier, any error resulting from the inclusion of these small areas is considered insignificant.

The main difficulty in reconstructing the Little Ice Age glacier is interpreting the former ice margin in the Tide Lake basin, where there is no terminal moraine. The Little Ice Age terminal moraine can be mapped along the southern periphery of Berendon Glacier (Fig. 33), but it is not evident in the Tide Lake basin because the glacier calved into the lake (Clague and Mathews, 1992). The Little Ice Age glacier margin was, therefore, extended along the lake basin from the terminal moraine to the trimline on the west side of the

valley (Fig. 33). The potential error associated with this issue is discussed in the following section.

Reconstructed Glacier Equilibrium-line Altitudes

Lillooet Glacier

The differences in Little Ice Age ELA values calculated by the different methods (Table 5) likely reflect a complex mass balance relationship created by the second northern accumulation area. This complexity is illustrated by the 90 m difference in elevation between the highest lateral moraine of the northern tributary glacier and the highest lateral moraine of the main Lillooet Glacier valley. Although the ELAs determined from the highest lateral moraine and using the AAR method agree, the moraine is discontinuous and it may not be representative of the highest moraine deposited during the Little Ice Age.

The median altitude method appears to be insensitive to changes in glacier area because it gives equal ELA values for the modern and Little Ice Age glaciers. This insensitivity is due to similar elevation ranges used to reconstruct both glaciers (Appendix F). The Little Ice Age value is probably in error. While the modern ELAs calculated by the median altitude and AAR methods are relatively similar compared to those of the Little Ice Age, the two modern values do not overlap within error.

Moore (1993) estimated the ELA of Lillooet Glacier for the years between 1970 and 1980. He assumed that climate at Lillooet Glacier is intermediate between that of Place and Sentinel glaciers. He obtained modern ELA values of 1800-2200 m asl by varying model parameters until he obtained ELA values between those calculated for Place and Sentinel glaciers. Photographs taken on a flight over Lillooet Glacier at the beginning of September 2002 show that snowline was approximately 1780 m asl. While snowline only approximates ELA, this observation suggests that modern ELA is at the lower end of the range suggested by Moore (1993) and slightly higher than, but within the error of, the ELA calculated here using the AAR method.

Diadem Glacier

The Little Ice Age ELA of Diadem Glacier (2290 m asl) calculated using an AAR of 0.65 gives an acceptable THAR value, and the ELA area-elevation plot shows a relatively even distribution of mass. In contrast, the modern glacier possesses a large concentration of mass at high elevations. Assuming the glacier is in equilibrium, its hypsometry dictates a larger AAR value. If the AAR value, however, is increased to give a reasonable THAR value, the ELA drops to 2320 ± 90 m asl. This large drop in elevation is due to the convex shape of the ELA curve, which produces significant changes in elevation with small changes in AAR. This second, lower modern ELA value, while theoretically more representative of the glacier's hypsometry, is problematic because it overlaps the Little Ice Age ELA range. The overlap occurs because of the large extrapolated error envelopes of both ELA values, which again is a function of the shape of the ELA curve.

The lower modern ELA value is preferred to the first value of 2500 ± 40 m asl, which gives an anomalously high ELA depression of 210 m. The average Little Ice Age ELA depression calculated by Hurley (1996) for a set of North Cascade glaciers just east of the crest of the range is approximately 100 m (see Fig. 38), and the ELA depression calculated for a small cirque moraine at Mt. Shuksan in the North Cascades is 65 m (Burrows et al., 2000). Diadem Glacier has a more continental climate than the glaciers studied by Hurley (1996) and Burrows et al. (2001), thus an ELA depression of 100 m or less would be expected. Using the same argument, the ELA depression for Diadem Glacier should be less than the 120 m calculated for Lillooet Glacier. Accordingly, 2320 ± 90 m asl is accepted as the modern ELA of Diadem Glacier.

ELAs calculated by the median altitude method are probably equal, as in the case of Lillooet Glacier, because of the insensitivity of the method to large changes in area with relatively small changes in altitude. The ELA derived from the highest moraine elevation is anomalously low due to erosion of the moraine off of steep valley walls.

Berendon Glacier

Mayo (1984) suggests that the modern net balance of Berendon Glacier is zero at approximately 1375 m asl. The point of zero mass balance should be equal to the ELA, but this value is problematic because it is only 5 m higher than the calculated Little Ice Age ELA.

One possible explanation for this inconsistency is that the Little Ice Age ELA calculated here is incorrect due either to an erroneous reconstruction of the ice margin or to the margin calving in Tide Lake. Because over half of the Little Ice Age terminal moraine is still preserved, it is unlikely that the extrapolated section is significantly in error. Furthermore, because this moraine represents the terminus of the glacier for a lengthy period, regardless of calving, the THAR method can still be used to evaluate ELA values. The calculated Little Ice Age THAR value of 0.47 is reasonable, providing some support for a calculated Little Ice Age ELA of 1370 m asl.

A second possibility is that the glacier's mass distribution is skewing the modern ELA value. Based on the hypsometric curve presented in Figure 34, the modern ELA calculated by Mayo (1984) requires an AAR of approximately 0.75. A higher AAR should correspond with a relatively greater amount of mass in the accumulation area. The profile of the reconstructed hypsometric curve for the Berendon Glacier, however, does not indicate a greater mass of ice in the accumulation area. As a result, the AAR is probably closer to 0.65 than the 0.75 required by Mayo's ELA. A modern ELA of 1420 m asl is further consistent with Little Ice Age depressions calculated by Hurley (1996) and Burrows et al. (2000).

Climatic Interpretation of Reconstructed Equilibrium-line Altitudes

Climate data at the equilibrium-line altitudes of the three glaciers is not available, thus two methods were used to estimate the relative climate change associated with the Little Ice Age advances and the advances responsible for the outer moraines.

Upper air data collected at Port Hardy (Appendix I), located at the northern tip of Vancouver Island, B.C., were used to reconstruct relative temperature change. September daily temperature and altitude values, collected at standard pressure

surfaces for the years 1951 – 1960 and 1994 – 2003, were used to construct 10-year average curves. September was chosen as this month typically represents the end of the ablation season when the ELA can be approximated by the upper limit of the perennial snow cover. Calculated ELA depressions for the three glaciers were then plotted on the curves to establish the associated temperature changes (Fig. 35). While lapse rates over land do not necessarily correspond to those in the free atmosphere, it is acceptable to use the upper air data here as only relative changes in temperature, and not absolute temperature values, were extrapolated to reflect the ELA depressions.

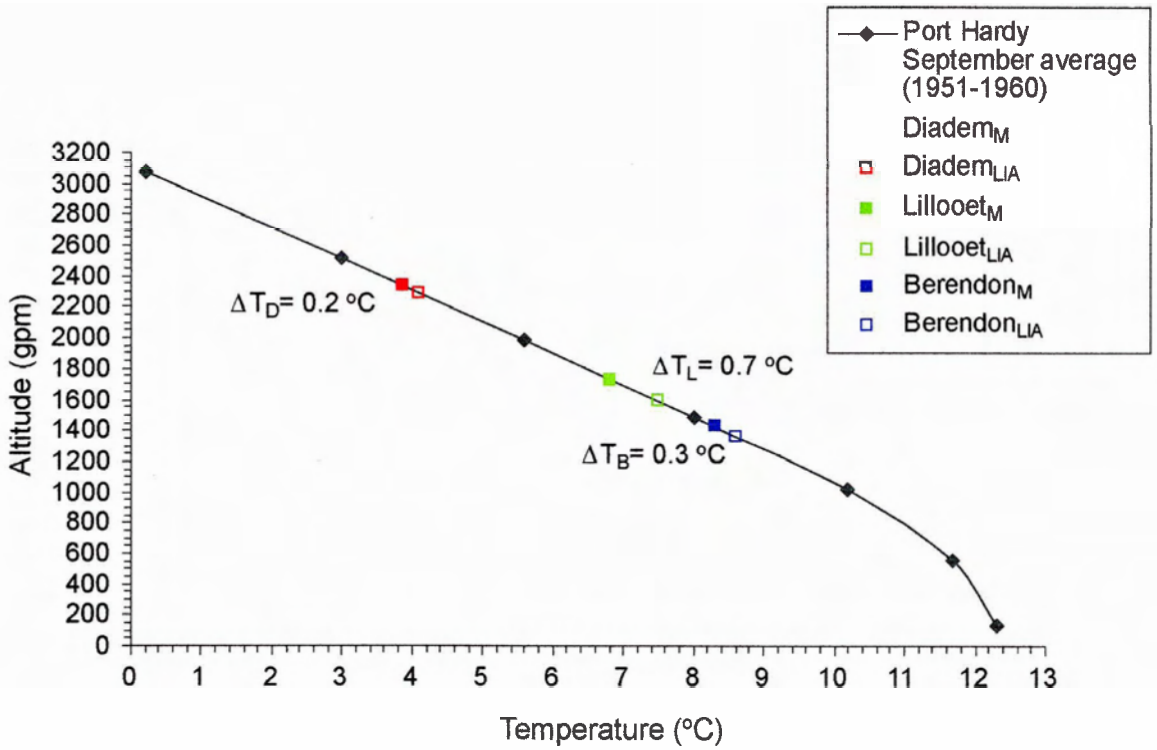

Figure 35. Plot of average September upper air temperature change with altitude at Port Hardy, B.C. The curve reflects a ten-year average for the years between 1951 and 1960. ΔT_L, ΔT_D, and ΔT_B are relative temperature depressions corresponding to the equilibrium-line altitude depressions calculated for the Lillooet, Diadem, and Berendon glaciers, respectively. M and LIA denote the modern and Little Ice Age equilibrium-line altitudes of each glacier. See Appendix I for details.

Of the two records, the 1951-1960 record is preferred as it provides more standard pressure surfaces with which to build the curve (Appendix I). Using this dataset, relative temperature depressions of 0.7 °C, 0.2 °C, and 0.3 °C are predicted for the Lillooet, Diadem, and Berendon glaciers, respectively (Fig. 35; Table 6). Given the difficulties in ELA calculation for the Diadem Glacier, however, this value should be treated as a minimum.

Precipitation and temperature data were also compiled for 29 climate stations located along the length of the Coast Mountains in British Columbia (Appendix J). Three temperature variables and two precipitation variables were compared to elevation: mean annual temperature, mean ablation season temperature (May to August), mean July temperature, mean annual precipitation, and mean accumulation season precipitation (October to April). Of the three temperature variables, only mean annual temperature correlates significantly with elevation (Fig. 36; Appendix K). Separation of the data geographically gives stronger correlations for southern stations (r^2= 0.89) than for northern stations (r^2 = 0.83). None of the precipitation variables correlate with elevation.

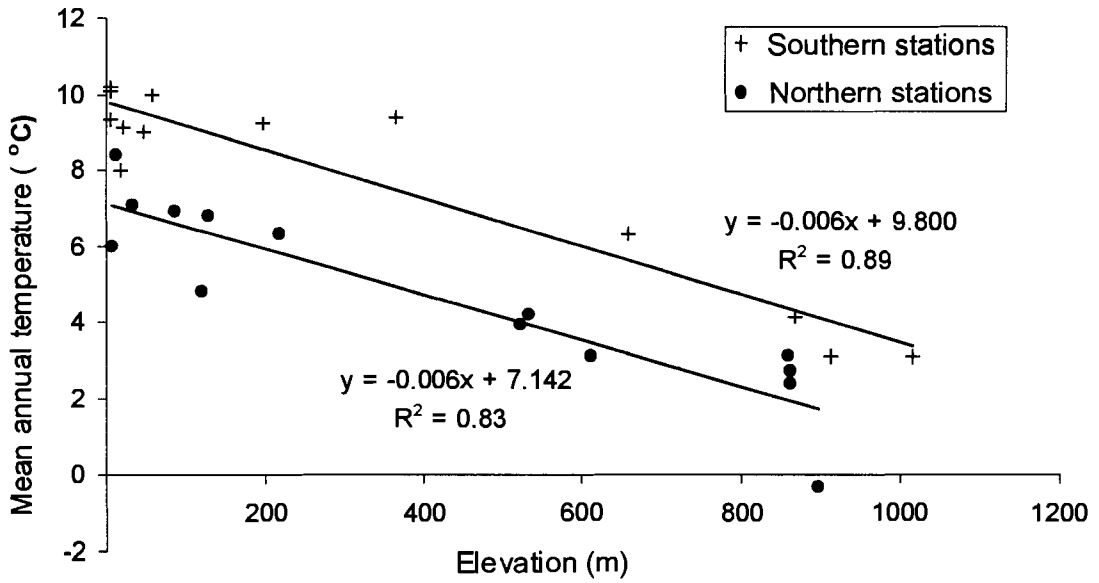

Figure 36. Mean annual temperature lapse rates calculated for northern and southern climate stations in the Coast Mountains. See Appendix J for climate data.

Extrapolation from the mean annual temperature curves gives modern free air lapse rates of 0.72 °C/100 m for both the southern and northern climate stations (Fig. 36). Applying these to the Little Ice Age ELAs gives temperature depressions of approximately 1.0 °C, 0.2 °C, and 0.4 °C for Lillooet, Diadem, and Berendon glaciers, respectively. The Diadem value should again be treated as a minimum.

Of the temperature values obtained, those calculated from the upper air data are preferred as the modern free air lapse rates calculated using the climate station data are higher than expected. Porter (1977) obtained an ablation season lapse rate of 0.62 °C/100 m and a July lapse rate of 0.67 °C/100 m for glaciers in Cascade Range, Washington, while Clague and Mathewes (1989) use a lapse rate of 0.65 °C/100 m for a site in southern British Columbia, under the assumption that adiabatic lapse rates are usually between 0.64 and 0.65 °C/100 m. The predicted temperature depressions using the calculated lapse rates are, however, still in close agreement with those calculated using the upper air data (Table 6).

Table 6. Comparison of temperature depressions (in °C) calculated using an ablation season temperature lapse rate and Port Hardy upper air data. See text for details of calculations and Appendixes I and J for details of climate data.

Glacier	Ablation season T lapse rate	Upper air September T (1951-1960)	Upper air September T (1994-2003)
Lillooet	1	0.7	0.6
Diadem	> 0.2	> 0.2	> 0.1
Berendon	0.4	0.3	0.3

These temperature depression values provide an approximation of Little Ice Age climate change, but they ignore a likely coeval increase in precipitation. Poor correlations between precipitation and altitude data, however, preclude reliable estimates of precipitation lapse rates. Porter (1977) examined the relation between accumulation season precipitation and glaciation level in the Cascade Range and found precipitation to be significantly better correlated with longitude (i.e., east or west of the range crest) than with altitude. A similar correlation is observed here, as precipitation data fall naturally into eastern and western components, and as comparable amounts of precipitation fall at stations that differ by over 800 m of altitude within their respective geographic groups

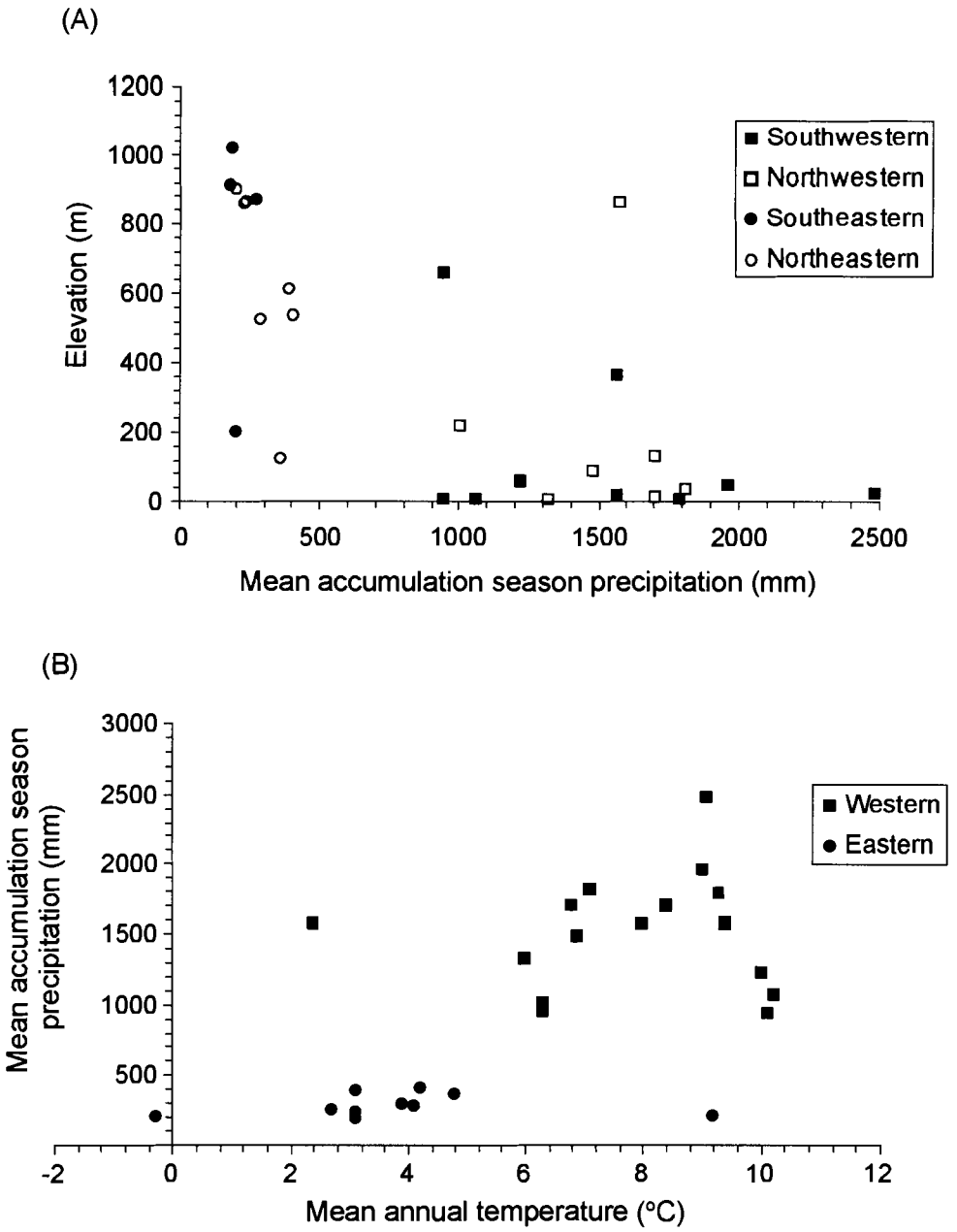

Figure 37. Plots of mean accumulation season precipitation (October to April) against (A) elevation and (B) mean annual temperature at climate stations in different areas. See Appendix J for climate data.

(Fig. 37). The influence of continentality on the position and temperature of ELA is further illustrated by the precipitation gradient inferred from the positive correlation between mean annual temperature and accumulation season precipitation (Fig. 37). The consequence of these trends is that modern precipitation data cannot be used to extrapolate regional precipitation lapse rates. Rather, local precipitation at various modern ELA elevations must be compared. Such comparisons are not possible because of the lack of available climate data at these sites. However, the increase in precipitation in the Coast Mountains during the Little Ice Age was likely 5 % or less, based on Porter's (1977) estimate of a 20-30 % increase in precipitation associated with a 4.2 ± 1.0 °C decrease in mean annual temperature for late Pleistocene glaciers.

Regional Comparison

A comparison of estimated ELAs of the three studied glaciers to those of other glaciers in the Coast Mountains is shown in Figure 38. The plot indicates a general decrease in ELA from southeast to northwest, along the northwest grain of the Coast Mountains.

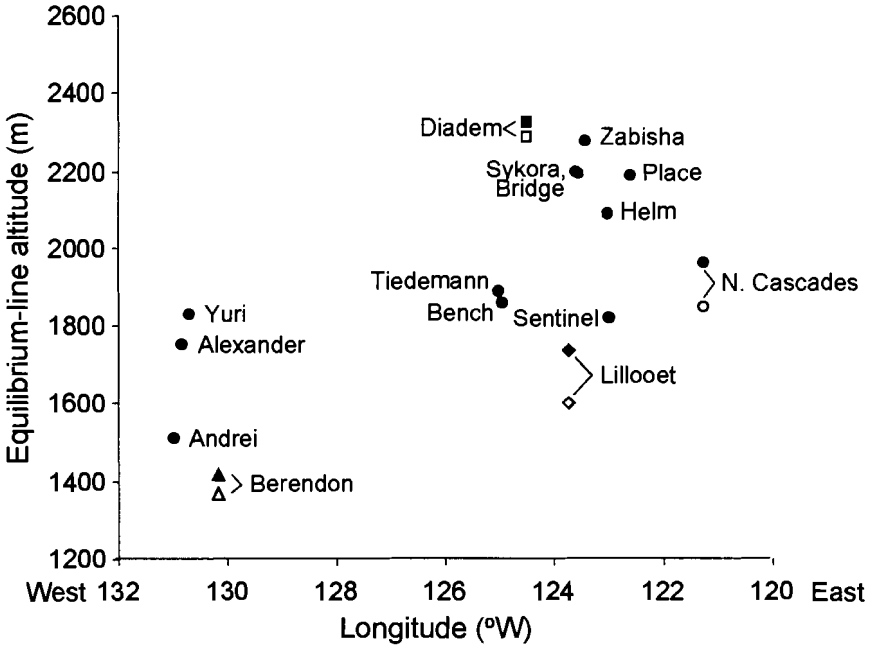

Figure 38. Calculated equilibrium-line altitudes of glaciers in the North Cascade Range, Washington, and Coast Mountains, British Columbia. See Appendix L for glacier locations and altitudes. Closed and open symbols represent modern and Little Ice Age values, respectively.

Compared to Bridge Glacier, the Lillooet Glacier modern ELA is lower than expected, as Bridge Glacier is just north of Lillooet Glacier. The apparently low Lillooet ELA value may be due to the unique mass balance relationship between Lillooet and Bishop glaciers. Lillooet Glacier, however, is approximately 5-10 km west of the crest of the Coast Mountains, whereas Bridge Glacier is 15-20 km east of it. Given the strong precipitation gradient, a higher ELA is expected for the more easterly Bridge Glacier. The modern ELA of Lillooet Glacier also overlaps, within error, that of Sentinel Glacier, which similarly lies approximately 15 km west of the Coast Mountain crest. These observations affirm the modern Lillooet ELA value.

Diadem Glacier is similar in many ways to Place Glacier (Fig. 38), which has a comparable area (3.4 km^2) and extends over a similar elevation range (1800 – 2600 m) (Moore and Demuth, 2001). Diadem Glacier is approximately 5 km farther east of the Coast Mountain crest than Place Glacier, which likely explains its slightly higher ELA.

The modern ELA of Andrei Glacier is similar to that of Berendon Glacier (Fig. 38). Both glaciers are of similar size and flow eastward out of major icefields. The Berendon ELA is, however, slightly lower than might be expected, perhaps due to penetration of moist air from Portland Inlet to the south.

Conclusion

The AAR method is the best technique for estimating modern and former ELAs when direct mass balance measurements are not available. The insensitivity of the AAR method to some of the reconstructed mass distribution curves, however, clearly demonstrates the need to evaluate glacier geometry to obtain reasonable ELA values. The THAR method proved to be a useful check in determining appropriate AAR values. The median altitude method is unsuitable for the larger glaciers in this study, because it overestimates ELA and does not recognize changes in glacier geometry. The highest moraine elevations are similarly unsuitable, as they generally underestimate ELA, probably due to erosion of moraines on steep valley walls.

Calculated modern ELAs of Lillooet, Diadem, and Berendon glaciers are similar to ELAs of other glaciers of similar character and geographic location. Examination of modern

precipitation data reveals strong longitudinal gradients that can account for variability among glacier ELAs, but prevents a reconstruction of past precipitation conditions.

Little Ice Age ELA depressions for the three studied glaciers range from 30 m to 140 m, with associated increases in glacier mass of up to 75%. Using modern upper air data, a relative decrease in temperature of up to 0.7 °C is predicted for the Little Ice Age, which was likely associated with a coeval increase in precipitation. Given the slightly greater ice extents indicated by the outer moraine at each of the three sites, climate change similar to that at the Little Ice Age maximum occurred during the advances that deposited the outer moraines.

5 Conclusion

This thesis provides reconstructions of late Quaternary glacier fluctuations at three sites in the Coast Mountains of British Columbia using a variety of methods. Data presented in the thesis indicate advances of glaciers at four times: prior to approximately 7000 cal yr BP and likely during the late-glacial; around 2900 cal yr BP (the Tiedemann event); between 1400 and 900 cal yr BP; and between 500 and 300 cal yr BP (Little Ice Age maximum).

The advances help to define Holocene climatic conditions in the Coast Mountains. The stratigraphic records of the Lillooet and Diadem sites suggest warmer and drier conditions during the early Holocene, similar to other paleoclimate reconstructions for British Columbia (Clague and Mathewes, 1989; Hebda and Whitlock, 1997; Brown, 2000; Walker, 2001). Sedimentological and paleobiological evidence further suggests that cooler-than-present climate conditions persisted between the Tiedemann and Little Ice Age advances. The correlation of middle and late Holocene advances at the three sites also suggests that the advances were not the result of local climate change but rather regional climate change throughout the Coast Mountains. Glacier advance prior to the Little Ice Age maximum further indicates that the late Neoglacial was characterized by an extended period of variable but generally cool climate.

The earliest recognized glacier advances at the three sites may also provide insight into the deglacial history of the Cordilleran Ice Sheet. Although these advances are still poorly dated, it is likely that they are latest Pleistocene in age, given their magnitude and independent evidence for a warmer climate during the early Holocene. The outer moraines at the three sites may reflect glacier readvances soon after the Cordilleran Ice Sheet disappeared. If correct, this conclusion implies that these older advances occurred under the influence of regional climate and were not due to local glaciological or climate factors.

This final point highlights the most important conclusion of this study. With continued research, glacial deposits in the British Columbia Coast Mountains will yield critical information on late-glacial climate that is required for a more comprehensive understanding of future climate change and its impact on montane environments.

6 References

Aruscavage, P.J., and Campbell, E.Y. 1983. An ion-selective electrode method for determination of chloride in geologic materials. Talanta, **30**: 745-749.

Bartington Instruments Ltd. 1993. Operation manual for MS2 magnetic susceptibility system, 20 pp.

Beget, J.E. 1981. Early Holocene glacier advance in the North Cascade Range, Washington. Geology, **9**: 409-413.

Beget, J.E. 1984. Tephrochronology of Late Wisconsin deglaciation and Holocene glacier fluctuations near Glacier Peak, North Cascade Range, Washington. Quaternary Research, **21**: 304-316.

Benn, D.I., and Evans, D.J. 1998. Glaciers and glaciation. Arnold, London, 734 pp.

Bethe, H.A., Korff, S.A., and Placzek, G. 1940. On the interpretation of neutron measurements in cosmic radiation. Physics Reviews, **57**: 573-587.

Bierman, P.R., and Gillespie, A. 1991. Range fires: A significant factor in exposure-age determination and geomorphic evolution. Geology, **19**: 641-644.

Bierman, P.R., Marsella, K.A., Patterson, C., Davis, P.T., and Caffee, M. 1999. Mid-Pleistocene cosmogenic minimum-age limits for pre-Wisconsinan glacial surfaces in southwestern Minnesota and southern Baffin Island: A multiple nuclide approach. Geomorphology, **27**: 25-39.

Briner, J.P., Swanson, T.W., and Caffee, M. 2001. Late Pleistocene cosmogenic ^{36}Cl glacial chronology of the southwestern Ahklun Mountains, Alaska. Quaternary Research, **56**: 148-154.

Brown, K.J. 2000. Late Quaternary vegetation, fire history, and GIS mapping of Holocene climates on southern Vancouver Island, British Columbia, Canada. Unpublished Ph.D. thesis, University of Victoria, Victoria, B.C., 253 pp.

Brugger, K.A., and Goldstein, B.S. 1999. Paleoglacier reconstruction and late Pleistocene equilibrium-line altitudes, southern Sawatch Range, Colorado. *In* Glacier processes past and present: Boulder, Colorado. *Edited by* D.M. Mickelson, and J.W. Attig. Geological Society of America Special Paper 337, pp. 103-112.

Burrows, R.B., Kovanen, D.J., Easterbrook, D.J., and Clark, D.H. 2000. Timing and extent of cirque glaciation near Mts. Baker and Shuksan, Cascade Range, Washington. Geological Society of America, Abstracts with Programs, **32**: 7.

Calkin, P.E., Wiles, G.C., and Barclay, D.J. 2001. Holocene coastal glaciation of Alaska. Quaternary Science Reviews, **20**: 499-461.

Clague, J.J. 1989. Quaternary geology of the Canadian Cordillera. Chapter 1 *In* Quaternary geology of Canada and Greenland. *Edited by* R.J. Fulton. Geological Survey of Canada, Geology of Canada, no.1, pp. 15-95.

Clague, J.J., and James, T.S. 2002. History and isostatic effects of the last ice sheet in southern British Columbia. Quaternary Science Reviews, **21**: 71-87.

Clague, J.J., and Mathewes, R.W. 1989. Early Holocene thermal maximum in western North America: New evidence from Castle Peak, British Columbia. Geology, **17**: 277-280.

Clague, J.J., and Mathewes, R.W. 1996. Neoglaciation, glacier-dammed lakes, and vegetation change in northwestern British Columbia, Canada. Arctic and Alpine Research, **28**: 10-24.

Clague, J.J., and Mathews, W. H. 1992. The sedimentary record and Neoglacial history of Tide Lake, northwestern British Columbia. Canadian Journal of Earth Sciences, **29**: 2383-2396.

Clague, J.J., Evans, S.G., Rampton, V.N., and Woodsworth, G.J. 1995. Improved age estimates for the White River and Bridge River tephras, western Canada. Canadian Journal of Earth Sciences, **32**: 1172-1179.

Clague, J.J., Wohlfarth, B., Ayotte, J., Eriksson, M., Hutchinson, I., Mathewes, R., and Walker, L. submitted. Late Holocene environmental change at treeline in the northern Coast Mountains, British Columbia. Quaternary Science Reviews.

Crandell, D.R., and Miller, R.D. 1974. Quaternary stratigraphy and extent of glaciation in the Mount Rainier region, Washington. United States Geological Survey Professional Paper 847, 59 pp.

Desloges, J.R., and Ryder, J.M. 1990. Neoglacial history of the Coast Mountains near Bella Coola, British Columbia. Canadian Journal of Earth Sciences, **27**: 281-290.

Duk-Rodkin, A., Barendregt, R.W., Tarnocai, C., and Phillips, F.M. 1995. Late Tertiary to late Quaternary record in the Mackenzie Mountains, Northwest Territories, Canada; stratigraphy, paleosols, paleomagnetism, and chlorine-36. Canadian Journal of Earth Sciences, **33**: 875-895.

Faegri, K., and Iverson, J. 1975. Textbook of pollen analysis. Munksgaard, Copenhagen, 295 pp.

Friele, P.A., and Clague, J.J. 2002a. Younger Dryas readvance in Squamish river valley, southern Coast Mountains, British Columbia. Quaternary Science Reviews, **21**: 1925-1933.

Friele, P.A. and Clague, J.J. 2002b. Readvance of glaciers in the British Columbia Coast Mountains at the end of the last glaciation. Quaternary International, **87**: 45-58.

Gaisser, T.K. 1990. Cosmic rays and particle physics. Cambridge University Press, Cambridge, 279 pp.

Gosse, J.C., and Phillips, F.M. 2001. Terrestrial in situ cosmogenic nuclides: Theory and application. Quaternary Science Reviews, **20**: 1475-1560.

Gosse, J.C., and Stone, O. 2001. Terrestrial cosmogenic nuclide methods passing milestones toward paleo-altimetry. EOS, **82**: 82,86,89.

Gosse, J.C., Reedy, R.C., Harrington, C.D., and Poths, J. 1996. Overview of the workshop on secular variations in production rates of cosmogenic nuclides on Earth. Radiocarbon, **38**: 135-147.

Grove, J.M. 1988. The Little Ice Age. Methuen, London, 498 pp.

Hallet, B., and Putkonen, J. 1994. Surface dating of dynamic landforms: Young boulders on aging moraines. Science, **256**: 937-940.

Hebda, R.J. 1983. Late-glacial and post-glacial vegetation history at Bear Cove Bog, northeast Vancouver Island, British Columbia. Canadian Journal of Botany, **61**: 3172-3192.

Hebda, R.J., and Whitlock, C. 1997. Environmental history. *In* The Rainforests of home. *Edited by* P.K. Schoonmaker, B. von Hagen, and E.C. Wolf. Island Press, Washington, D.C., pp. 227-254.

Heine, J.T. 1998. Extent, timing and climatic implications of glacier advances at Mount Rainier, Washington, U.S.A., at the Pleistocene/Holocene transition. Quaternary Science Reviews, **17**: 1139-1148.

Hurley, T.M. 1996. Late-glacial equilibrium-line altitudes of glaciers in the southern North Cascade Range, Washington. Unpublished M.Sc. thesis, University of Washington, Seattle, Washington, 82 pp.

Jackson, L.E., Phillips, F.M., and Little, E.C. 1999. Cosmogenic ^{36}Cl dating of the maximum limit of the Laurentide Ice Sheet in southwestern Alberta. Canadian Journal of Earth Sciences, **36**: 1347-1356.

Kershaw, J.A. 2002. Formation and failure of moraine-dammed Queen Bess Lake, southern Coast Mountains, British Columbia. Unpublished M.Sc. thesis. Simon Fraser University, Burnaby, B.C., 130 pp.

Kovanen, D.J., and Easterbrook, D.J. 2002. Timing and extent of Allerod and Younger Dryas age (ca. 12,500-10,000 ^{14}C yr BP) oscillations of the Cordilleran Ice Sheet in the Fraser Lowland, western North America. Quaternary Research, **57**: 208-224.

Kurz, M.D., and Brook, E.J. 1994. Surface exposure dating with cosmogenic nuclides. *In* Dating in exposed and surface contexts. *Edited by* C. Beck. University of New Mexico Press, Albuquerque, New Mexico, pp. 139-159.

Lal, D. 1991. Cosmic ray labeling of ersosion surfaces: In situ nucliide production rates and erosion models. Earth and Planetary Science Letters, **104**: 424-439.

Lal, D., and Peters, B. 1967. Cosmic ray produced radioactivity on the earth. *In* Handbuch der Physik. *Edited by* K. Sitte. Springer-Verlag, Berlin, pp. 551-612.

Laxton, S., Smith, D., Desloges, J.R., and Day, A. 2003. Stratigraphic analysis of a mid-Holocene delta at Fyles Glacier, Coast Mountains, British Columbia. Canadian Association of Geographers, Annual Meeting of the Western Division, March 13-15, 2003. University of Northern British Columbia, Prince George, B.C., Abstracts.

Letreguilly, A. 1988. Relation between the mass balance of western Canadian mountain glaciers and meteorological data. Journal of Glaciology, **34**: 11-18.

Luckman, B.H. 2000. The Little Ice Age in the Canadian Rockies. Geomorphology, **32**: 357-384.

Mackinnon, A., Pojar, J., and Coupe, R. 1992. Plants of northern British Columbia. Lone Pine Publishing, Edmonton, Alberta, 338 pp.

Mathews, W.H. 1973. Record of two jökulhlaups. *In* Symposium on the Hydrology of Glaciers. *Edited by* J.W. Beck, R.J. Adie, and D.M. Johnson. International Association of Scientific Hydrology Publication, **95**: 99-110.

Mathews, W.H., and Clague, J.J. 1993. The record of jökulhlaups from Summit Lake, northwestern British Columbia. Canadian Journal of Earth Sciences, **30**: 499-508.

Mayo, L.R. 1984. Glacier mass balance and runoff research in the U.S.A. Geografiska Annaler, **66A**: 215-227.

McCrumb, D.R. 2001. Age constraints for a late-glacial morainal shoal in Howe Sound, British Columbia. Unpublished M.Sc. thesis, University of Washington, Seattle, Washington, 40 pp.

McCrumb, D.R., and Swanson, T.W. 1998. Cosmogenic ^{36}Cl age constraints on the deglaciation history of the Cordilleran ice sheet from Howe Sound, British Columbia. Geological Society of America, Abstracts with Programs, **30**: 135.

Meidinger, D., and Pojar, J. (eds.) 1991. Ecosystems of British Columbia. British Columbia Ministry of Forests, Research Branch, Special Report Series, no. 6, 330 pp.

Meierding, T.C. 1982. Late Pleistocene equilibrium-line altitudes in the Colorado Front Range: A comparison of methods. Quaternary Research, **18**: 289-310.

Moore, P.D., and Webb, J.A. 1978. An illustrated guide to pollen analysis. Hodder and Stroughton, London, 133 pp.

Moore, R.D. 1993. Application of a conceptual streamflow model in a glacierized drainage basin. Journal of Hydrology, **150**: 151-168.

Moore, R.D., and Demuth, M.N. 2001. Mass balance and streamflow variability at Place Glacier, Canada, in relation to recent climate fluctuations. Hydological Processes, **15**: 3474-3486.

Ohmura, A., Kasser, P., and Funk, M. 1992. Climate at the equilibrium line of glaciers. Journal of Glaciology, **38**: 397-411.

Ostrem, G. 1966. The height of the glaciation limit in southern British Columbia and Alberta. Geografiska Annaler, **48A**: 126-138.

Ostrem, G. 1973. The transient snowline and glacier mass balance in southern British Columbia and Alberta, Canada. Geografiska Annaler, **55A**: 93-106.

Pellatt, M.G., and Mathewes, R.W. 1994. Paleoecology of post-glacial treeline fluctuations on the Queen Charlotte Islands, Canada. Ecoscience, **1**: 71-81.

Pelto, M.S., and Riedel, J. 2001. Spatial and temporal variations in annual balance of North Cascade glaciers, Washington 1984-2000. Hydrological Processes, **15**: 3461-3472.

Phillips, F.M., and Plummer, M.A. 1996. CHLOE: A program for interpreting *in-situ* cosmogenic nucliide data for surface exposure dating and erosion studies. Radiocarbon, **38**: 98-99.

Phillips, F.M., Stone, W.D., and Fabryka-Martin, J.T. 2001. An improved approach to calculating low-energy cosmic-ray neutron flux near the land/atmosphere interface. Chemical Geology, **175**: 689-701.

Phillips, F.M., Zreda, M.G., Benson, L.V., Plummer, M.A., Elmore, D., and Sharma, P. 1996a. Chronology for fluctuations in late Pleistocene Sierra Nevada glaciers and lakes. Science, **274**: 749-751.

Phillips, F.M., Zreda, M.G., Flinsch, M.R., Elmore, D., and Sharma, P. 1996b. A reevaluation of cosmogenic chlorine-36 production rates in terrestrial rocks. Geophysical Research Letters, **23**: 949-952.

Phillips, F.M., Zreda, M.G., Smith, S.S., Elmore, D., Kubik, P.W., and Sharma, P. 1990. Cosmogenic chlorine-36 chronology for glacial deposits at Bloody Canyon, eastern Sierra Nevada. Science, **248**: 1529-1532.

Porter, S.C. 1964. Composite Pleistocene snowline of Olympic Mountains and Cascade Range, Washington. Geological Society of America Bulletin, **81**: 477-482.

Porter, S.C. 1977. Present and past glaciation threshold in the Cascade Range, Washington U.S.A.: Topographic and climatic controls, and paleoclimatic implications. Journal of Glaciology, **18**: 101-116.

Putkonen, J., and Swanson, T. 2003. Accuracy of cosmogenic ages for moraines. Quaternary Research, **59**: 255-261.

Rama, and Honda, M. 1961. Cosmic-ray induced radioactivity in terrestrial materials. Journal of Geophysics Research, **66**: 3533-3539.

Reasoner, M.A. 1993. Equipment and procedure improvements for a lightweight, inexpensive, percussion core sampling system. Journal of Paleolimnology, **8**: 273-281.

Reyes, A. 2003. Late Holocene fluctuations of Lillooet Glacier, southern Coast Mountains, British Columbia. Unpublished M.Sc. thesis. Simon Fraser University, Burnaby, B.C.

Ryder, J.M., and Thomson, B. 1986. Neoglaciation in the southern Coast Mountains of British Columbia: Chronology prior to the late Neoglacial maximum. Canadian Journal of Earth Sciences, **23**: 273-287.

Smith, D. 2003. Late Holocene glacier activity in the Tchaikazan Valley, T'syl-os Provincial Park, British Columbia. Canadian Association of Geographers, Annual Meeting of the Western Division, March 13-15, 2003. University of Northern British Columbia, Prince George, B.C., Abstracts.

Stone, J.O. 2000. Air pressure and cosmogenic isotope production. Journal of Geophysical Research, **105**: 23,753-23,759.

Stone, J.O., Evans, J.M., Fifield, L.K., Allan, G.L., and Cresswell, R.G. 1998. Cosmogenic ^{36}Cl production in calcite by muons. Geochimica and Cosmochimica Acta, **62**: 433-454.

Stuiver, M., and Reimer, P. J. 1993. Extended ^{14}C database and revised CALIB radiocarbon calibration program. Radiocarbon, **35**: 215-230.

Stuiver, M., Reimer, P.J., Bard, E., Beck, J.W., Burr, G.S., Hughen, K.A., Kromer, B., McCormac, F.G., v. d. Plicht, J., and Spurk, M. 1998. INTCAL98 radiocarbon age calibration 24,000 - 0 cal BP. Radiocarbon, **40**: 1041-1083.

Swanson, T.W., and Caffee, M.L. 2001. Determination of ^{36}Cl productions rates derived from the well-dated deglaciation surfaces of Whidbey and Fidalgo Islands, Washington. Quaternary Research, **56**: 366-382.

Swanson, T.W., and Porter, S.C. 1997. New cosmogenic isotope ages for the last glaciation in the eastern North Cascade Range. Geological Society of America, Abstracts with Programs, **29**: 108.

Titus, R.L. 1965. Upper air climate of Canada- Average, extreme and standard deviation values, 1951-1960. Canadian Department of Transport, Meteorological Brach, Toronto, Ont., 70 pp.

Thomas, P.A., Easterbrook, D.J., and Clark, P.U. 2000. Early Holocene glaciation on Mount Baker, Washington State, U.S.A. Quaternary Science Reviews, **19**: 1043-1046.

Thompson, R., and Oldfield, F. 1986. Environmental magnetism. Allen and Unwin, London, 227 pp.

Walden, J., Oldfield, F., and Smith, J. 1999. Environmental magnetism: A practical guide. Quaternary Research Association, Technical Guidebook 6, 243 pp.

Walker, L.A. 2001. Late Pleistocene and Holocene vegetation, climate, sea level and fire history of Effingham Island Bog, Vancouver Island, British Columbia. Unpublished B.Sc. thesis, University of Victoria, Victoria, B.C., 67 pp.

Zreda, M.G., and Phillips, F.M. 1994. Surface exposure dating by cosmogenic chlorine-36 accumulation. *In* Dating in exposed and surface contexts. *Edited by* C. Beck. University of New Mexico Press, Albuquerque, New Mexico, pp. 161-183.

Zreda, M.G., and Phillips, F.M. 1995. Insights into alpine moraine development from cosmogenic ^{36}Cl buildup dating. Geomorphology, **14**: 149-156.

Zreda, M.G., Phillips, F.M., and Elmore, D. 1994. Cosmogenic ^{36}Cl accumulation in unstable landforms 2: Simulations and measurements on eroding moraines. Water Resources Research, **30**: 3127-3136.

Appendix A. Published radiocarbon ages from Berendon and Spillway ponds.

Radiocarbon age[1] (^{14}C yr BP)	Calibrated age[2] (cal yr BP)	Laboratory[3] number	Location Lat. (N), Long. (W)	Elevation[4] (m)	Depth[5] (cm)	Dated material
Berendon Pond						
505 ± 80	550-670	LuA-5113	56°14.5', 130°03.7'	837	1.21-1.40	Conifer cone fragment
615 ± 85	590-710	LuA-5114	56°14.5', 130°03.7'	835	3.42-3.47	Conifer needle fragments
Spillway Pond						
400 ± 50	380-560	TO-4090	56°14.5', 130°04.0'	839	0.28	Twig
520 ± 60	560-670	TO-4092	56°14.5', 130°04.0'	839	0.29	Twig
600 ± 70	590-700	TO-4152	56°14.5', 130°04.0'	839	0.14	*Abies* needles
720 ± 50	700-730	TO-4091	56°14.5', 130°04.0'	839	0.35	Bark

Note: Ages reported in Clague and Mathewes (1996).

[1] Age error terms are 1-sigma.

[2] Reference datum is AD 1950. Calibrated from data of Stuiver and Reimer (1993) and Stuiver et al. (1998). The values given are 2-sigma age ranges, determined using an error multiplier of 2.0.

[3] Laboratories: LuA, University of Lund; TO, IsoTrace (University of Toronto).

[4] Approximate elevation of sample.

[5] Depth below lake floor.

Appendix B. Moraine boulder sample data.

Sample ID	Lithology	Elevation (m)	Location Lat. (N) , Long. (W)	Boulder dimensions[1] (cm)	$^{36}Cl/Cl$[2] $[10^{-15}]$	Cl[3] [ppm]	CaO[3] [wt%]	K_2O[3] [wt%]	Comments
SF-LG-15	Granite	1512	50°45.78'123°44.88'	ca. 150,150,110	186	10.76	3.05	0.51	Maximum weathering rind is 2 mm
SF-LG-28	Granite	1376	50°45.20' 123°43.30'	420,300,300	126	31.51	3.77	1.51	Weathering rind minimal
SF-QB-4	Granodiorite	1739	51°15.57'124°30.52'	360,245,145	373	43.77	4.21	1.35	Pitted surface (2-3 mm)
SF-QB-5	Granodiorite	1733	51°15.56' 124°30.53'	275,220,140	73	41.62	4.28	1.44	Pitted surface, weathering rind 3-5 mm
SF-BG-1	Dacite	864	56°14.40'130°03.93'	180,120,110	28	88.22	4.42	2.56	Weathering rind <1 mm
SF-BG-3	Dacite	860	56°14.44'130°03.84'	280,210,150	34	132.30	4.22	2.57	Surface cracks weathered to 2 mm

[1] Boulder measurements are length, width, and height, respectively.

[2] $^{36}Cl/Cl$ measurements performed by the Centre for Accelerator Mass Spectrometry at Lawrence Livermore National Laboratory, California.

[3] Total Cl and oxides measurement performed by the New Mexico Bureau of Geology and Mineral Resources, New Mexico Institute of Mining and Technology, Socorro.

Appendix C. Major element data for moraine boulder samples.

Sample ID	SiO_2 [wt. %]	TiO_2 [wt. %]	Al_2O_3 [wt. %]	Fe_2O_3(T) [wt. %]	MnO [wt. %]	MgO [wt. %]	CaO [wt. %]	K_2O [wt. %]	Na_2O [wt. %]	P_2O_5 [wt. %]	LOI [wt. %]	Total [wt. %]	Ba [ppm]
SF-LG-15	74.47	0.18	14.47	1.89	0.04	0.37	3.05	0.51	4.56	0.03	0.53	100.10	334
SF-LG-28	69.81	0.28	15.80	2.66	0.05	0.90	3.77	1.51	4.25	0.02	0.50	99.56	513
SF-QB-4	71.00	0.28	15.13	2.89	0.06	1.04	4.21	1.35	3.74	0.02	0.67	100.39	415
SF-QB-5	69.20	0.26	16.53	2.64	0.05	0.91	4.28	1.44	4.35	0.02	0.67	100.34	587
SF-BG-1	64.28	0.44	16.58	4.34	0.11	1.41	4.42	2.56	3.77	0.04	1.77	99.72	2092
SF-BG-3	63.87	0.47	16.98	4.24	0.10	1.34	4.22	2.57	3.97	0.02	1.54	99.32	2170

Notes: LOI is loss on ignition. Fe_2O_3(T) is total iron expressed as Fe_2O_3. Analyses performed by the New Mexico Bureau of Geology and Mineral Resources, New Mexico Institute of Mining and Technology, Socorro.

Appendix D. Trace element data for moraine boulder samples.

Sample ID	Rb [ppm]	Sr [ppm]	Pb [ppm]	Th [ppm]	U [ppm]	B [ppm]	Gd [ppm]
SF-LG-15	4	618	ND	ND	ND	<3	<1
SF-LG-28	24	549	8	ND	1	12	1
SF-QB-4	20	448	11	4	1	8	3
SF-QB-5	22	574	11	2	2	6	2
SF-BG-1	63	545	1	2	2	8	3
SF-BG-3	66	525	ND	ND	1	9	2

Notes: ND is below the lower limit of determination. Analyses performed by the New Mexico Bureau of Geology and Mineral Resources, New Mexico Institute of Mining and Technology, Socorro, except for B and Gd, which were done at SGS Laboratories, Don Mills, ON.

Appendix E. Magnitude of errors in apparent ^{36}Cl ages on moraine boulders.

Sample characteristics	Error
Surface geometry correction	1%
Shielding correction	1%
Thickness	1%
Erosion rate and style	2%
Sample preparation and analysis	
Weighing of sample	2%
Addision of carrier	2%
XRF (U,Th)	<2%
XRF (all other elements)	<2%
PGES (B, Gd)	<2%
Total chlorine	<5%
AMS	3%

Notes: Errors are from Gosse and Phillips (2001) and laboratories that performed the analyses. Total errors were calculated using equation 6.1 of Gosse and Phillips (2001); they include only random, not systematic, errors.

Appendix F. Modern and Little Ice Age contour interval areas calculated for Lillooet Glacier.

Elevation range (ft)	Relative area on map	Area of increment (% total area)	Cumulative area below (% total area)
Modern			
9000-9400	0.06	0.3	100
9000-9300	0.14	0.7	99.7
8500-9000	4.23	21.2	99.0
8000-8500	2.99	15.0	77.8
7500-8000	1.30	6.5	62.8
7000-7500	0.76	3.8	56.2
6500-7000	1.04	5.2	52.4
6000-6500	1.26	6.3	47.2
5500-6000	2.02	10.1	40.9
5000-5500	2.43	12.2	30.8
4500-5000	1.64	8.2	18.6
4000-4500	1.08	5.4	10.3
3500-4000	0.65	3.3	4.9
3000-3500	0.26	1.3	1.7
2700-3000	0.07	0.4	0.4
Sum area	19.93	100.0	
Little Ice Age			
9000-9400	0.06	0.2	100
9000-9300	0.17	0.5	99.8
9000-9200	0.10	0.3	99.3
8500-9000	5.26	15.1	99.1
8000-8500	4.60	13.2	84.0
7500-8000	2.30	6.6	70.8
7000-7500	1.41	4.0	64.2
6500-7000	1.22	3.5	60.2
6000-6500	2.32	6.6	56.7
5500-6000	3.11	8.9	50.0
5000-5500	4.13	11.8	41.1
4500-5000	2.63	7.5	29.3
4000-4500	1.65	4.7	21.7
3500-4000	1.36	3.9	17.0
3000-3500	1.80	5.2	13.1
2600-3000	2.78	8.0	8.0
Sum area	34.90	100	

Appendix G. Modern and Little Ice Age contour interval areas calculated for Diadem Glacier.

Elevation range (ft)	Relative area on map	Area of increment (% total area)	Cumulative area below (% total area)
Modern			
9500-9800	0.18	4.9	100.0
9000-9500	0.18	4.7	95.1
9000-9150	0.09	2.4	90.4
9000-9050	0.05	1.4	88.0
8500-9000	1.38	37.3	86.6
8000-8500	0.81	21.9	49.3
7500-8000	0.32	8.7	27.3
7000-7500	0.35	9.5	18.7
6500-7000	0.12	3.2	9.2
6000-6500	0.12	3.2	6.0
5600-6000	0.10	2.7	2.7
Sum area	3.70	100.0	
Little Ice Age			
9500-9800	0.18	3.9	100.0
9000-9500	0.18	3.8	96.1
9000-9150	0.09	2.0	92.3
9000-9050	0.05	1.1	90.3
8500-9000	1.38	30.0	89.3
8000-8500	0.81	17.6	59.3
7500-8000	0.32	6.9	41.7
7000-7500	0.35	7.6	34.7
6500-7000	0.12	2.6	27.1
6000-6500	0.24	5.2	24.5
5600-6000	0.89	19.3	19.3
Sum area	4.61	100.0	

Appendix H. Modern and Little Ice Age contour interval areas calculated for Berendon Glacier.

Elevation range (ft)	Relative area on map	Area of increment (% total area)	Cumulative area below (% total area)
Modern			
7000-7200	0.28	1.3	100.0
6500-7000	0.39	1.8	98.7
6500-6700	0.04	0.2	96.9
6000-6500	2.08	9.7	96.7
6000-6300	0.20	0.9	86.9
6000-6200	0.05	0.2	86.0
5500-6000	3.66	17.2	85.8
5000-5500	3.95	18.5	68.6
4500-5000	5.14	24.1	50.1
4000-4500	2.52	11.8	26.0
3500-4000	1.94	9.1	14.2
3000-3500	0.68	3.2	5.1
2500-3000	0.41	1.9	1.9
Sum area	21.34	100	
Little Ice Age			
7000-7200	0.28	1.1	100.0
6500-7000	0.39	1.5	98.9
6500-6700	0.04	0.2	97.4
6000-6500	2.08	8.1	97.2
6000-6300	0.20	0.8	89.1
6000-6200	0.05	0.2	88.3
5500-6000	3.66	14.3	88.1
5000-5500	4.36	17.0	73.8
4500-5000	5.66	22.1	56.8
4000-4500	2.94	11.5	34.7
3500-4000	2.43	9.5	23.2
3000-3500	0.91	3.6	13.7
2500-3000	1.18	4.6	10.1
2000-2500	1.41	5.5	5.5
Sum area	25.59	100	

Appendix I. Ten-year average September altitude and temperature values for standard pressure surfaces at Port Hardy, B.C. (1951 -1960 and 1994-2003).

Pressure (mb)	Altitude (gpm)	Temperature (°C)
1951-1960		
1000	136	12.3
950	565	11.7
900	1018	10.2
850	1491	8.0
800	1992	5.6
750	2519	3.0
700	3073	0.2
1994-2003		
1000	143	11.4
925	789	10.4
850	1492	7.6
700	3072	0.1

Notes: Altitudes given are standardized geopotential heights. Soundings taken at 1200 GMT. 1951-1960 data from Titus (1965); 1994-2003 data from Global Radiosonde Data, available on-line through the University of Wyoming (http://www.weather.uwyo.edu/upperair/sounding.html).

Appendix J. Climate data used to calculate modern lapse rates.

Climate station	Location Lat.(N)	Long.(W)	Elevation (m)	Mean temperature (°C) June	July	August	Mean T_{J-A} (°C)	Mean annual T (°C)	Mean P_{O-A} (mm)	Mean annual P (mm)
Southern										
Abbotsford	49°01',	122°21'	58	15.1	17.5	17.7	16.8	10.0	1220	1573
Addenbroke Island	51°36',	127°52'	21	12.8	14.7	15	14.2	9.1	2483	3286
Bella Coola	52°22',	126°41'	18	14.4	16.8	16.7	16.0	8.0	1293	1652
Burnaby (SFU)	49°16',	122°59'	366	14	16.8	17	15.9	9.4	1570	2020
Cortes Island	50°05',	125°10'	6	15.4	17.9	17.9	17.1	10.2	1062	1379
Dryad Point	52°11',	128°06'	4	13.4	15.4	15.7	14.8	9.3	1792	2527
Hope Airport	49°22',	121°30'	39	15.7	18.3	18.8	17.6	9.9	1593	2008
Hope Slide	49°16',	121°14'	674	12.2	14.8	14.9	14.0	6.1	917	1210
Kleena Kleen 2	51°58',	124°59'	914	11.6	14.1	13.7	13.1	3.1	180	330
Lillooet Seton	50°40',	121°55'	198	18.4	21.4	21	20.3	9.2	206	330
Lunch Lake	51°49',	124°28'	1017	11.1	13.6	13.5	12.7	3.1	188	373
Squamish Upper	49°54',	123°16'	46	15.2	17.7	17.8	16.9	9.0	1966	2367
Tatlayoko Lake	51°40',	124°24'	870	11.3	13.8	13.8	13.0	4.1	273	434
Vancouver Airport	49°12',	123°10'	4	15.2	17.5	17.6	16.8	10.1	944	1199
Whistler	50°07',	122°57'	659	13.2	15.9	16.1	15.1	6.3	946	1229
Northern										
Bob Quinn AGS	56°58',	130°15'	612	11.9	14.1	13.4	13.1	3.1	387	642
Green Island	54°34',	130°42'	12	12.7	14.4	14.6	13.9	8.4	1708	2447
Hazelton Temlehan	55°12',	127°43'	122	13.8	16.3	15.9	15.3	4.8	361	614
Kemano	53°33',	127°56'	87	13.6	16	16.1	15.2	6.9	1480	1897
Kitimat Townsite	54°03',	128°37'	128	13.6	16.2	16.2	15.3	6.8	1708	2191
Ootsa Lake	53°46',	126°00'	861	10.9	13.8	13.8	12.8	3.1	232	426
Prince Rupert Airport	54°17',	130°26'	35	11.1	13.1	13.5	12.6	7.1	1817	2594
Smithers Airport	54°49',	127°10'	522	12.6	15	14.6	14.1	3.9	289	513
Stewart	55°56',	129°59'	7	13.7	15.1	14.3	14.4	6.0	1323	1843
Suskwa Valley	55°17',	127°10'	534	12.4	14.5	13.9	13.6	4.2	403	746
Tahtsa Lake West	53°37',	127°42'	863	8.2	11.5	11.7	10.5	2.4	1574	1978
Terrace Airport	54°28',	128°34'	217	13.7	16.4	16.3	15.5	6.3	1004	1322
Togadin Ranch	57°36',	130°40'	899	9.4	11.6	11.1	10.7	-0.3	202	419
Wistaria Airport	53°49',	126°12'	863	10.7	13.3	13.2	12.4	2.7	239	438

Notes: T_{J-A}, mean ablation season temperature (June to August); P_{O-A}, mean accumulation season precipitation (October to April). Data calculated from Environment Canada's Canadian climate normals (1971-2000).

Appendix K. Variance values for linear regressions of climate data.

Variable	r^2 value		
	All stations	Northern stations	Southern stations
Mean annual temperature	0.71	0.83	0.89
Mean temperature (May-September)	0.43	0.55	0.43
Mean July temperature	0.38	0.47	0.37
Mean annual precipitation	0.47	0.45	0.49
Mean precipitation (October-April)	0.47	0.49	0.51

Appendix L. Equilibrium-line altitudes of glaciers in the North Cascade Range, Washington, and Coast Mountains, British Columbia.

	Location	Equilibrium-line altitude (m)	
Glacier	Lat. (N), Long. (W)	Modern	Little Ice Age
North Cascades[1]	47°30', 121°15'	1960	1850
Sentinel[2]	49°54', 122°59'	1818	
Helm[3]	49°58', 123°00'	2090	
Place[2]	50°26', 122°36'	2187	
Lillooet[4]	50°45', 123°44'	1740	1600
Zabisha[3]	50°48', 123°25'	2280	
Bridge[3]	50°49', 123°33'	2200	
Sykora[3]	50°53', 123°34'	2200	
Diadem[4]	51°15', 124°30'	2320	2290
Tiedemann[3]	51°20', 125°00'	1890	
Bench[3]	51°27', 124°56'	1860	
Berendon[4]	56°14', 130°10'	1420	1370
Andrei[3]	56°57', 130°59'	1510	
Yuri[3]	56°58', 130°42'	1829	
Alexander[3]	57°06', 130°49'	1750	

[1] Hurley (1996). Values shown are averages for the study area. Values calculated using an AAR of 0.65.

[2] Letreguilly (1988). Values calculated from data collected by Glaciological Division, Inland Waters Branch, Department of Energy, Mines and Resources, Canada.

[3] Ohmura et al. (1992). Values calculated from data collected by Glaciological Division, Inland Waters Branch, Department of Energy, Mines and Resources, Canada.

[4] This study. Elevations calculated using an AAR of 0.65, with the exception of modern Diadem Glacier (AAR = 0.80).